DISSERTATION

submitted to the
Faculty of Chemistry and Earth Sciences
of the University of Heidelberg, Heidelberg, Germany
in partial fulfillment of the requirements for the degree of
Doctor of Natural Sciences (Dr. rer. nat.)

sumitted by
Caitlin Howell (M.Sc. Botany and Plant Pathology)
born in Lewiston, Maine, USA

Oral examination: October 10th, 2011

In situ investigations of biological molecules using vibrational sum-frequency-generation spectroscopy

The dissertation was carried out at the

Institute of Physical Chemistry

University of Heidelberg, Heidelberg, Germany

and reviewed by

Prof. Dr. Michael Grunze
Institute of Physical Chemistry, University of Heidelberg

Prof. Dr. Marcus Motzkus
Institute of Physical Chemistry, University of Heidelberg

Nothing tends so much to the advancement of knowledge as the application of a new instrument. The native intellectual powers of men in different times are not so much the causes of the different success of their labours, as the peculiar nature of the means and artificial resources in their possession.

Sir Humphrey Davy

Published works related to this thesis:

- C. Howell, H. Hamoudi, P. Koelsch, and M. Zharnikov Orientation changes in surface-bound hybridized DNA undergoing preparation for *ex situ* spectroscopic analysis. *Chemical Physics Letters*, 513 (2011) 267–270.

- C. Howell, J. Zhao, P. Koelsch, and M. Zharnikov. Hybridization in ssDNA films: a multi-technique spectroscopy study. *Physical Chemistry Chemical Physics*, 13 (2011) 15512-15522.

- C. Howell, R. Maul, W. Wenzel, and P. Koelsch. Interactions of hydrophobic and hydrophilic self-assembled monolayers with water as probed by sum-frequency-generation spectroscopy. *Chemical Physics Letters*, 494 (2010) 193–197.

- D. Verreault, V. Kurz, C. Howell and P. Koelsch. Sample cells for probing solid/liquid interfaces with broadband sum-frequency-generation spectroscopy. *Review of Scientific Instruments*, 81 (2010) 06311/11–10.

- M.-O. Diesner, C. Howell, V. Kurz, D. Verreault and P. Koelsch. In vitro characterization of surface properties through living cell. *Journal of Physical Chemistry Letters*, 1 (2010) 2339–2342.

- C. Howell, R. Schmidt, V. Kurz and P. Koelsch. Sum-frequency-generation spectroscopy of DNA films in air and aqueous environments. *Biointerphases*, 3 (2008) FC47–FC51

- C. Howell, M.-O. Diesner, M. Grunze, and P. Koelsch. Probing the extracellular matrix with sum-frequency-generation spectroscopy. *Langmuir*, 24 (2008) 13819–13821.

Other works published as a PhD student:

- A.-C. Hastrup, C. Howell, F. Larsen, B. Goodell, and J. Jellison. Differences in modification of crystalline cellulose due to degradation by brown and white rot fungi. *FEBS Journal*, (2011) submitted.

- C. Howell, A.-C. Hastrup, R. Jara, F. Larsen, B. Goodell, and J. Jellison. Changes in wood crystalline cellulose structure caused by hot-water extraction and fungal decay. *Cellulose*, 18 (2011) 1179-1190.

- A.-C. Hastrup, C. Howell, B. Jensen, and F. Green. Non-enzymatic depolymerization of cotton cellulose by fungal mimicking metabolites. *Biodeterioration and Biodegradation*, 65 (2011) 553–559.

- S. Schreiner, A. Hatch, D. Shudy, C. Howell, J. Jianli, P. Koelsch, M. Zharnikov, D. Petrovykh, and A. Opdahl. Impact of DNA-surface interactions on the stability of DNA hybrids. *Analytical Chemistry*, 83 (2011) 4288–4295.

Works published as a masters student:

– C. Howell, J. Paredes, and J. Jellison. Decay resistance properties of hot water extracted oriented strand board. *Wood and Fiber Science*, 41 (2009) 201–208.

– C. Howell, A.-C. Hastrup, B. Goodell, and J. Jellison. Temporal changes in wood crystalline cellulose during degradation by brown rot fungi. *International Biodeterioration and Biodegradation*, 63 (2009) 414–419.

– J. Paredes, R. Mills, C. Howell, S. Shaler, D. Gardener, A. van Heiningen.Surface characterization of Red Maple strands after hot water extraction. *Wood and Fiber Science*, 41 (2009) 38–50.

– C. Howell, A.-C. Hastrup, B. Goodell, and J. Jellison. The use of X-ray diffraction for analyzing biomodification of crystalline cellulose by wood decay fungi. *International Research Group on Wood Protection Series*, (2007) IRG/WP 07-10622.

Works published as a bachelors student:

– C. Howell and J. Jellison. Biological variability in the oxalate/oxalate decarboxylase system among five isolates of the wood-degrading fungus *Meruliporia incrassata*. *International Research Group on Wood Protection Series*, (2006) IRG/WP 06-10573.

– C. Howell, L. Gott, and B. Meehan. Fun with soil block jars: teaching fungal wood decay in the classroom. *International Research Group on Wood Protection Series*, (2006) IRG/WP 06-10574.

– J. Jellison,C. Howell B. Goodell and S. Quarles. Investigations into the biology of *Meruliporia incrassata*. *International Research Group on Wood Protection Series*, (2004) IRG/WP 04-10508.

Acknowledgements

This work was performed at the Institute of Applied Physical Chemistry (APC) at the University of Heidelberg and at the Institute of Toxicology and Genetics (ITG) at the Karlsruhe Institute of Technology (KIT) Campus North in Eggenstein-Leopoldshafen. It was funded by a US National Science Foundation Graduate Research Fellowship.

I am grateful to all the people without whom this work would not have been possible:

To my advisor Prof. Dr. Michael Grunze. I am appreciative of the invitation to come join the APC, the constant support, the multiple opportunities provided to attend scientific conferences and visit other labs, the enlightening scientific discussions that always left me with more to think about, and finally for the review of this thesis. Many thanks also to Prof. Dr. Markus Motzkus, for agreeing to be the second referee of this work and for taking the time to come by the labs to share ideas and admire lasers.

To Priv.-Doz. Dr. Patrick Koelsch, for being a good group leader whose door was always open and to whom it was always exciting to come with new data and ideas, as well as for introducing me to the field of non-linear optics.

To my lab group: Dominique Verreault, Volker Kurz, Mark-Oliver Diesner, Anna Keese, Christoph Barth, and Markus Niermeyer, for being as fun to do science with as to party with. There is nothing quite so precious in science as a group of friendly, brilliant, like-minded people who are always willing to listen and lend their own knowledge and experience to a problem, and you all were it. I am particularly grateful to Volker for significant amounts of help with running complex SFG experiments, to Mark-Oliver for countless great discussions and for the experimental work on living cells, and to Dominique for his constant selflessness in sharing his knowledge, experience, and time.

To Dr. Dmitri Petrovykh, for being an excellent collaborator as well as an endlessly patient mentor always ready and willing to provide an eye-opening point of view, a clever solution, or a much-needed reality check. Without his collaborative projects I would have a lot fewer interesting things to do and without his willingness to listen and provide advice these last three years I probably would be a lot less sane.

To Dr. Michael Bruns and his group at the Institute of Material Research III: Dipl.-Ing. Vanessa Trouillet, Dip.-Ing. Florian Stemme, Vanessa Hermann and Udo Geckle, as well as Stefan Heissler at the Institute of Functional Interfaces at KIT, for help with wafer preparation and sample characterization, instrumental physics and theory lessons, interesting conversations (scientific and general), as well as *in situ* German lessons.

To Prof. (apl.) Dr. Michael Zharnikov for providing multiple opportunities for interesting and extremely efficient collaborative work, as well as for performing the synchrotron experiments and analyzing the resulting data. To my other collaborators over the years: Prof. Dr. Wolfgang Wenzel, Robert Maul, Hicham Hamoudi, Jianli Zhao,

Evgeniya Lock, Kenan Fears, Sabine Oberhansl, Asutosh Chilkoti, Vinalia Tjong, for providing the opportunity to share knowledge, experience, viewpoints, and ideas.

To my Spanish family: María de la Luz and Alvaro, as well as Eduardo, Ernesto and María Ángeles for welcoming me into their family, introducing me to their culture, being so patient with my attempts to speak Spanish, and for making me feel at home so far away from home.

To my mother Cindy for all the phone calls, care packages, and editorial help as well as all the visits and exciting European adventures we shared. To my parents Nicky and Frank for their unconditional love, support, and cheerleading that spanned two continents, as well as for always providing a happy home to come back to. To my sisters Ali and Julie and my brother Justin, for being my lifelines back home and for seamlessly rolling me back into the fray upon my annual return.

And finally to Adrián, whose emotional support, culinary prowess, sense of adventure, and love provided the motivation to finish this work. This is for you.

Summary

***In situ* investigations of biological molecules using vibrational sum-frequency-generation spectroscopy**

The molecular-level understanding of biological molecules on solid surfaces is critical in areas including medicine, biologically-based industry, and the development of biotechnologies. In order to gain further knowledge of the orientation and organization of biological molecules adsorbed on surfaces, we used the label-free, interface-specific technique of sum-frequency generation (SFG) spectroscopy. This technique has the distinct advantage of being able to be operated *in situ* as well as *ex situ*, allowing for direct comparison of changes in biological molecules between these two states. Films of surface-bound single-stranded DNA (ssDNA) on gold were chosen as model biological systems due to their numerous applications in genetic profiling, nano-assembly, and bio-computing, as well as their relative simplicity as biomolecular layers. Sensitivity and proof-of-principle tests on simple surface-bound, short alkane chains demonstrated the ability of SFG spectroscopy to detect molecular concentrations low enough to be useful in the investigation of biological molecules and to accurately detect the interactions of water with model hydrophobic and hydrophilic self-assembled monolayers. Investigations of multilayers of thymine, adenine, and cytosine nucleobases alone revealed a high degree of order in the thymine layers, with the signals from the methyl group unique to this base clearly visible. Films of both thiolated and non-thiolated surface-bound DNA in air showed little and moderate orientation, respectively, with the methylene stretches of the sugar-phosphate backbone dominating the spectra. Comparison of the changes in signal intensity among thymine, adenine, and cytosine ssDNA films in air and in H_2O revealed differences in their solubility, which agreed with current *ex situ* knowledge of the manner in which these differing DNA types adsorb on gold surfaces. These experiments also revealed the appearance of nucleobase-specific spectra upon exposure to water, which was tied to the higher mobility of the sugar-phosphate backbone under these conditions. Investigations of hybridized ssDNA films in air using SFG spectroscopy indicated that the hybridization process in surface-bound DNA molecules does not necessarily correspond with an increase in molecular order, as is known to happen with DNA molecules in solution, and furthermore that even gentle processing of such hybridized samples for *ex situ* analysis can significantly disrupt the hybrid structure. These results were confirmed using near-edge absorbtion fine structure spectroscopy. Finally, the results obtained from the model DNA films were applied to a more complex biomolecule, fibronectin, on gold surfaces. Experiments showed that SFG spectroscopy could detect a fibronectin film even under a layer of fixed cells. Further tests on living cells over alkanethiol self-assembled monolayers confirmed this observation. These results give new information on the orientation and organization of DNA films on solid surfaces both *in* and *ex situ*, and show how this knowledge can be applied to more complex biological systems. Furthermore, this work contributes to a knowledge base for the application of SFG spectroscopy to future questions in which the label-free, *in situ* knowledge of surface-bound biological molecules is of critical importance.

Kurzfassung

***In situ* Untersuchung von biologisch relevanten Molekülen mit Summenfrequenzerzeugungs-Spektroskopie**

Das Verständnis von Biomolekülen auf dem molekularen Niveau auf Oberflächen ist insbesondere in der Medizin, der biologischen Industrie und bei der Entwicklung von Biotechnologien essentiell. Die markerfreie und grenzflächenspezifische Summenfrequenzgeneration (SFG) Spektroskopie wurde angewandt um Orientierung und Konformation von Biomolekülen auf Oberflächen zu bestimmen. Diese Methode kann sowohl *in situ* als auch *ex situ* verwendet werden. Veränderungen der Biomoleküle zwischen beiden Zuständen werden sichtbar. Auf Gold gebunden Einzelstrang DNA (single-stranded DNA: ssDNA) wurde aufgrund der zahlreiche Anwendungen bei genetischem profiling, Biocomputing und in der Nanotechnologie als biologisches Modellsystem gewählt. Anhand von Messungen an selbstorganisierten Monoschichten, bestehend aus einem unterschiedlichen Verhältnis von deuterierten und undeuterierten Alkanthiolen auf Goldoberflächen, konnte gezeigt werden, dass bei der SFG Spektroskopie geringe Oberflächendichten, wie sie bei der Untersuchung von Biomolekülen vorkommen, ein hinreichendes Signal-Rausch-Verhältnis ergeben. Gleichermaßen wurden die Wechselwirkungen von Wasser mit hydrophoben und hydrophilen selbstaggregierenden Monolagen bestimmt. Messungen an Multilagen von Thymin, Adenin und Cytosin Basen ergeben einen hochgeordneten Zustand der Thyminschicht, der sich von einem starken Signal der basespecifischen Methylgruppe ableitet. Immobilizierung der ssDNA mittles Thiollinken resultierte in einem höhrer Ordgung im Vergleich zu nichttiolierten DNA, dabei dominierten die Methylenstreckschwingungen des Zuckers das Spektrum. Vergleich der Veränderungen des Signals von Thymin, Adenin und Cytosin ssDNA in Luft und Wasser legten Unterschiede in ihrer Löslichkeit dar, welche mit dem aus der Literatur bekannten *ex situ* Adsorbtionsverhalten der verschiedenen Nukleobasen auf Goldoberflächen korrelieren. Darüber hinaus zeigten die Spektren in wässriger Lösung nukleobasenspezifische Banden, welche sich durch eine erhöhte Mobilität des Zuckerrückgrats erklären lassen. SFG Spektren von hybridisierten ssDNA Filmen in Luft deuten an, dass der Hybridisierungsprozess von oberflächengebundenen ssDNA Molekülen nicht notwendigerweise mit einem Anstieg der molekularen Ordnung korreliert. Dieser Zusammenhang ist anders als es für DNA in Lösung bekannt ist. Ebenso kann selbst bei vorsichtigem Umgang von derartig Proben für die *ex situ* Untersuchung eine signifikante Störung in der hybridisierten Struktur entstehen. Diese Ergebnisse wurden mit Röntgen-Nahkanten-Absorptions-Spektroskopie (NEXAFS) bestätigt. Schließlich wurden die zuvor gewonnen Ergebnisse aus den DNA Studien auf das komplexere Biomolekül Fibronection angewandt. Die Experimente zeigten, dass SFG Spektroskopie die Fibronektionfilme selbst durch eine Schicht von fixierten Zellen hindurch detektieren kann. All diese neuen Erkenntnisse über die Orientierung und Organisation von DNA Filmen auf festen Oberflächen bilden die Grundlage für die weiterführende Anwendung der SFG Spektroskopie, bei denen markerfreie und oberflächengebundene Biomoleküle von großer Bedeutung sind.

Table of Contents

List of Figures

List of Tables

Chapter 1

Introduction

1.1 Biomolecules on Surfaces

Nature makes extensive use of surfaces in order to control biological reactions. Interfaces such as the cell surface/extracellular matrix (ECM), cell surface/protein, and ECM/protein are, in fact, where most biological reactions occur [1, 2]. In our effort to control and adapt biological mechanisms and processes to our own particular needs, surface science offers many unique advantages.

First, employing surface functionalization techniques adapted from chemistry allows for the fabrication of substrates for biological reactions that can be tailored to specifications such as hydrophobicity, charge, or the presence of a particular functional group, thus enhancing (or, in some cases, diminishing) the reaction in question. This advantage has been used to prevent protein adsorption [3, 4], create simple biomolecular computers [5, 6], and control cell behavior [7, 8]. Second, the use of particular surfaces can provide a measure to control the orientation and ordering of adsorbed molecules, which can further facilitate their biological reactivity or interaction with biological systems. This approach is currently being used in the developing field of tissue engineering, where for example surfaces functionalized with the temperature-switchable polymer poly(N-isopropylacrylamide)serve as a growth substrate for cells. The cells can be grown to a confluent state on such surfaces, then removed as an intact sheet by changing the temperature and inducing a conformational change in the polymer beneath [9, 10].

Finally, as immobilizing biomolecules generally involves fixing many molecules to a confined space it becomes possible to localize in 2D space a biological reaction that would perhaps in nature only occur in small amount spread out over a large and undefined 3D area. This strategy is being used commercially in the case of protein [11, 12], antibody [12, 13], and DNA [14, 15] arrays, where the immobilization of a large number of molecules together makes it possible to easily visualize the fluorescent signal when labeled target molecules are introduced to the system and binds.

In addition, the unwanted adsorption of biomolecules on surfaces is a major issue in a number of areas. In global shipping and other marine industries, biofouling by *Ulva* spores and other organisms causes significant increases in the costs associated with an increased need for fuel [16, 17], an issue which has been at the heart of a recent research efforts [18, 19, 20]. In the food industry, the formation of biofilms and colonization by bacteria causes problems in the diary, meat, and even grain industries [21, 17]. In medicine, the buildup of proteins on an implant surface can trigger an inflammatory response and the formation of fibrotic capsules around the device, resulting in implant failure and possibly serious complications [17, 22]. A more complete understanding of how biomolecules bind to surfaces and how they behave once attached may also contribute to new technologies which are able to prevent adsorption in these situations.

Biomolecules which are intentionally immobilized on solid substrates generally fall into one of five categories: proteins (including amino acids, polypeptides, and multi-protein aggregates), lipids, saccharides, nucleotides (including DNA and RNA), or composite molecules consisting of a combination of two or more molecules from the previously listed categories [1]. Yet

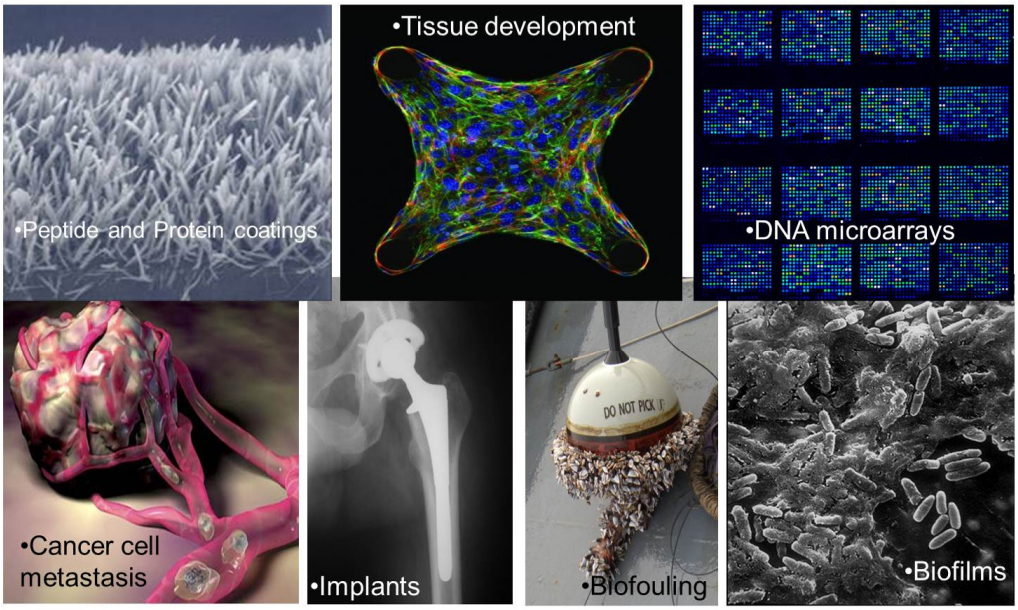

Figure 1.1: Examples of areas in which biomolecule-surface interactions play an important role. All images used are copyright-free and in the public domain.

despite this variety and the examples given above, the field of biointerface science is still relatively new, and a number of limitations still need to be overcome before full realization of the potential of these systems can occur.

Among the most pressing of these is perhaps the ability to understand on the most basic levels what exactly occurs in systems where biomolecules are bound to a solid substrate [1, 2, 23, 24]. Biomolecules tend to be quite complex, and can give complex results in experiments. Of the molecules listed above, DNA and RNA are some of the most simple. Furthermore, they offer unique advantages due to their relative simplicity, versatility, and specific hybridization properties. Thus these molecules offer a good starting point for a bottom-up approach to the further understanding of biomolecules at interfaces.

1.2 DNA and Biotechnology

1.2.1 Applications

DNA (Deoxyriobnucleic acid) holds great promise as the basis for new nano-scale biotechnologies due to its unique recognition and coupling abilities [25, 26]. In recent years it has become possible to order DNA sequences of any arbitrary sequence and of almost any length desired. This technological advance has had significant effects on DNA biotechnology.

In solution, the exploitation of the sequence-specific recognition of DNA has resulted in the creation of 3D scaffolds on which proteins can be immobilized in order to either position them more effectively for use in enzyme and other reactions, or as a means to crystallize them for structure determination using X-ray crystallography [25]. Relatively recently, P. Rothemund demonstrated that DNA can be synthesized to fold into almost any arbitrary shape [27]. These

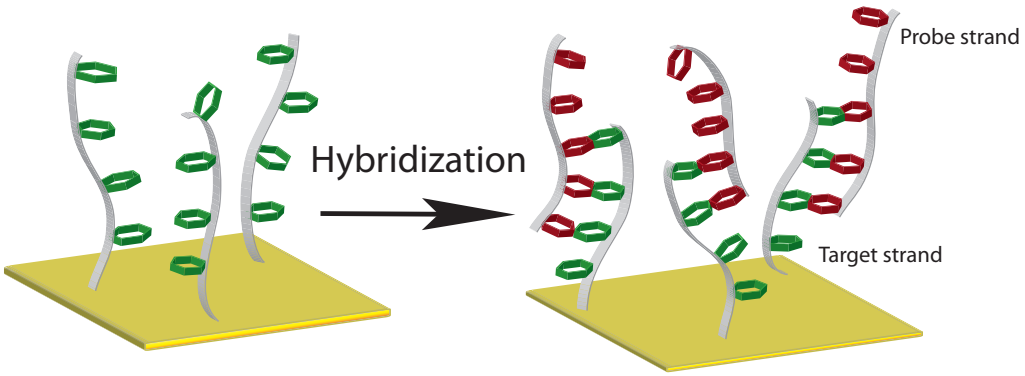

Figure 1.2: Cartoon of hybridization in a surface-immobilized DNA film. The target molecules are immobilized on the surface, and the probe molecules are introduced and bind to the surface-bound moities.

technologies are based on the concept of a DNA "sticky end": a trailing DNA edge of a particular sequence that will only bind with its compliment. Through a well-considered choice of the sequence of this end, its placement and thus the resulting shape of the overall DNA strand to which it is attached, can be determined.

Surface-bound DNA has also begun to be more heavily used in biotechnological applications. Previously, the attachment of these molecules to a solid surface was done primarily in the form of DNA microarray fabrication. DNA microarrays are detection tools which take advantage of the specific binding properties of DNA and RNA. They are currently used in applications such as measuring expression levels, assessing genetic variability, and disease profiling [28]. DNA microarrays are created by attaching thousands of single strands of DNA of a known sequence to a surface. When single stranded DNA (ssDNA) of an unknown sequence is passed over the microarray, complimentary strands will bind (Fig. 1.2) and activate a fluorophore which can be visually detected and quantified (Fig. 1.7) allowing for the processing of thousands of genetic tests simultaneously [15, 14]. This useful technology continues to be heavily used in biological applications, even as other uses for surface-bound DNA are being developed.

Mirkin and colleagues [29, 30] applied the "sticky end" concept to DNA strands immobilized on gold nanoparticles. They showed that through this method they could control the aggregation of the nanoparticles by controlling the length of the sequences used to decorate the surface. The use of DNA-decorated nanoparticles for diagnostic purposes is currently a field of active research [31].

Other fascinating developments in the field of DNA biotechnology have been the advent of DNA computing and the use of DNA for the direction of cell settlement. DNA computing was first demonstrated by Adleman, who used DNA in solution to solve a seven-point Hamiltonian path problem [32]. Since then, this field has evolved to include using DNA immobilized on surfaces [5]. Using DNA patterning to control where cells settle on a surface requires attaching a DNA strand with a "sticky end" to the membrane of a living cell. This was achieved by Francis and colleagues [33], who then proceeded to arrange these cells in a precise way using DNA microarrays functionalized with the compliment strands [8, 7].

Further interesting properties unique to DNA molecules are also being discovered and exploited. For example, research into the properties of the various DNA nucleobases has shown that adenine and adenine-containing DNA strands have a relatively high preference for gold and will adhere to it relatively strongly [34], even to the point of out-competing DNA sequences of cytosine, guanine, and thymine, in that order [35]. Thymine in particular has shown to have only a very weak affinity for gold [36]. Using this knowledge, Opdahl and co-workers [37] designed DNA strands which consisted of a block of adenine followed by a block of thymine (called block

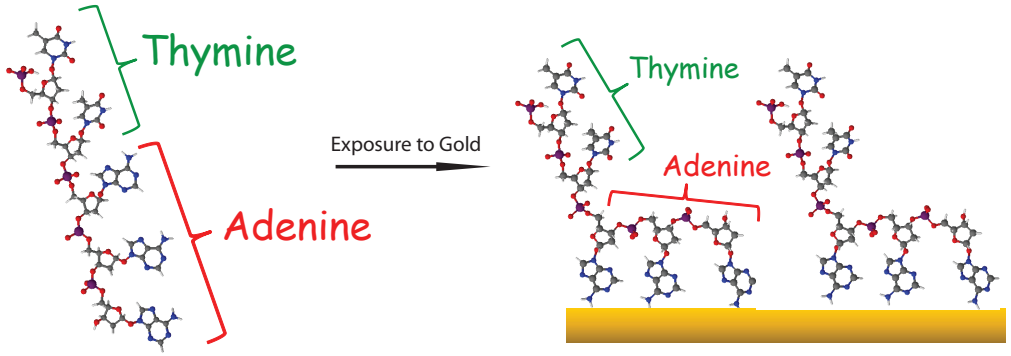

Figure 1.3: Graphic example of an block-oligonucleotide with 2 thymine and 3 adenine subunits. The molecule bends into an L-shape with the adenine adsorbed to the substrate and the thymine extending away from the surface upon exposure to gold.

or di-block oligonucleotides). They demonstrated that these special strands would adsorb on a gold surface in an L-shaped conformation, with the adenine block adhered to the surface and the thymine block extending away into the ambient (Fig. 1.3). This had the effect of significantly lowering the cost of DNA needed to make arrays, as these block-oligonucleotides did not need to be functionalized in order to adhere to a substrate. This method also allows for a certain degree of control over the density of the DNA in the film, a parameter which is of critical importance in hybridization efficiency [38, 39, 40], through the shortening or lengthening of the adenine block.

1.2.2 DNA Structure

DNA is composed of repeating nucleotide units consisting of of a phosphoralated β-D-2'-deoxyribose sugar attached to one of four different types of nucleobase (monocyclic pyrimidines thymine or cytosine, or bicyclic purines adenine or guanine) via a β-glycosyl $C_{1'}$-N linkage [41] (Fig. 1.4). The nucleotide units making up the DNA strand are referred to as thymidine, adenosine, cytidine, and guanosine, and are abbreviated (dT), (dA), (dC), and (dG), respectively. In the case of the synthetic DNA primarily used in this work, in which the entire strand consists of only one type of base, the total number of nucleotide units is generally given as a subscript after the chain abbreviation, e.g. $(dT)_{25}$. Futhermore, when modifications such as the addition of a thiol group are present in the DNA molecule, they are denoted by the chemical symbol after, e.g. $(dT)_{25}$-S.

A DNA nucleotide can twist itself in a number of ways. A list of the possible angles in which torsion can occur (Fig. 1.5) and the atoms which create these angles are listed in Table 1.6. Of the angles listed, α, β, γ, ϵ, ζ, which describe the rotation around the backbone, and χ, which describes the rotation of the base relative to the furanose sugar, would be expected to contribute most significantly. The other angles listed (δ, v_0-v_4) primarily describe potential areas of twist within the 5-member ring, which is expected to be more constrained. However, it is known that this ring is generally non-planar, with the atoms transitioning between an arrangement in either a twist with two atoms displaced on opposite sides of a plane or an envelope with one of the atoms in a different plane than the other four [41].

The plane of the nucleobase is generally approximately normal to the plane of the sugar. The torsion angle describing the rotation of the nucleobase around the sugar, χ, can be described as either *syn* or *anti*. In *syn*, the six-member ring in purines or the O_2 group in pyrimidines are positioned over the sugar, while in *anti* they are pointing away [41]. The angle γ relates the position of the $O_{5'}$ atom relative to the line of the $C_{3'}$ and $C_{4'}$ atoms in the sugar, and can be used to describe the rotation of the phosphate group relative to the sugar moiety. This angle can rotate 360°, and so is most often described using three terms: +sc or gauche-gauche, in which γ is less than 90°, ap or gauche-trans, in which γ is between 90° and 180°, and -sc or trans-gauche, in which

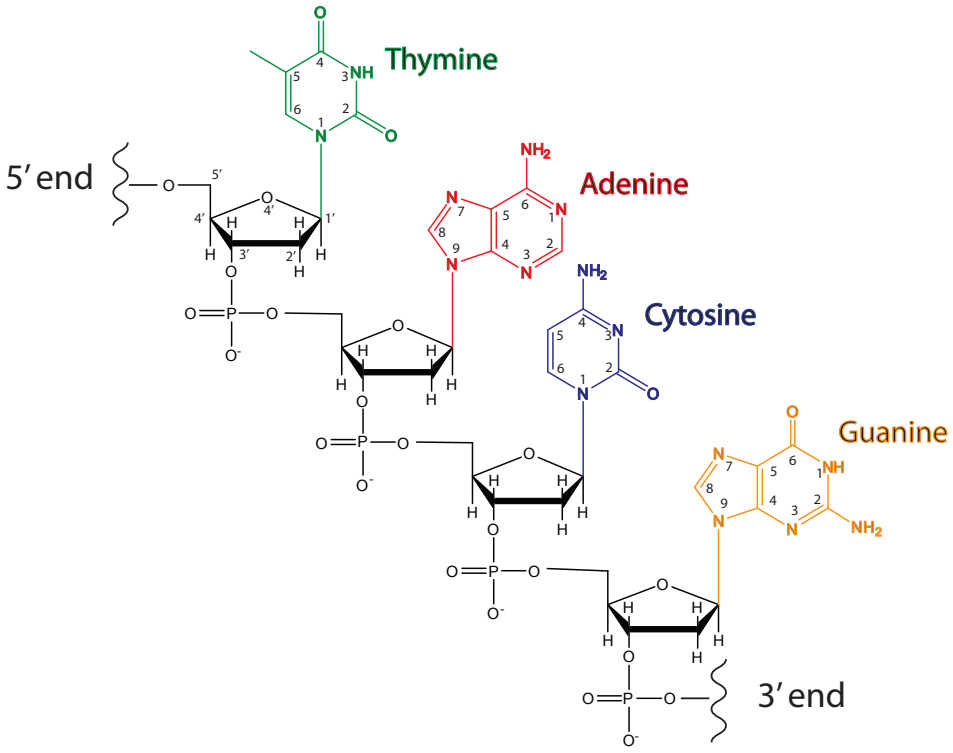

Figure 1.4: Chemical structure of a single DNA strand with a thymine, an adenine, a cytosine, and a guanine nucleobase. The atom numbers for each base are shown. The color scheme for the various nucleobases in this figure are used throughout the rest of this work.

γ is greater than 180° [41]. Previous studies have shown that some oligonucleotides in solution can stabilize via hydrogen bonding between the backbone and nucleobase in conformation in which χ is in the anti position and γ in the +sc position [42].

When adhered in an upright conformation on a surface, a single nucleotide in a DNA strand is generally assumed to take up approximately 0.34 nm vertically and approximately 1 nm laterally [43, 41]. Nucleobases in solution, in the solid state, and immobilized on surfaces have been shown to stack [41, 44], giving rise to stable, single-stranded helices, with purine-purine stacks being the most stable and pyrimidine-pyrimidine stacks the least [41]. These stacks are dynamic in solution and can transition back and forth between a stacked and unstacked state. The stabilization of these stacks is mainly through permanent dipoles in the C=O or C-NH_2 groups of the nucleobases which superimpose over the π-electronic systems of the adjacent bases [41].

Given the high number of ways in which a single strand of DNA can bend, it is convenient to discuss its flexibility in terms of persistence length. Persistence length in polymers is a measure of rigidity, and is defined as the length before the molecule begins to bend away from its original direction at any given point. Reports on short (100-200 base pairs, bp) double-stranded DNA (dsDNA) adsorbed in mica have reported persistence lengths of 80 nm. Persistence length can also depend on nucleobase composition, temperature, and ionic strength of the environment of the DNA strands. Mills *et al.* measured persistence lengths of 0.31 nm and 0.78 nm for 100-200bp (dT) and (dA) homo-oligonucleotides, respectively, measured at 4°C. They attributed this difference to an improved base-stacking of adenine at these temperatures [45]. Tinland and co-workers found that the persistence length for single-stranded DNA (ssDNA) in solution appeared to increase almost exponentially with a decreasing solution ionic strength [46]. For a 3000 bp sequence at room temperature, they measured a persistence length of approximately 8 nm at 0 M salt concentration. A more recent study done by Murphy and colleagues using fluorescence spectroscopy systematically investigated the persistence length of short-chain (dT) (between 10

Angle	Atoms which form Angle
α	$O_{3'}$-P-$O_{5'}$-$C_{5'}$
β	P-$O_{5'}$-$C_{5'}$-$C_{4'}$
γ	$O_{5'}$-$C_{5'}$-$C_{4'}$-$C_{3'}$
δ	$C_{5'}$-$C_{4'}$-$C_{3'}$-$O_{3'}$
ε	$C_{4'}$-$C_{3'}$-$O_{3'}$-P
ζ	$C_{3'}$-$O_{3'}$-P-$O_{5'}$
χ (A and G)	$O_{4'}$-$C_{1'}$-N_1-C_2
χ (T and C)	$O_{4'}$-$C_{1'}$-N_9-C_4
υ_0	$C_{4'}$-$O_{4'}$-$C_{1'}$-$C_{2'}$
υ_1	$O_{4'}$-$C_{1'}$-$C_{2'}$-$C_{3'}$
υ_2	$C_{1'}$-$C_{2'}$-$C_{3'}$-$C_{4'}$
υ_3	$C_{2'}$-$C_{3'}$-$C_{4'}$-$O_{4'}$
υ_4	$C_{3'}$-$C_{4'}$-$O_{4'}$-$C_{1'}$

Figure 1.5: Torsion angles in nucleotides and the atoms which form them. Adapted from Ref.[41].

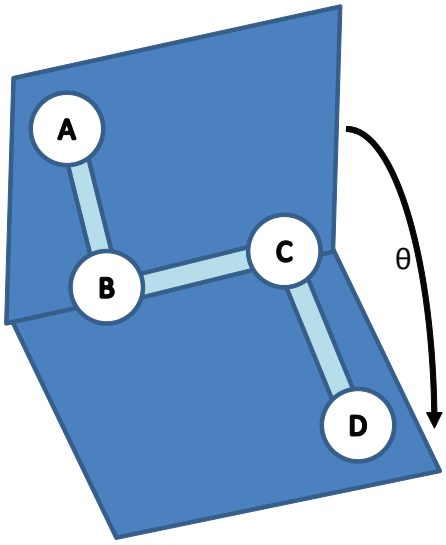

Figure 1.6: Definition of a torsion angle as described in the sketch to the left. The four atoms form three bonds, with the outer two bonds rotating relative to each other through the central bond.

and 70 bp) in solutions of increasing ionic strength reported a persistence length ranging from 1.5 nm in 2 M NaCl to 3 nm in 25 mM NaCl [47]. For ssDNA adsorbed on solid surfaces there is significantly less information available on the persistence length, and a length of 2 nm derived from the solution data is therefore generally used [48, 49].

DNA can be attached to solid surfaces through either covalent attachment using a gold-thiol interaction or a silanization procedure, physical adsorption relying on non-covalent interactions such as hydrogen bonding or electrostatic effects, or through the use of other specific molecular interactions such as biotin-streptavidin [50]. As a result, DNA films have been reported on such diverse substrates as gold [51, 52], diamond [53, 54], silicon [55, 56], glass [57], platinum [58] and amorphous carbon [59]. However, of these, the immobilization of ssDNA on gold is frequently used due to the ease of film formation when the ssDNA molecules are modified with a sulfur-terminated short-chain alkanethiol linker. Furthermore, this approach to DNA immobilization has been found to produce more dense and highly ordered films due to the self-assembly effects of thiolated molecules on gold substrates.

Assuming a cylindrical geometry with a 1 nm cross section, the theoretical upper density limit for a film of tightly-packed, vertically-oriented DNA strands on a solid surface is approximately $1\text{x}10^{14}$ molecules/cm^2. However, achievement of such high densities is nearly impossible due to such things as the relatively high electronegativity of the sugar-phosphate backbone [41]. For this reason, very high salt solutions are necessary when fabricating dense ssDNA films. Petrovykh *et al.* further showed that the cation valence has a significant effect on immobilization density, with buffers made with divalent cations producing significantly denser films [60]. Molecular re-organization also plays a role, as ssDNA molecules tend to initially adsorb flat on the surface, requiring time to re-arrange themselves into a more upright conformation in order to permit the adsorption of further molecules [60].

In the producing of dense ssDNA films, nucleobase composition also plays an important role. Experiments by Kimura-Suda and co-workers showed that adenine ssDNA would outcompete guanine, cytosine, and thymine ssDNA for adsorption sites on a gold substrate [35]. In further work examining the nucleobase composition on immobilization of thiolated versus non-thiolated ssDNA, Gorgiadis and co-workers observed that nucleobases with higher affinities

for gold, such as poly(dA), tended to adsorb to the surface initially by both the thiol and the nucleobases and remain in that conformation, hindering the further adsorption of other poly(dA) molecules and resulting in overall lower ultimate densities. Conversely, DNA strands composed of less strongly-binding bases, such as poly(dT), tended to adsorb most strongly through the thiol bond, ultimately leading to the formation of more densely-packed films [52].

The usefulness of ssDNA adsorbed on solid surfaces comes from its ability to be hybridized. DNA hybridization occurs when cytosine bases hydrogen bond to guanine bases, and adenine bases hydrogen bond to either thymine (in DNA) or uracil (in RNA). In solution the hybrids may adopt a number of forms, the most common of which are A-DNA with 11 nucleotides per turn and an axial rise of 2.56 , or B-DNA, with 10 nucleotides per turn and an axial rise of 3.3 to 3.4 [41]. It is known that hybridization causes the DNA molecules to become stiffer and more highly ordered, with a persistence length of around 45 nm [61, 46]. Hybridization in films of surface-bound oligonucleotides is less well understood and has been an area of active research for the past two decades. During this time it has been found that the efficient functioning of these systems is highly dependent on a variety of parameters including density [62], location of the nucleation site [63], length of the surface-bound DNA strands (targets) and incoming hybridizing strands (probes) [63], target orientation [64], and degree of target mismatch [65]. Of these, packing density and molecular orientation of the surface-bound strands are probably the most important factors [38, 39, 40].

1.2.3 Characterization Techniques

In order to gain more sophisticated and detailed knowledge of systems such as DNA at interfaces one needs efficient experimental tools which not only give specific information about the composition of the molecules at the surface, but also their orientation and relationship to the molecules and environment surrounding them.

Over the years there has been a significant amount of research energy dedicated to finding ways to answer these questions, involving many different techniques [1, 2]. The challenge still remains, though, to develop techniques with high sensitivity and resolution that can be operated *in situ* and provide information in real time on ordering and orientation as well as composition and structure. This list of desired properties is long enough that no single technique can fulfill all of them, but there are several promising candidates that are currently in the process of being refined or developed.

1.2.3.1 *In Situ* Techniques

Formation, hybridization, and interaction of DNA films with different environments can be monitored by a number of *in situ* techniques. Of these, fluorescence imaging is probably the most common [66, 67, 15, 68, 47], making use of fluorescent markers to track the formation of hybrids and even DNA conformation [47]. Radiometric labeling can also be used to detect both probe density and hybridization efficiency [38, 69].

Label-free methods are currently favored in the scientific community due to the lack of complications or artifacts stemming from the use of labels. One of the most popular methods is surface plasmon resonance (SPR) spectroscopy and imaging [70, 71, 72, 73, 39, 74], which uses light to excite plasmons which can then be detected. The plasmon is very sensitive to optical changes at the metal/liquid interface and can thus be used to detect adsorption or desorption of molecules to the surface. Similarly, quartz crystal microbalance with dissipation can be used to measure DNA attachment to surfaces [75, 76], although this process becomes difficult in the high salt concentrations needed for high density film formation. Electrochemical procedures such as cyclic voltammetry and chronocoulometry have also been used to infer adsorption of DNA molecules onto electrode surfaces [77]. *In situ* ellipsometry can also be used to gather information about the thickness of DNA films through a layer of solution [2, 1, 78]. Electrochemical *in situ* scanning-tunneling microscopy [79] and atomic force microscopy [80] have also been used to visualize DNA molecules immobilized on solid surfaces.

However, it can often be difficult to deduce specific, molecular-level information from these techniques, especially in terms of the orientation of particular parts of the molecule. For such

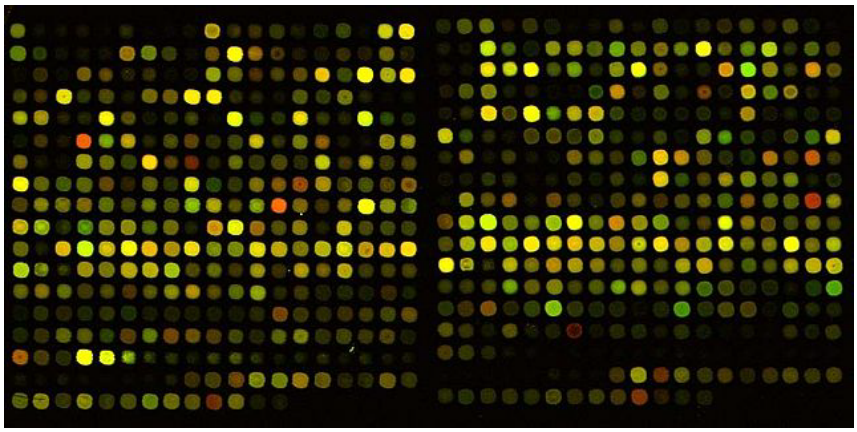

Figure 1.7: An example of the use of fluorescence in detecting DNA immobilized on surface: a DNA microarray showing a fluorescent signal at the sites of hybridization.

information, researchers generally turn to more specific *ex situ* techniques.

1.2.3.2 *Ex Situ* Techniques

Ex situ molecular spectroscopy generally does not require any labeling and probes individual functional moieties and structural motifs within the DNA molecules. A number of vacuum-based techniques have been employed to investigate thin films of DNA on solid surfaces, including X-ray photoelectron spectroscopy (XPS or ESCA), near edge x-ray absorption fine structure (NEXAFS) spectroscopy , and time-of flight secondary ions mass spectrometry (ToF-SIMS). XPS can be used to quantitatively determine the elemental composition and chemical state of a sample by measuring the kinetic energy of electrons ejected from the sample after irradiation with an x-ray beam. It has been used to examine the changes occurring upon the adsorption of DNA to a surface, particularly in the N 1s peak [64, 81, 39, 82]. In 2003 and 2004, Petrovykh and colleagues devised a way to calculate the density of DNA molecules on gold surfaces using the attenuation of the gold signal and the atomic percent of nitrogen calculated from the XPS spectra [60, 51]. Since then, XPS has proven valuable as a quality control measure for DNA films [44, 74, 40, 83, 84, 37].

NEXAFS spectroscopy samples the electronic structure of the unoccupied molecular orbitals to provide information about the chemical identity of a thin film. A further benefit of this technique is that information about orientational order in the system can be obtained by examining the difference between spectra obtained using different angles of incidence for the incoming x-ray beam [63]. This technique has been used to examine the overall orientation of the nucleobases in films of ssDNA [44, 39, 85, 83]. Examining the orientation of thiol-modified DNA strands versus unmodified strands, Lee *et al.* concluded that the thiolated strands were oriented upright with the nucleobases stacked parallel to the surface, while the unthiolated strands were lying down on the surface with the nucleobases adsorbed in a more or less perpendicular orientation [39]. Petrovykh *et al.* compared thymine ssDNA with long ($[dT]_{25}$) and short ($[dT]_5$) chain lengths. They found that the short-chain DNA had a higher degree of overall order than the long-chain, which they attributed to the increased flexibility of the longer strands [44].

ToF-SIMS relies on the analysis of secondary ions ejected from the surface of a film after sputtering with a focused primary ion beam, and can give information on the composition of a film as well as, in some situations, orientation. Lee and co-workers used ToF-SIMS to examine the effects of impurities on the formation of thiolated ssDNA films, detecting an excess of sulfur used as a reducing agent in the molecule preparation process which apparently had a strong tendency to remain in the final film [86]. Other work has presented this technique as a way to verify the immobilization of DNA onto surfaces functionalized with other polymers such as ethylene glycol

[87]. Other applications for this technique include DNA sequencing [88] and imaging [89].

Vibrational spectroscopic analysis of solid/liquid interfaces and thin films *in situ* holds great potential for answering some of the most crucial questions in the fields of environmental, biomedical, and materials sciences [1, 2, 23, 24], in part due to the fact that it can be operated under ambient conditions. Of these techniques currently applied to DNA, Fourier-transform infrared (FTIR) spectroscopy is one of the most convenient. Probing the absorption of infrared light by molecules over a range of 400-4000 cm^{-1}, FTIR gives distinct signatures from the four nucleobases in the amide I region [81] due to the distinct structures of these bases. This has made it useful for determining the composition of a surface-adsorbed DNA film after competition experiments between different types of homo-oligonucleotides [35], as well as determining the orientation of (dT) films by examining the intensities of peaks attributed to chemisorbed C=O versus non-chemisorbed C=O [44, 37].

Raman spectroscopy, which examines changes in the inelastic scattering of laser light unique to particular molecules, can also be used to detect DNA on surfaces. Like FTIR spectroscopy, Raman spectroscopy on DNA samples gives unique peaks, primarily in the amide I region, which are related to the composition of the nucleobases [90]. Although for the most common forms of Raman spectroscopy rather large quantities of DNA are needed in order to generate a signal, making analysis of thin films of DNA using the setups most commonly available not possible. This can be overcome, however, by using surface enhanced Raman spectroscopy [91, 92], which makes use of rough metal surfaces to increase the Raman signal. One particular benefit of this approach is that it can be used both *in situ* and *ex situ* [91]. However, the use of a rough metal surface compromises the formation of a well-ordered films made through self-assembly mechanisms [93]. Recently tip-enhanced Raman spectroscopy has been proposed as a way to overcome these limitaitions [94].

Most of methods offer a substantial understanding of the chemical composition, surface density, orientation and ordering of DNA films under non-aqueous conditions. However, the ability to characterize ssDNA films in aqueous environment is important because it allows for the examination of these films *in situ* - the conditions under which they are actually used. Furthermore, the ability to compare results obtained *in situ* and *ex situ* can provide a way to determine whether the results obtained in air or under vacuum conditions are applicable in aqueous environments. SERS can be operated *in situ*, however it requires the use of rough metal surfaces which may disrupt the natural organization of the DNA molecules in a film. In order to overcome this limitation and still retain the ability to compare *in situ* and *ex situ* states in DNA films, the technique of sum-frequency-generation (SFG) spectroscopy can be used.

1.3 SFG Spectroscopy

The technique of sum-frequency-generation (SFG) spectroscopy relies on the frequency mixing that when two pulsed laser beams achieve temporal and spacial overlap at an interface. The light emitted at the sum of the two incident frequencies can be resonantly enhanced when the frequency of one of the incoming beams matches a resonant frequency of vibrational modes of the molecules located at the interface [95]. SFG spectroscopy has emerged as a tool well-suited to the investigation of liquid/solid interfaces, due to the surface sensitivity arising from the particular selection rules of this technique, a molecular-level detection capability, and the ability to function under ambient conditions [96, 97, 98, 99]. Furthermore, this technique offers the potential for probing the same sample in air and in liquid [84, 26, 10], making it possible to bridge the gap between measurements *in situ* and those that need to be performed under ultrahigh vacuum or other non-standard conditions. The selection rules of SFG dictate that a signal can only be generated in a non-centrosymmetric environment, resulting in the suppression of isotropic bulk signal (see Chapter 2). This feature makes SFG spectroscopy inherently surface specific [100] with submonolayer resolution, allowing for the tracking of subtle modifications even in ultra thin films. Being an all optical technique, SFG is also non-invasive and non-destructive, making this technique useful for the characterization DNA films both *in situ* and *ex situ*.

Only a few measurements of ssDNA films by SFG spectroscopy have been reported [26]. Sartenaer *et al.* used SFG spectroscopy to probe thiolated ssDNA immobilized on platinum in

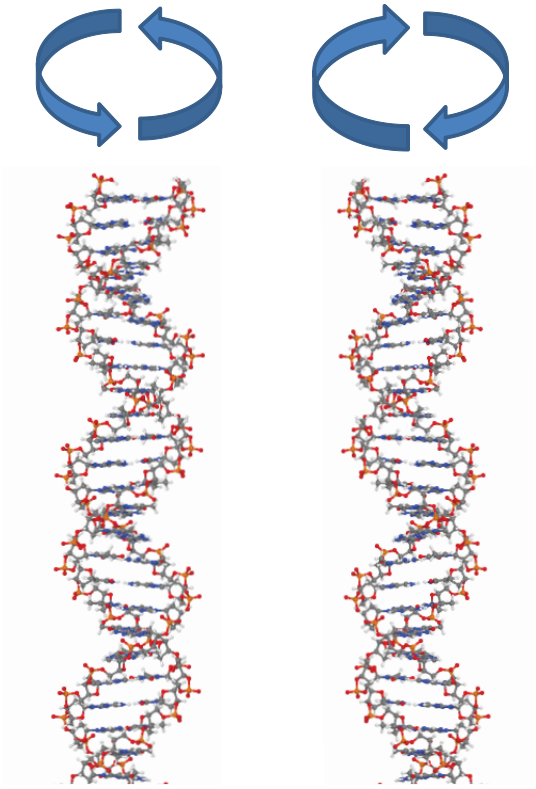

Figure 1.8: Example of DNA helices with a right-handed twist (left) and a left-handed twist (right) such as the samples investigated by Stokes *et al.* in Ref. [57]

the CH stretching region. They found a strong disordering in the films with the SFG spectra dominated by the linker group anchoring the ssDNA strands to the surface [58]. However, the densities of these films were not quantified and were likely very low, given that sulfur does not have as high an affinity for platinum as it does gold. Furthermore, that the buffer solution used in these experiments was only 10μM, which does not completely electrostatically shield the DNA molecules and causes them to repel each other, decreasing the film density, as discussed in Section 1.2.2.

Asanuma and co-workers used SFG spectroscopy to examine the effects of metal cations of different valencies on the overall order in a ssDNA film on silicon in air. They reported that the divalent cations Mg^{2+} and Ca^{2+} produced a greater degree of disordering than the monovalent cations K^{+} and Na^{+}, which they attributed to a greater affinity of the divalent cations for the highly charged phosphate groups in the backbone of the DNA molecules [101]. Stokes and colleagues used polarization-resolved SFG spectroscopy to examine the handedness of DNA helices immobilized on silica in air. By comparing spectra taken with light polarized $\pm 45^{\circ}$ relative to the plane of incidence. They were able to see differences between dsDNA hybridized to have a right-handed rotation and those hybridized to have a left-handed rotation [57] (Fig. 1.8).

However, despite the potential of SFG to be used to compare DNA films *in situ* and *ex situ*, to date there has only been one report of such an experiment, carried out by our group in 2008 [84]. In that work, (dA) and (dT) films were compared in air, D_2O, and buffer in the CH and amide I regions. A more thorough analysis is needed in order to establish this technique as a viable tool for the examination of DNA and other biological molecules *in situ* and to fully understand how these systems change in different environments.

1.4 Aims of this work

The overarching goal of this work was to obtain molecular-level, label-free information about the organization and orientation of the biological molecules immobilized on a solid surface, especially pertaining to how they change *in situ* and how this knowledge can be further applied to more complex systems. This goal was achieved by using DNA as a model biomolecule and by reaching the following smaller aims:

[i] Gaining label-free, molecular-level information in air about DNA molecules immobilized on solid surfaces using SFG spectroscopy

[ii] Comparing results in air to results *in situ* to obtain an understanding how these films change when exposed to liquid

[iii] Furthering the understanding of the more complex system of hybridized DNA, specifically gathering more information about the level of order in these systems before and after hybridization

[iv] Beginning to apply the knowledge obtained by the relatively simple biomolecular systems of DNA to understanding more complex biological systems such as the extracellular matrix under a layer of cells

These goals were accomplished by first testing the sensitivity of the SFG instrument to confirm that the detection level was low enough for ssDNA films and by testing the accuracy of this technique when comparing model hydrophobic and hydrophilic self-assembled monolayers (Chapter 3). Then, the way in which SFG detects nucleobases alone, unmodified DNA, and modified DNA in air were measured in order to gain a solid understanding of these systems *ex situ* (Chapter 4). Next, thiolated DNA films were measured *in situ* in buffer, D_2O, and extensively in H_2O (Chapter 5). Further tests were then done on hybridized DNA samples in air, using both SFG and NEXAFS to confirm changes seen in ordering (Chapter 6). Finally, more complex systems of cells on surfaces were measured (Chapter 7).

Chapter 2

Materials, Methods, and Instruments

2.1 Film Preparation

2.1.1 Chemical Acquisition and Control Parameters

Alkanethiols used in these experiments were ordered from Sigma-Aldrich Chemie Gmbh (Munich, Germany), while deuterated 1-dodecanethiol for sensitivity determination (98.9% deuteration) was ordered from C/D/N Isotopes (Montreal, Canada). Thymine, adenine, and cytosine powders were also purchased from Sigma-Aldrich.

HPLC-purified custom thymine, adenine, or cytosine homo-oligonucleotides (ssDNA) were purchased from Operon Biotechnologies (Cologne, Germany, VBC Genomics (Vienna, Austria), or Sigma-Aldrich (Taufkirchen, Germany). Oligos modified with a C6 linker and thiol group on the 5′ end ordered from Operon were received with a HS-$(CH)_6$OH protective group attached to the thiol linker, while thiol-modified oligos from Sigma were deprotected with dithiothreitol (DTT) by the vendor prior to shipping, and trace amouunts of these molecules remained present in the final product. All DNA were used as-received with no further purification. It is possible that the trace DTT in the films made with the oligonucleotides purchased from Sigma disrupted the layer formation to some extent, as previous studies have shown that this can be the case [86]. However, examination of these films with XPS showed no significant amounts of excess sulfur in these films, and comparison of the SFG spectra of these films and those made from Operon oligos showed no significant differences between the two, and density calculations remained constant.

Upon receipt, DNA concentrations were verified using a Thermo-Fischer NanoDrop UV-vis spectrophotometer (NanoDrop, somewhere)and separated into aliquots to be frozen until use.

2.1.2 Gold wafer parameters and cleaning procedures

Gold films were fabricated at the in the lab of Dr. M. Bruns using radio frequency magnetron sputtering. Silicon wafers (Si-Mat Silicon Materials, Kaufering, Germany) were covered with a chromium adhesion later, followed by a gold layer to produce a 100 nm-thick polycrystalline gold film. The resulting metal films were polycrystalline, with a predominant (111) orientation. Wafers were cut into appropriate sizes and cleaned either by submersion in warm piranha solution (70% H_2SO_4 / 30% H_2O_2) for 10 minutes or by exposure to UV/ozone (UV cleaner 42-220, Jelight) for 2.5 hrs. All wafers were rinsed thoroughly with HPLC-grade water or ethanol immediately prior to film deposition.

2.1.3 Film Deposition

Alkanethiol SAMs were made by placing the clean gold wafers into 3 mM solutions of the molecules in ethanol and incubating them at room temperature for at least 18 hrs. Samples were then removed from the solutions, rinsed in ethanol, dried under flowing N_2.

Nucleobase multilayers were fabricated according to the procedures outlined by Ostblom *et al.* [102], using 50 μm solutions of adenine, thymine, and cytosine dissolved in pure ethanol. A

drop of the nucleobase solution was placed on the gold wafer and allowed to evaporate, forming the multilayer.

For DNA film formation, gold wafers were placed in 2 mL of 1 M phosphate buffered saline (PBS) solution or 1 M $CaCl_2$ solution with 10mM Tris-HCl and 1mM EDTA[74] ($CaCl_2$-TE) at pH 7.3 and containing 3-5 μM DNA. Samples were incubated at either room temperature or 37° for between 24 and 40 hours. After the incubation, all samples were rinsed with flowing HPLC-grade or Mili-Q water (resistivity > 18.2 mΩ) for 1 min to remove excess buffer salt and dried under flowing nitrogen. Using these procedures, DNA densities of between 7×10^{12} and 7×10^{13} DNA molecules/cm^2 were generally achievable.

Films were hybridized by placing them in 1 M NaCl-TE solution containing 10mM Tris-HCl, 1 mM EDTA, and 3 μM target solution for 6-8 hours at room temperature, followed by rinsing for 1 min with 1 M NaCl and dipping briefly in HPLC water to remove excess buffer salts. The extent of hybridization was generally confirmed using the N 1s signal.

2.2 X-Ray Photoelectron Spectroscopy (XPS)

2.2.1 Instrument Specifications

XPS measurements were performed on one of two instruments in the laboratories of Dr. Michael Bruns of the Institute for Applied Materials at the Karlsruhe Institute of Technology (KIT). The first was an ESCALAB 5 spectrometer equipped with an Alpha 110 hemispherical electron energy analyzer (ThermoFischer Scientific). Measurements on this instrument were performed at pressures of <10^-9 bar using non-monochromatized MgKα radiation. A pass energy of 20eV with an energy resolution of $\approx$ 1 eV was used. The second instrument was a K-Alpha XPS spectrometer (ThermoFisher Scientific, East Grinstead, UK). Data acquisition using the Thermo Avantage software is described elsewhere. All DNA and SAM thin films examined using this instrument were analyzed using a microfocused, monochromated Al Kα X-ray source (400 μm spot size).

All photoelectrons were detected at a take-off angle of 0° relative to the sample surface normal. In addition to survey scans to detect unexpected species, spectra of specific areas were collected in the Au 4f, C 1s, and O1s regions. The N 1s and P 2p regions were monitored for samples containing DNA, and the S 2p region was examined for samples made with thiolated molecules. All spectra were referenced to the C 1s peak at 285.0 eV binding energy and the Au $4f_7/2$ peak assumed to be at 84.0 eV. No charge compensation was needed. The Au reference spectra used to calculate the DNA density of the layers were obtained by sputter-cleaning the films *in situ* using Ar ions.

2.2.2 Data Processing Procedures

The spectra were fitted with one or more Voigt profiles using UNIFITii [103] (BE uncertainty: +0.2eV) and Scofield sensitivity factors were applied for quantification. The number of peaks was chosen according the work published by Petrovykh and co-workers [60]. The peaks were fit simultaneously with the background, which consisted of a combination of Shirley and linear functions.

After fitting the peaks, the surface density of the DNA molecules was determined according to the procedures of Petrovykh *et al.* [51] The thickness t of the DNA film relative to the Ar sputter-cleaned gold was calculated by:

$$t = -\ln\left[\frac{I_{DNA}}{I_{Au}}\right] \times L \tag{2.1}$$

where I_{DNA} is the intensity of the DNA film, I_{Au} the intensity of the sputter-cleaned gold, and L the estimated practical effective attenuation length for electrons in Au with a DNA overlayer [51]. Once the layer thickness had been determined, the relative DNA coverage $\frac{\theta_N}{N_{Au}}$ could be obtained by applying the formula:

$$\frac{\theta_N}{N_{Au}} = \frac{\frac{N_N}{N_{Au}} \times t}{100 - \frac{N_N}{N_{Au}}} \tag{2.2}$$

where $\frac{N_N}{N_{Au}}$ is the atomic density relative to Au. From the relative coverage, the absolute DNA density n_{DNA} expressed in molecules/cm^{2}was determined using the equation:

$$n_{DNA} = \frac{\theta_N}{N_A u} \times \frac{5.892 \times 10^{22}}{10 \times 10^{-7} \times n_N} \tag{2.3}$$

where n_{DNA} is the number of nitrogen atoms per DNA strand in the film. The factor 5.892×10^{22} is the atomic density of gold and 10×10^{-7} accounts for the film thickness expressed in nm [51]. It should be noted that this approach assumes that a minimal amount of signal is stemming from contaminants at the surface. This assumption was further supported by examining the C 1s spectra, which showed a major peak at 285 eV for samples that were heavily contaminated, as opposed to a major peak at 287 eV for samples that were composed primarily of DNA.

2.3 Infrared Reflection-Adsorption Spectroscopy (IRRAS)

2.3.1 Instrumentation

Infrared reflection-adsorption spectroscopy (IRRAS) was performed at the Institute for Functional Interfaces (IFG) at KIT on a Vertex 80 Infrared spectrometer (Bruker Optics, Ettlingen, Germany) using an A518 IRRAS sampling stage with an 80° fixed-angle gracing incidence. The signal was recorded by a D313 narrow-band MCT detector cooled by liquid N_2. Background measurements were performed with 1024 scans, and suppression of the water signal in samples was usually achieved between 1000 and 3000 scans. Baseline correction and data evaluation were performed using the Opus 6.5 IR software package (Bruker Optics).

2.4 Synchrotron Measurements

2.4.1 High-Resolution X-Ray Photoelectron Spectroscopy

The high-resolution x-ray photoelectron spectroscopy (HRXPS) experiments were performed at the D1011 beamline (bending magnet) at the MAX II storage ring of the MAX-lab synchrotron radiation facility in Lund, Sweden, by Prof. (apl.) Dr. Michael Zharnikov and members of his lab group. The spectra were acquired in normal emission geometry at photon energies (PEs) ranging from 350 and 580 eV. The energy resolution was better than 100 meV allowing a clear separation of individual spectral components. The energy width of the individual emissions was close to the intrinsic energy spread of the respective core-level photoemission process. The binding energy (BE) scale of every spectrum was individually calibrated using the Au 4f7/2 emission line of the underlying Au substrate at 83.95 eV [104], which is the value given by the ISO standard. HRXPS spectra were fitted by symmetric Voigt functions and a Shirley-type background. The fits were performed self-consistently: identical fit parameters were used for the same spectral regions.

2.4.2 Near-Edge X-Ray Absorption Fine Structure Spectroscopy

The near-edge x-ray absorption fine structure (NEXAFS) spectroscopic experiments were also performed by Prof. Zharnikov at the same beamline as the HRXPS measurements. The spectra acquisition was carried out both at the carbon and nitrogen K-edges in the partial electron yield mode with retarding voltages of 150 and 300 V, respectively. Linear polarized synchrotron light with a polarization factor of 95 percent was used. The energy resolution was better than 100 meV. The incidence angle of the light was varied from 90˚ (E-vector parallel to the surface plane) to 20˚ (E-vector nearly normal to the surface) in steps of 10˚-20˚ in order to monitor the orientational order of the target molecules within the films.

The raw NEXAFS spectra were normalized to the incident photon flux by division through the spectrum of a clean, freshly sputtered gold sample. Furthermore, the spectra were reduced to the standard form by subtraction of a linear pre-edge background and normalization to the unity edge jump (as determined by a nearly horizontal plateau 40-50 eV above the respective absorption edges). The energy scale was referenced to the most intense π^* resonance of highly oriented pyrolytic graphite (HOPG) at 285.38 eV [105].

2.5 Density Functional Theory

Density Functional Theory (DFT) was performed by Dr. Robert Maul in the group of Prof. Dr. Wolfgang Wenzel at the Institute for Nanotechnology at KIT and were used to provide supplemental information on peak positions for some alkanethiol films. DFT as implemented in the Turbomole simulation package [106] using a localized basis set and effective core potentials to model the electron-ion interaction was used. The Kohn-Sham equation was solved for a given exchange-correlation (XC) functional for the valence electrons, and the well-established PBE-functional was used [107]. To take into account van-der-Waals interactions between alkanethiols and water, the DFT+D approximation [108] was employed incorporating the long-range dispersion contribution to the XC-functional. The vibrational frequencies were calculated in the framework of the frozen-phonon method [109]. Calculations for alkanethiol molecules in H_2O were made using a single molecule of water. Simulations were performed assuming a single molecule in a vacuum and neglecting the presence of a metallic substrate, therefore a deviation between calculated and experimental values of up to 20 cm^{-1} was considered acceptable.

2.6 Sum-Frequency-Generation Spectroscopy (SFG)

2.6.1 Theory

SFG spectroscopy probes vibrations of molecular groups at interfaces through a non-linear response. It is a relatively new technique as it requires the use of reliable high powered lasers which first became available a few decades ago. The first reports of the detection of molecular vibrations via SFG spectroscopy were by Shen [110, 111] and Harris [112] in the late 1980s.

In general, an electric field $\mathbf{E}$ induces a dipole moment μ in atoms or molecules, which can be described by:

$$\mu = \mu_0 + \alpha\mathbf{E} \tag{2.4}$$

in which μ_0 is the permanent dipole of the atoms or molecules and α the polarizability [95]. The sum of the dipole moment per unit volume or bulk polarization $\mathbf{P}$ induced by the $\mathbf{E}$ field is given as:

$$\mathbf{P} = \varepsilon_0\chi^{(1)}\mathbf{E} \tag{2.5}$$

where ε_0 is the vacuum permittivity (8.854 $\times 10^{-12}$ C/V·m) and $\chi^{(1)}$ is the macroscopic average of α, also known as the first-order or linear susceptibility. When the $\mathbf{E}$ field is increased to the point at which it is comparable to the $\mathbf{E}$ field experienced by the electrons in a molecule, as is possible with high-power, coherent laser beams, the polarization can be expressed as a Taylor series:

$$\mathbf{P} = \varepsilon_0(\chi^{(1)}\mathbf{E} + \chi^{(2)}\mathbf{E}^2 + \chi^{(3)}\mathbf{E}^3 + ...) \tag{2.6}$$

In this equation, $\chi^{(2)}$ and $\chi^{(3)}$ are the second- and third-order non-linear susceptibilities, respectively [95]. $\mathbf{P}$ can be expressed as a convolution of its first-, second-, and higher-order components (Fig. 2.1). If two incoming $\mathbf{E}$ fields, $\mathbf{E}_1$ and $\mathbf{E}_2$ oscillating with frequencies of ω_1 and ω_2 are considered, the second-order term of the polarization, $\mathbf{P}^{(2)}$ can be expressed as:

$$\mathbf{P}^{(2)} = \varepsilon_0\chi^{(2)}(\mathbf{E}_1 cos\omega_1 t + \mathbf{E}_2 cos\omega_2 t)^2 \tag{2.7}$$

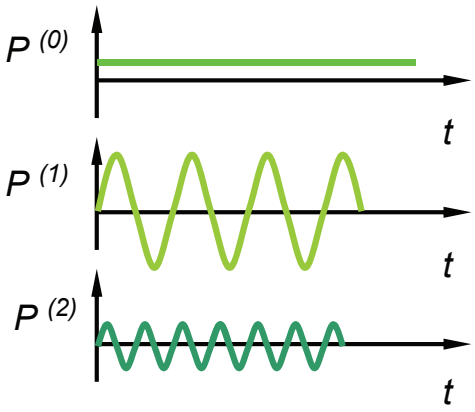

Figure 2.1: Graphic illustration of the oscillations of the first-, second-, and third order polarizability with respect to time

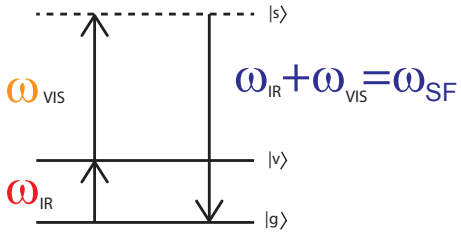

Figure 2.2: Energy levels associated with the generation of an SF signal. $|g\rangle$ represents the ground state, $|v\rangle$ the excited vibrational state, and $|s\rangle$ any other higher state

Equation 2.7 can be expanded to give four terms: one describing a DC field with no frequency dependence (optical rectification), a term in which the frequency of the emitted light is doubled (second harmonic generation), a term in which one frequency is subtracted from the other (difference- frequency generation) and one in which one frequency of the emitted light is added to the other (sum-frequency generation) [95]. In SFG spectroscopy we measure the latter.

When SFG light is measured from a sample on a gold substrate, its intensity can be described as:

$$I_{SFG} \propto \left|\mathbf{P}^{(2)}\right|^2 \propto \left|\chi^{(2)}\right|^2 I_{IR} I_{VIS} \tag{2.8}$$

in which I_{IR} and I_{VIS} are the two incident beams at a tunable IR and a fixed 800 nm visible [1] wavelength. In this equation, $\chi^{(2)}$ consists of two different contributions: one from the substrate (non-resonant) and one from the adsorbate (resonant) [113]:

$$\chi^{(2)} = \chi^{(2)}_{NR} + \chi^{(2)}_{R} = \chi^{(2)}_{NR} + \sum_k \left| \frac{A_k}{(\omega_{IR} - \omega_v) + i\Gamma_k} \right| e^{i\phi_k} \tag{2.9}$$

where the non-resonant contribution $\chi^{(2)}_{NR}$ is generated by electronic inter-band transitions occurring within metal substrates [114]. The resonant contribution $\chi^{(2)}_{R}$ is generated from molecular vibrations and modeled as a sum of Lorentzian oscillators with resonance frequency ω_k, linewidth Γ_k, phase difference ϕ_k relative the non-resonant contribution, and strength A_k. The term A_k is a

1. Although technically in the near-IR region, this beam has historically been called "visible" to distinguish it from the tunable IR beam.

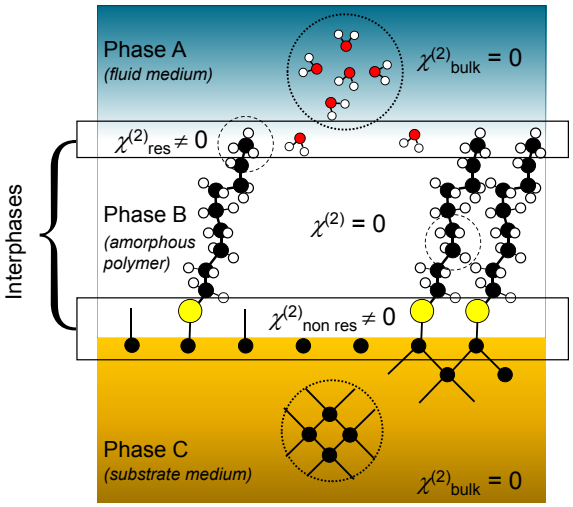

Figure 2.3: Graphic illustration of the selection rules governing the generation or suppression of an SFG signal

Table 2.1: Incident beam polarization combinations and the elements of $\chi^{(2)}$ which they probe. Polarizations are listed in the order of decreasing frequency: SFG,VIS,IR. Adapted from Ref. [95]

Polarization combination	Probed elements of $\chi^{(2)}_{ijk}$
pss	$\chi^{(2)}_{zyy}$
sps	$\chi^{(2)}_{yzy}$
ssp	$\chi^{(2)}_{yyz}$
ppp	$\chi^{(2)}_{zzz}$, $\chi^{(2)}_{zxx}$, $\chi^{(2)}_{xzx}$, $\chi^{(2)}_{xxz}$

complex third-rank tensor dependent on the Fresnel factors as well as the IR and Raman transition moments of the probed material [114]. The SFG signal is resonantly enhanced when (ω_{IR} is equal to ω_v (Fig. 2.2).

The second-order non-linear susceptibility $\chi^{(2)}_{ijk}$ (where i, j, and k has a total of 27 possible components which can the non-linear response of of a molecule to all polarization combinations. However, in a molecule containing a C_∞ rotation axis only 4 of these components contribute [95] (Table 2.1). Further information about such molecules at the surface may be gathered by changing the polarization of the incident **E** field, as different polarization combinations probe different elements of $\chi^{(2)}$. For instance, the **E** field of s-polarized light has a component solely in the y-direction, resulting in only those elements with transition dipole moments perpendicular to the plane of incidence giving rise to an SFG signal. The **E** of p-polarized light, on the other hand, has components in both the x and z directions, resulting in SFG signals from elements with transition dipole moments both parallel and perpendicular to the plane of incidence [23]. More complex molecules do not have a perfect C_∞ axis of rotation; however, even for these species more elements will be probed in ppp polarization than in ssp polarization.

The surface specificity of SFG spectroscopy arises from the fact that in a centrosymmetric environment, the elements of $\chi^{(2)}_{ijk}$ must be equivalent in all directions, giving:

$$\chi^{(2)}_{ijk} = \chi^{(2)}_{-i-j-k} = -\chi^{(2)}_{-i-j-k} \tag{2.10}$$

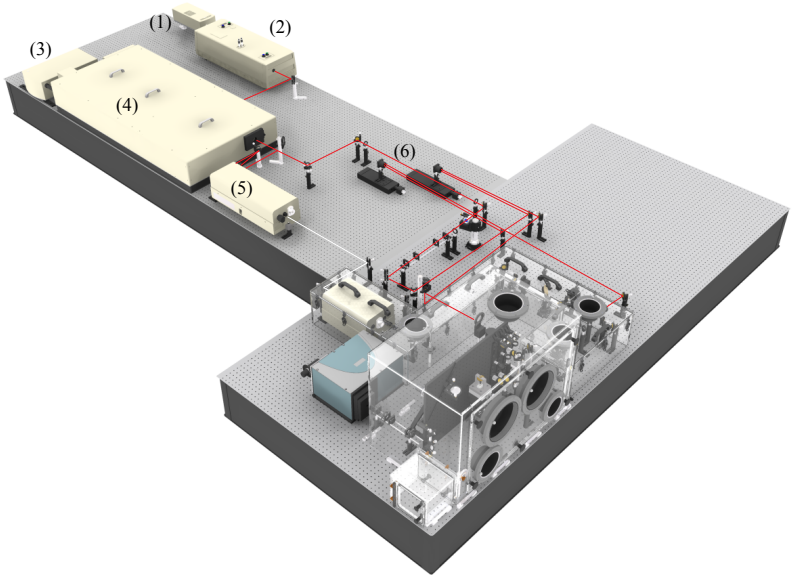

Figure 2.4: Setup of the optical table. The labels denote: (1) Millenia Pro, (2) Tsunami, (3)Empower, (4) Spitfire, (5) Topas, and (6) delay stages. The VIS and Signal/Idler beams are represented by red and white solid lines, respectively. For clarity the beams paths are only illustrated up to purge chamber (clear box).

This can only be true when $\chi^{(2)}_{ijk} = 0$, rendering the process of SFG signal generation forbidden in centrosymmetric media such as air or water [23, 95]. At interfaces, however, the centrosymmetry is broken and SFG can occur (Fig. 2.3).

2.6.2 Instrument Specifications

SFG measurements were performed on a home-built spectrometer located in the Institute of Toxicology and Genetics (ITG) at KIT [115]. This laser consists of a fs regenerative amplifier (RGA) (Spitfire Pro 35F XP, Spectra-Physics; sub-35 fs, 1 kHz) seeded by a mode-locked Ti:sapphire oscillator (Tsunami 3941-MS, Spectra-Physics; sub-30 fs, 80 MHz) with a tunable wavelength centered at 800 nm. The regenerative amplifier and seed laser are pumped by frequency-doubled Q-switched Nd:YLF (Empower 30, Spectra-Physics; 30 W, 1 kHz, 527 nm) and Nd:YVO_4 (Millenia Pro 5s, Spectra-Physics; 5 W, 532 nm) solid-state lasers, respectively. The RGA generates 120-fs duration pulses centered at 800 nm with a repetition rate of 1 kHz and an average power of 4 W. The amplified output beam is then split up and the larger fraction (80%) is used to pump an automated optical parametric amplifier (OPA) (TOPAS-C, Light Conversion) coupled to a non-collinear difference-frequency generator (NDFG) (Light Conversion). This generates broadband (FWHM∼70-200 cm^{-1}) IR pulses which can be tuned from 2.6 to 12 μm. The signal and idler beams are spatially separated and spectrally filtered by a Ge plate (Crystec). The remaining fraction of the output beam (20%) is fed into an air-spaced Fabry-Perot etalon (SLS Optics; spacing $d = 12.5$ μm, free spectral range FSR = 398.29 cm^{-1}, effective finesse $F_{eff} = 57.48$ at 790 nm) which gives narrowband (FWHM∼1 nm), asymmetric ps 800 nm (VIS) pulses. A 3D graphic of the optical table setup is shown in Fig.2.4.

The linearly-polarized IR and VIS beams were independently directed and focused on the sample surface with incident angles (relative to the surface normal) of 60°, 68° and 70°, respectively. These beams were then spatially (through the use of mirrors) and temporally (through the use of delay lines) overlapped at the sample surface within a spot ∼200 μm in diameter (Fig. 2.6). The elliptical shape is due to the angle of incidence of the beams. Maximum energies of ∼30 μJ/pulse for the IR beam and ∼40 μJ/pulse for the VIS beam can be obtained immediately before the sample. However, for these experiments the incoming beams were adjusted by

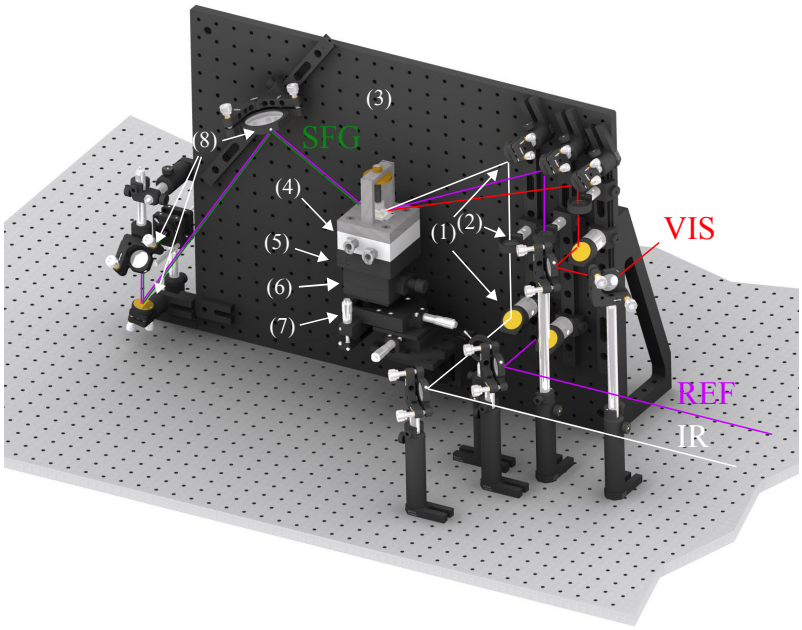

Figure 2.5: 3D image of the sample stage area. The labels denote: (1) input mirrors, (2) input lenses, (3) breadboard, (4) measuring cell, (5) kinematic plates, (6) 1-axis goniometer, (7) 3-axis rolling block, and (8) output mirrors. The IR, REF, SFG, and VIS beams are represented by white, purple, green, and red solid lines, respectively. The reflected IR and VIS beams are not shown for clarity.

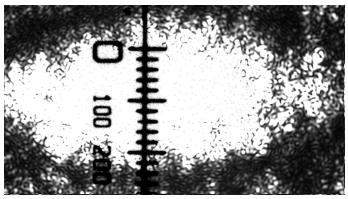

Figure 2.6: Beam profile of the VIS pulse at the sample stage. The scale shown is in μm units. This image was acquired using a microscope mounted above the sample stage.

pinholes to a maximum of $\sim$7 μJ/pulse for the IR and $\sim$5 μJ/pulse for the VIS to prevent bubble formation or sample ablation.

The outgoing SFG beams is collimated by lenses, filtered through a short-pass filter (3rd Millenium 770SP, Laser Components), and dispersed in an imaging spectrograph (Shamrock SR-301i-B, Andor Technology; focal length $f = 303$ mm, 1200 grooves/mm grating blazed at 500 nm) equipped with both a photomultiplier (R9110, Hamamatsu) and an air-cooled, back-illuminated high-resolution CCD camera (iDus DU420A-BR-DD, Andor Technology; 254 $\times$1024 pixels). Using this setup, it was possible to obtaine SFG spectra with reasonable SNR on a time scale of ms to s. For alignment, spectra were recorded in real-time (every 0.1s) allowing more accurate intensity optimization and frequency adjustment. Spectra were taken with either *ppp*, *ssp*, or *sps* polarization combination for the SFG, VIS, and IR beams, respectively, acheived by the rotation of the IR and VIS beams through the use of half-wave plates and/or a periscope.

Films in liquid were probed using a liquid cell inspired by the IR spectroscopy cell of Skoda *et al.* [116]. The cell, designed by V. Kurz, consists of a hemicylindrical CaF_2 prism with optically polished curved and basal surfaces (Crystec; 10×20 mm), a Teflon® base and prism adapter, and

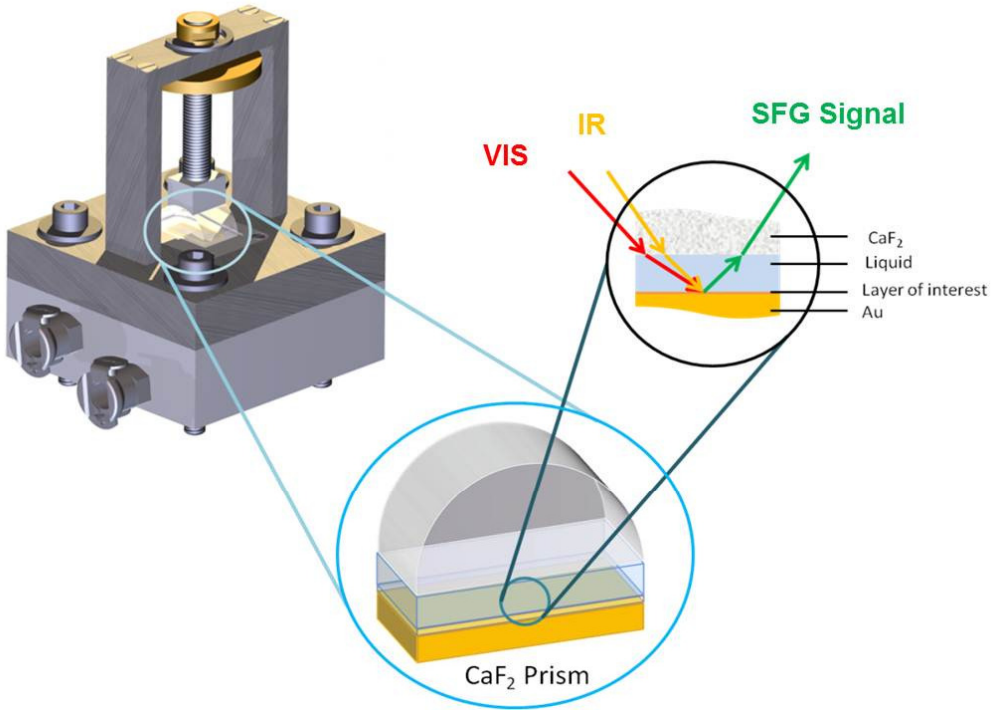

Figure 2.7: Measurement cell for *in situ* characterization of liquid/solid interfaces. The surface is probed through a half-cylindrical CaF_2 crystal located on top of the sample. The liquid is entrapped between the crystal base plate and the sample surface.

a threaded rod to hold the prism on place on top of the sample [115]. In this setup, the sample is placed on the Teflon® base with a drop of liquid on its surface. The prism is then placed gently on top of the liquid, creating an aqueous layer located between the sample and an IR-transparent prism thin enough for the beams to reach the surface and be reflected back without significant energy loss (Fig. 2.7).

A custom-built purge chamber was used in order to collect spectra more accurately in regions where water absorption is a problem. This acrylic glass-enclosed, air-proof chamber covers the optical path of the IR beam from the NDFG module to the spectrograph. The air inside the chamber is air-dried ($\leq 1\%$ RH) by an FTIR purging gas generator (75-45-12VDC, Parker-Balston; 14 L/min) coupled to two additional coalescing pre-filters to remove air particulates and hydrocarbon residues. The humidity and temperature in the chamber are monitored by a thermohygrometer (Hytelog-USB, Hygrosens) mounted on the top panel. Using this setup, near complete elimination of the signals arising from water vapor in the air is achievable.

2.6.3 Data Processing Procedures and Considerations

SFG spectra from samples on gold consist of a convolution of the signal arising from electronic transitions of the gold substrate and vibrational transitions from the sample, as shown in Eq. 2.9. These spectra can therefore be presented either as (i) a full, raw spectrum consisting of a combination of the non-resonant and resonant components,(ii) as background-subtracted spectra in which the non-resonant background emanating from the gold is assumed to have a Gaussian shape and is divided by the spectrum, or (iii) as a background-suppressed (BGS) spectrum in which a small shift in the temporal overlap of the VIS and IR beams minimize the contributions from the NR background (Fig. 2.8). Very noisy data can also be smoothed with either averaging

or Savitzky-Golay routines, generally using between 5 and 15 data points.

Analyzing the raw spectra (type [i]) minimizes the errors associated with data processing, however spectra presented in this way are often difficult to understand with those not familiar with SFG spectroscopy, as the non-resonant background contributions are significantly more prominent than the resonant contributions from the sample (Fig. 2.8i).

To obtain background-subtracted spectra (type [ii]), the raw SFG output can be fitted by Eq. (2.8) using a Gaussian shape for the non-resonant contribution (reflecting the fs IR profile) and Lorentzian oscillators for the resonant contributions (Fig. 2.8ii). The major drawback associated with this type of presentation, however, is the fact that the phase of the resonant contributions relative to the non-resonant background, ϕ_k, are unknown. This could potentially cause complications in numerical analysis of such spectra, as in order to fit the SFG spectra using Eq. (2.8)these phase values must be assumed. However, for purely qualitative comparison purposes, presentation of the SFG data as type (ii) can be highly useful.

Background-suppressed (BGS) spectra (type [iii]) are generated by shifting the incidence timing of the VIS beam slightly with respect to the IR beam. In 2007, Dlott and colleagues [117] introduced a method by which the non-resonant contributions coming from a metal solid substrate such as gold could be suppressed, allowing the resonant contributions to become dominant in the spectrum. This method relies on the fact that electronic transitions that create the non-resonant background signal have a much shorter lifetime than the vibrational resonant contributions [117]. By shaping the VIS beam through the use of a Fabry-Perot étalon, it becomes possible to create an asymmetric beam profile with a 100fs rise and a smooth 1ps ring-down [117]. When this pulse is overlapped with the IR pulse with a time delay of 300fs, a spectrum is obtained in which the large Gaussian peak observable in the raw spectra is nearly gone, leaving behind only the resonant contributions (Fig. 2.8iii). If theoretically modeled and plotted over time, it can be seen that the NR background disappears slowly as the delay is increased, with the resonant contributions becoming more prominent at approximately 300 fs before receding as the delay difference between the two beams continues to lengthen.

In a BGS spectrum, the phase of the peaks is no longer an issue. This is due to the fact that when considering a spectrum with only one resonant contribution, the SFG intensity can be expressed as:

$$I_{SFG} \propto \left|\chi^{(2)}_{NR} + \chi^{(2)}_{R}\right|^2 = \left|\chi^{(2)}_{NR}\right|^2 + \left|\chi^{(2)}_{R}\right|^2 + 2\left|\chi^{(2)}_{NR}\chi^{(2)}_{R}e^{i\delta}\right| \tag{2.11}$$

where δ is the phase difference between the resonant and non-resonant components. In this picture, when the non-resonant component of the spectra is very large, the cross-term is also large and the phase plays an important roll in the spectra. When the non-resonant component is small, however,

$$I_{SFG} \propto \left|\chi^{(2)}_{NR} + \chi^{(2)}_{R}\right|^2 \propto \left|\chi^{(2)}_{R}\right|^2 \tag{2.12}$$

leading to a suppression of the cross-term as well as the non-resonant background and effectively removing all phase contributions. This has the added benefit of facilitating the identification of peak positions, especially in complex molecules such as DNA. The peak positions, used in conjunction with the raw SFG data, can then be used to determine fit phase simultaneously with the other peak parameters such as intensity and width. In this work, a Voigt function was used to fit the BGS peak positions to the raw SFG spectra.

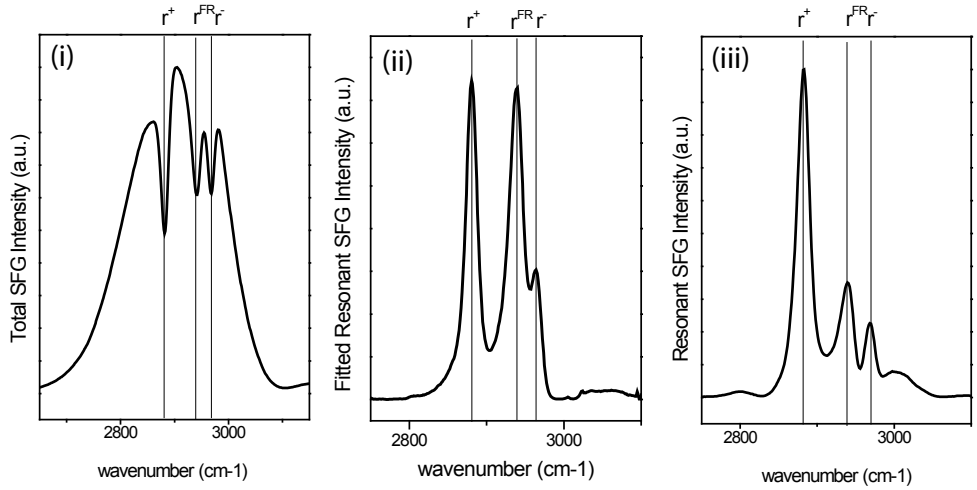

Figure 2.8: The raw SFG spectrum of DDT SAM (i) consists of a large, Gaussian non-resonant contribution with smaller Lorenzian resonant contributions appearing as peaks with a 180° phase difference distorting the Gaussian shape. The Gaussian peak can be fitted, divided through the spectrum, and the resonant contributions inverted to give a background-subtracted SFG spectrum (ii). When a delay between the incoming VIS and IR beams is introduced, however, the non-resonant contribution can be suppressed, leaving the resonant contributions behind in a BGS spectrum (iii). The labels of r^+, r^{FR}, and r^- stand for the CH_3 symmetric, Fermi-resonant, and asymmetric vibrations, respectively.

Chapter 3

Sensitivity and Proof-of-Principle Experiments

3.1 Summary

When dealing with a new system of measurement, it is important to have a firm grasp on limitations of the system in order to avoid incorrect interpretations or overstatements of the acquired data. Sensitivity tests of this system yielded a signal-to-noise ratio of 100 at a surface coverage of 0.2 molecules per nm^2. It is also essential to have simple proof-of-principle experiments in which the expected outcome is known in order to confirm that the system is operating in a predictable way. For this, hydrophilic and hydrophobic self-assembled monolayers of alkanethiols were examined in air and in water. Hydrophilic films showed significant changes in peak intensity and position upon exposure to water, indicating extensive interaction of water molecules with the film, as expected. Spectra of hydrophobic films were similar in air and water, indicating no interaction of water with the film, also as expected. Density Functional Theory (DFT) calculations were also performed to identify the vibrational modes contributing most significantly to the observed effects. These results confirm that SFG spectroscopy can be used to accurately detect the interaction of water with molecules in thin films at interfaces.

3.2 Sensitivity Measurements

3.2.1 Experimental Details

In order to experimentally determine the lower detection limit of the SFG system, mixed SAMs consisting of increasingly deuterated molecules were fabricated via solution deposition and measured in the CH stretching region. Silicon wafers sputter-coated with 100 nm of gold were cleaned by a UV/ozone cleaner for 2.5 hrs as described in Chapter 2 Section 2.1.2. The clean wafers were rinsed and placed in either pure or mixed 3 mM solutions of 1-dodecanethiol (Sigma-Aldrich) and deuterated 1-dodecanethiol (98.9% deuteration) in ethanol and incubated at room temperature for 18 hrs. Samples were then removed from the solutions, rinsed in ethanol, dried under flowing N_2, and immediately measured. SFG spectra were accumulated for 1 min, smoothed with a Savitzky-Golay routine using 15 data points, analyzed according to the background subtraction procedures outline in Chapter 2 Section 2.6.3 and plotted as the resonant contributions without the non-resonant background. The resonant SFG intensity as a function of surface coverage of the undeuterated dodecanethiol was then calculated (Fig. 3.1). X-ray photoelectron and IR spectroscopy measurements were also performed as outlined in Chapter 2 to ensure sample quality.

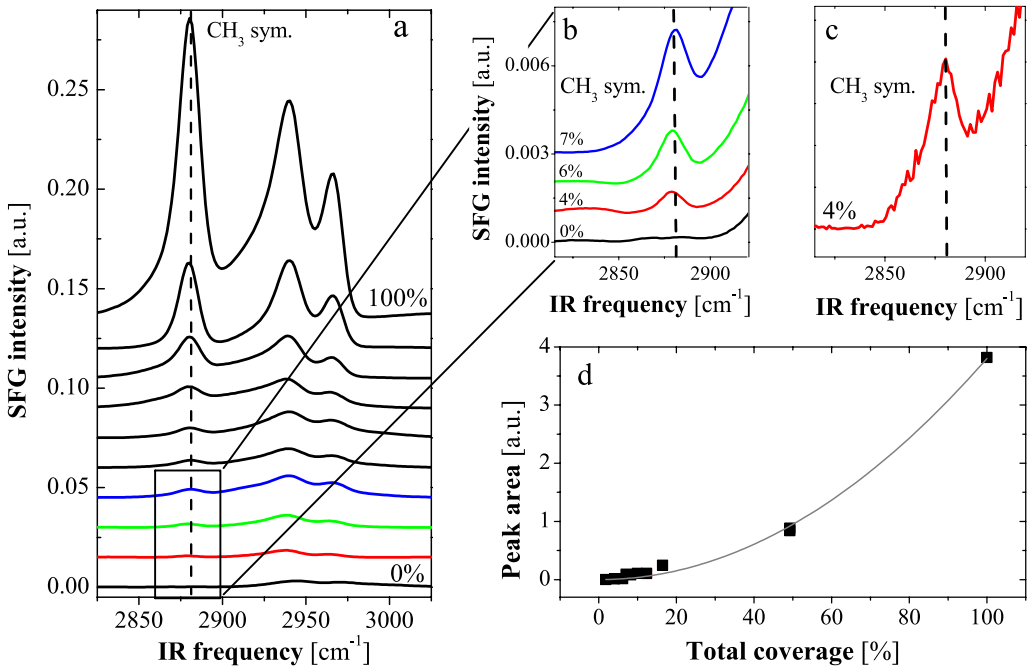

Figure 3.1: Spectra of DDT SAMs for calculation of the lower detection level of the SFG system. (a) Spectra of a fully deuterated SAM (0%, bottom trace), a fully undeuterated SAM (100%, top trace), and mixtures in between (from top: 50%, 16%, 12%, 10%, 8%, 7%, 6% and 4%). (b) Magnified spectra of the four lowest surface coverages highlighting the decrease in the CH_3 symmetric stretch. (c) Unsmoothed spectrum at 4% surface coverage for SNR determination. (d) Intensity of the symmetric CH_3 vibration as a function of surface coverage with the corresponding quadratic fit. The peak area was quantified using Lorentzian fits of the resonant SFG spectra.

3.2.2 Results and Discussion

The residual peaks present in the spectrum of the fully deuterated monolayer can be assigned to CH_2 vibrations and are related to incomplete deuteration. However, the peak at 2880 cm^{-1} arising from the symmetric vibrations of the terminal CH_3 group could be used to accurately assess the SFG intensity as a function of concentration, and hence the sensitivity of the spectrometer. Note that this peak was completely absent in the fully deuterated monolayer but still present in the mixed monolayer with the lowest undeuterated content tested (4% surface coverage, corresponding to 0.19 molecules per nm^2 assuming 0.21 nm^2 per alkanethiol molecule [118]) (Fig. 3.1b). The intensity of the SFG signal can be expressed as:

$$I_{SFG} \propto N^2 |\langle\beta\rangle|^2 \tag{3.1}$$

where $\langle\beta\rangle$ is the average molecular hyperpolarizability and N the molecular surface coverage. This quadratic relationship was supported by the experimental data. Ultimately, the lower detection limit of this system was found experimentally to be 4% with an SNR of 100. Theoretically, it should be possible to achieve a signal at 2% coverage with an SNR of 25, or even at 1% coverage with an SNR of 6.25. This detection limit is lower than previously reported values for other homodyne-detected systems (10% coverage) and comparable to heterodyne-detected systems, with lower reported limits of 1% coverage [119].

In this work, DNA films with an experimentally calculated density between 7×10^{12} and 7×10^{13} DNA molecules/cm^2 were used. Given that oligonucleotides consisted of at least 5 nucleosides, this translates into a lower CH_2 or CH_3 oscillator density of 4.5×10^{13} and $4.5 \times$

10^{14} oscillators/cm^2, above the experimentally demonstrated lower detection limit of 2×10^{13} oscillators/cm^2 from these experiments.

3.3 Proof-of-Principle Experiments: Model Hydrophilic and Hydrophobic SAMs

3.3.1 Background

Analyzing *in situ* SFG spectra of larger molecules or dynamic processes can be difficult, not only because of the inherent complexity of the molecules and processes themselves, but also because the coupling of water molecules to polar groups in samples *in situ* can lead to conformational changes which alter the resulting spectra. Due to the relatively recent appearance of SFG as an *in situ* spectroscopic technique, however, there is currently comparably less literature available which examines these changes [120, 121, 122, 123, 124, 125]. Furthermore, there is little information on these changes in basic contrasting systems - simple hydrophobic- and hydrophilic- functionalized surfaces - despite the fact that this information could be highly useful in interpreting *in situ* spectra of more complex samples such as biomolecules and polymers.

Self-assembled monolayers (SAMs) of alkanethiols often serve as model systems due to their relative simplicity and ability to be used to easily create hydrophilic and hydrophobic surfaces [**?** 126]. To date, there have been many theoretical and experimental studies performed on SAMs with methyl-terminated hydrophobic and hydroxyl-terminated hydrophilic tail groups. The majority of these studies have focused on structural and dynamic properties of water at the interface, and have found a substantially reduced water density in the direct vicinity of methyl terminal groups for hydrophobic films and a partially solvated state for hydroxyl terminal groups in hydrophilic films [127, 128, 129]. However these studies did not examine the effect of water interaction on the internal structure of the film itself. Bain and coworkers investigated the relationship between macroscopic contact angles and molecular-level details in methyl-terminated SAMs in air and in increasingly polar liquids. In order to vary the water contact angle between 77° and 112°, they used alkanthiols with oxygen atoms at varying distances relative to the terminal methyl group [120, 121]. Other studies have focused on structural changes within the SAMs, although using more complicated molecules [125, 123, 130]. Here we examine hydroxyl-terminated alkanethiol SAMs in air and in water using broadband SFG spectroscopy. These molecules are often employed as a protective group in the manufacturing of a variety of thiolated biomolecules including DNA [83, 84, 58, 131] and are also used as backfilling molecules to increase order in films of biological molecules [39]. Furthermore, we compare these results to hydrophobic methyl terminated SAMs and use Density Functional Theory (DFT) calculations to support peak assignments for both systems.

3.3.2 Experimental Details

Gold-coated wafers were placed in solutions of 1-dodecanethiol (DDT) (Fig. 3.3) to form hydrophobic surfaces or 11-mercaptoundecanol (MCU) (Fig. 3.5) to form hydrophilic surfaces (Sigma-Aldrich) in accordance with the methods outlined in Chapter 2 Section 2.1.3. Contact angles reported in literature for hydroxyl-terminated SAMs were $< 10°$ and 112° for methyl-terminated SAMs [132]. After 36 hrs of incubation at room temperature samples were removed from the solutions, rinsed thoroughly in ethanol, and dried under flowing N_2. Sample quality was verified via X-ray photoelectron and infrared spectroscopy. SFG Spectra were recorded using the femtosecond SFG spectrometer described in Chapter 2 Section 2.6. All spectra were recorded in ppp polarization in the order of increasing wavelengths (SFG, visible and infrared). Each sample was first measured in air, then in H_2O. The spectra were then background corrected, smoothed using a Savitzky-Golay fit (5 points) and normalized to the spectral profile of the broadband IR pulse as described in Section 2.6.3

Density Functional Theory (DFG) calculations were made according to the procedures described in Chapter 2 Section 2.5. In order to permit direct comparison between experiments and theory we calibrated the calculated frequencies to match those observed for the symmetric and

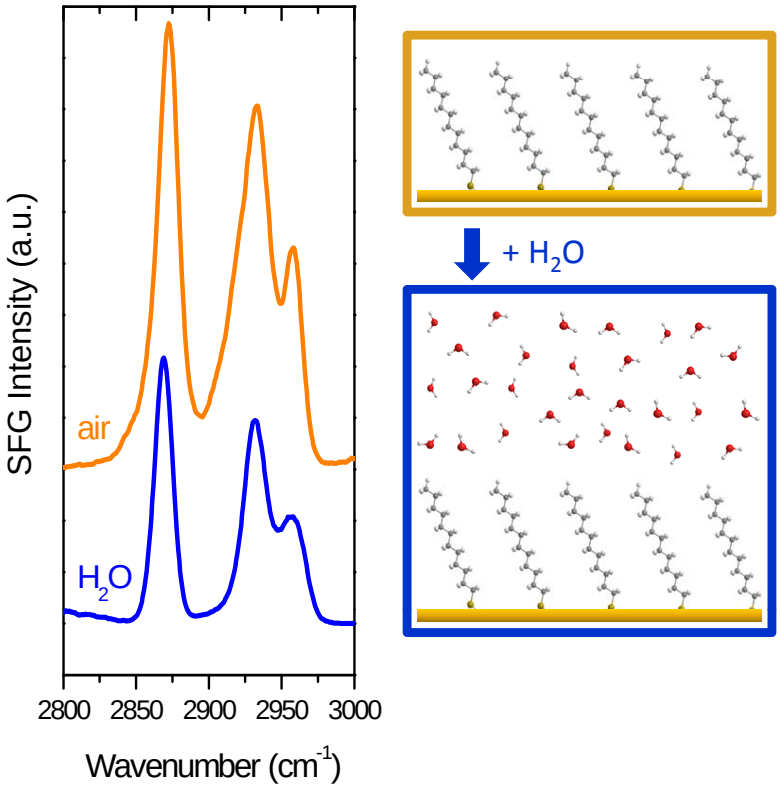

Figure 3.2: SFG spectra of a self-assembled monolayer of hydrophobic, methyl-terminated 1-dodecanethiol SAM on gold in air (above) and in water (below). No significant changes in relative peak intensities or positions were observed upon exposure to water, indicating that there is only a weak interaction (e.g. induced dipole, van-der-Waals) between water molecules and the film.

asymmetric CH_3 vibrations of the methyl terminal group in the DDT film. This yielded a redshift of the calculated spectra by 99.5 cm^{-1}.

3.3.3 Results and Discussion

3.3.3.1 Hydrophobic SAMs

Fig. 3.2 shows the SFG spectra of self-assembled monolayers of methyl-terminated DDT on gold in air (orange, upper trace) and in water (blue, lower trace) in the region between 2800 and 3000 cm^{-1}. The major bands present in these spectra are attributed to vibrations of the methyl terminal groups (located at 2880, 2940, and 2968 cm^{-1}) [133, 134]. Vibrations from methylene groups within the alkane chain can not be observed in the SFG spectra, with the exception of minor contributions from the methylene groups adjacent to the sulfur atom (located at 2885 and 2928 cm^{-1}) (Tab. 3.1).

This is due to the selection rules for second order nonlinear optical processes which dictate that only molecular arrangements with broken inversion symmetry can contribute to an SFG response. In air, the close-packed DDT film is assumed to have a highly ordered structure with an all-trans conformation of the alkane chains [135]. In this configuration a center of inversion is located in between the methylene groups in the alkane chain, leading to the suppression of the corresponding SFG signal. Indeed, the DFT calculation for the all-trans conformation reveals that none of the collective alkane chain CH_2 vibrations in the observed spectral range are both Raman and IR active. Note, that according to group theory, (SFG active) vibrations with broken inversion

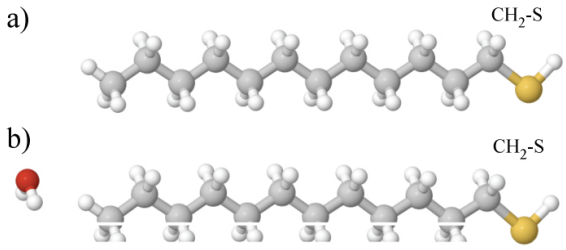

Figure 3.3: Graphic of a single DDT molecule as used for DFT calculations. a) molecule as used for calculations in air and b) molecule as used for calculations in water.

symmetry must be both Raman and IR active. In addition, the absence of bands originating from gauche defects in the alkane chain (see Tab. 3.1) confirms the presence of an ordered SAM.

Furthermore, the CH_3 as vibration has both in-plane (ip, 2965 cm^{-1}) and out-of-plane (op, 2955 cm^{-1}) contributions. In the polarization combination used in these experiments (ppp, in the order of increasing wavelength - SFG, visible, and IR), the observed SFG intensity of the vibrational modes with a component of the IR transition dipole moment perpendicular to the interface is maximized, while this polarization combination does not sample modes with transition dipole moments oriented parallel to the surface. The presence of the ip vibration and absence of the op vibration in these spectra indicate that the methyl groups are oriented perpendicular to the substrate, as is expected for a highly-ordered film of this type [135].

It was observed that placing the DDT films in water (Fig. 3.2, lower blue trace) did not significantly change the spectrum in either band position or relative intensity, in agreement with previous results [120, 121]. This indicates that the water molecules have only weak interactions with terminal methyl groups of the film and that the orientation of the methyl groups of this film remains the same. As a high density or close proximity of water molecules near the methyl groups would cause a change in the vibrations and thus a change in the spectra, these findings support previous results obtained by MD simulations [127], neutron [136], and x-ray-relfectivity [128, 129], suggesting a reduced water density near the surface of this hydrophobic film [127, 128, 129].

3.3.3.2 Hydrophilic SAMs

In Fig. 3.4, SFG spectra of the hydrophilic, OH-terminated MCU SAMs are shown. According to our DFT calculations, the only Raman and IR active bands in this region are collective CH_2 vibrations mainly located at the second CH_2 group from the OH-termination (CH_2(2)) and the CH_2 group adjacent to the sulphur atom (CH_2-S). (Tab. 3.1 and Fig. 3.5). A peak at 2964 cm^{-1} is also apparent in the MCU spectra in both air and water, but as this peak was not present in the DFT calculations we refrain from assigning it here. Collective vibrations located primarily at the first group from the OH-termination (CH_2(1)) are found to be located in the region below 2800 cm^{-1}, which was not probed in these experiments. The high overall intensity of this spectrum and presence of peaks due only to terminal or near-terminal groups indicate that this film also has a high degree of order, as the alkane chain methylene vibrations are suppressed (see discussion in the previous section on symmetry arguments in an all-trans conformation).

When this film is exposed to water, however, drastic changes occur (Fig 3.4, lower blue trace). First, the overall intensity of the peaks decreases significantly compared to the peaks in air (both spectra were normalized to the nonresonant background). Second, the relative intensities of these peaks are substantially changed. Third, new peaks attributed to CH_2 vibrations from further down the alkyl chains appear at 2909 and 2945 cm^{-1}. These are now visible due to the appearance of gauche defects caused by the water molecules interacting with this film and causing a change in the orientation of the hydroxyl terminal groups. This assignment is supported by the DFT calculations showing that these vibrations are only present in CH_2 groups adjacent to a kink in the alkyl chain. It should be noted, however, that the positions of the peaks assigned to CH_2-S vibrations remain unchanged. This indicates that while the interaction with water is disrupting

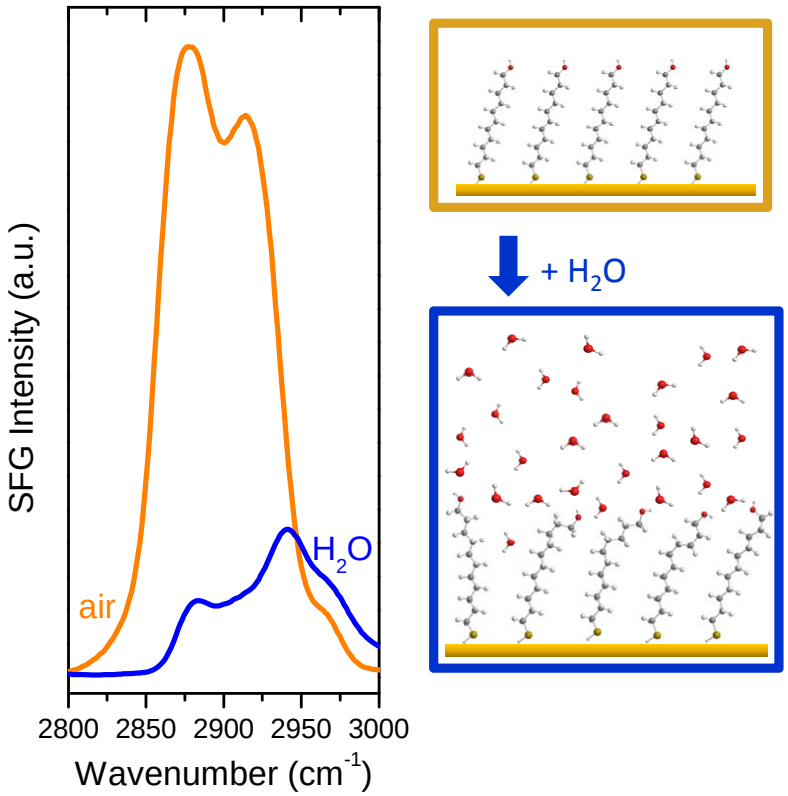

Figure 3.4: SFG spectra of hydrophilic, hydroxyl-terminated 1-mercaptoundecanol in air (upper trace), and in water (lower trace). Peak positions changed drastically upon exposure to water, as did both relative and overall intensities, indicating significant interaction of the water molecules with the film.

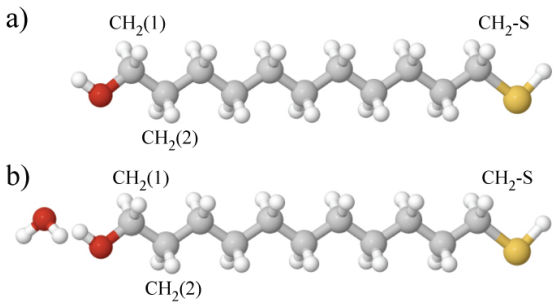

Figure 3.5: Graphic of a single MCU molecule as used for DFT calculations. a) molecule as used for calculations in air and b) molecule as used for calculations in water.

the upper part of the film, it is not disrupting lower part of the film, as would be expected for a well-formed SAM.

In summary, hydrophobic methyl- and hydrophilic hydroxyl-terminated self-assembled monolayers in air and in water using SFG spectroscopy were examined. Hydrophobic SAMs with methyl terminal groups showed similar spectra both in air and in water, demonstrating that these films do not change in either conformation or orientation upon exposure to solution, in agreement with previous results and supporting the concept of a reduced water density in close proximity to the hydrophobic interface suggested by other techniques. Hydrophilic SAMs with

Assignment	DDT					MCU				
	Positions					Position				
	Air			H_2O		Air			H_2O	
	Exp.	Calc.	Lit.[a]	Exp.	Calc.	Exp.	Calc.	Lit.[b]	Exp.	Calc.
CH_3 as, ip	2965	2957	2968	2965	2952	-	-	-	-	-
CH_3 s, FR	2940	2946	2940	2939	2929	-	-	-	-	-
CH_3 s	2880	2864	2880	2876	2865	-	-	-	-	-
CH_2-S as	2928	2939	-	2928	2933	2928	2938	-	2929	2934
CH_2-S s	2885	2877	-	2885	2877	2885	2877	-	2882	2870
CH_2(2) as	-	-	-	-	-	2911	2919	2910	-	-
CH_2(2) s	-	-	-	-	-	2865	2866	2956	-	-
CH_2 gauche	-	-	-	-	-	-	-	-	2945	2955
CH_2 gauche	-	-	-	-	-	-	-	-	2909	2924

Table 3.1: Peak positions and assignments for DDT and MCU monolayers in air and in water. s: symmetric, as: asymmetric, FR: Fermi resonance. The CH_2(2) group in MCU indicates that this resonance is centralized 2 carbon atoms away from the OH terminal group as depicted in Fig. 3.5. [a]Ref.[135] [b]Ref.[58]

hydroxyl terminal groups revealed substantially different SFG spectra in air and H_2O, attributed to a significant decrease in order and interaction of water molecules with the film. DFT calculations made for these molecules substantiate the peak assignment and the presence of gauche defects in the alkane chain when the film is exposed water.

3.4 Conclusions

Both the sensitivity measurements and the proof-of-principle results from model SAMs yield results that indicate that the technique of SFG can be used to examine and obtain accurate information about DNA films. The sensitivity measurements show that the current experimental setup can detect as few as 2×10^{13} oscillators/cm^2, which is below the lowest calculated density for DNA films used in these experiments, 4.5×10^{13} oscillators/cm^2. The proof-of-principle experiments have shown that SFG can give accurate and predictable information about SAMs measured in air versus in water, lending confidence to the analysis of the more complex systems of DNA through similar changes in environment.

Chapter 4

Surface-Bound DNA in Air

4.1 Summary

Thymine, adenine, and cytosine ssDNA and nucleobases immobilized on gold were examined in air in the CH stretching region using sum-frequency-generation spectroscopy. It was expected that the methyl group in thymine would give clues as to the changes in orientation of these molecules adsorbed on the surface as either ssDNA or nucleobase multilayers, with adenine and cytosine ssDNA and nucleobases acting as controls. Multilayers of the nucleobases alone showed clear peaks from the methyl group in thymine that were not visible in adenine and cytosine. Comparison of these peaks using different polarization combinations suggested an average orientation that was not completely planar with the sample surface, in agreement with previous results. Examination of films of unmodified short-chain DNA revealed a high degree of similarity among the spectra of thymine, cytosine, and adenine homo-oligonucleotides, indicating that the methylene vibrations of the sugar-phosphate backbone were the primary contributors to these spectra and suggesting that the DNA molecules on the surface were oriented in a way that was independent of nucleobase composition. Films of thiol-bound DNA, known for their relatively high degree of ordering, also showed highly visible differences between thymine, adenine, and cytosine ssDNA. This result suggested that, as was the case for the unthiolated films, the methylene vibrations from the backbone as well as the methylene groups from the thiol linker attaching the molecules to the substrate were dominating the spectra. The origin of these signals was verified by inducing order in the films through continuous wetting and drying, revealing increases in similar peaks for thymine, cytosine, and adenine ssDNA films. These results show that overall, the CH groups in films of surface-immobilized DNA are initially mostly disordered, likely due to the flexibility of single-stranded DNA molecules.

4.2 Background

Orientation and ordering in films of ssDNA immobilized on gold are essential to the optimal use of these systems [137]. In order to more accurately gather information on these parameters, we employed a bottom-up approach in which multilayers of the nucleobases were first examined, followed by unmodified DNA, and finally the more highly-ordered layers of thiol-modified DNA in air. Such an approach has been used before, most notably by Stokes *et al.* [57] who examined both individual DNA components as well as complete DNA molecules on glass using SFG spectroscopy. However, in those experiments the density of the DNA molecules was relatively low (on the order of 10^{12} molecules/cm^2, which is usually associated with a low degree of order). Furthermore, only thymine and its derivatives were tested. In these experiments, adenine and cytosine nucleobases and ssDNA were also tested for comparison.

The goal of these experiments was to gain a clear understanding of which CH oscillators in the DNA molecules gave rise to which signals, and to use that information to deduce order parameters from the samples tested. Although spectra in the Amide I region were also taken, these experiments focused mainly on the CH stretching region, as it was hoped that the CH_3 group

unique to thymine would be distinguishable and would yield clues as to the level of alignment of the nucleobases either alone or in a DNA strand. Previous work on the tilt angle of methyl groups in simple CH_3-terminated SAMs has shown that this information can be inferred by a comparison of the intensities of the asymmetric (r^-) to the symmetric (r^+) stretch [138] in ppp polarization or by comparison of the intensities of either the symmetric stretch in ssp to ppp polarization or the asymmetric stretch in ppp to ssp polarization [139]. However, both of these systems were developed assuming constraints based on alkanethiol chains, including the average degree of tilt of the entire chain (ϕ) relative to the surface normal, the rotation of the molecule around its axis (ψ), and the average degree of tilt of the methyl groups (θ) relative to the surface normal which is generally either 27°, for chains with an odd number of C atoms), or 58°, for chains with an even number of C atoms [138]. The fact that the latter dictates that the methyl groups are roughly pointing away from the sample surface means that the phase is generally assumed to be 180° relative to the surface normal [113, 125].

While some of these parameters may also be generally applicable to a methyl-containing thymine nucleobase in a DNA molecule, due to the flexibility of DNA strands there are also many more parameters that may influence the methyl peaks, including the rotation of the nucleobase relative to the pentose sugar, the rotation of the nucleobase and sugar relative to the phosphate groups, and kinks in the sugar-phosphate backbone which may result in the displacement of one nucleobase with respect to the others [41]. Furthermore, multiple studies using NEXAFS spectroscopy to determine the average orientation of thymine nucleobases relative to the substrate in films of thymine ssDNA on gold have revealed that they adopt an overall parallel orientation, although the degree of order is not extremely high [85, 44, 83]. Such an orientation would place the methyl groups in the thymine nucleobases nearly parallel to the sample surface, a condition which is generally not seen in the investigation of alkanethiol SAMs.

4.3 Experimental Details

All films were formed on 100 nm polycrystalline Au(111)-coated silicon wafers described in Chapter 2. Films were UV-cleaned for 2.5 hours and rinsed thoroughly with either pure ethanol or Mili-Q water prior to deposition.

Nucleobase multilayers were formed by placing a 50 μm solution of adenine, thymine, or cytosine dissolved in pure ethanol on a clean gold wafer and allowing the excess solvent to evaporate as described in Ref. [102] and in Section 2.1.3. DNA films were fabricated by placing the freshly cleaned gold wafers in 1M $CaCl_2$-TE buffer and incubating them at 37° for approximately 40 hours as described in Ref. [74] and Section 2.1.3. Following incubation, DNA films were rinsed for 1 min under flowing Mili-Q water to remove residual salt and excess DNA, then gently dried with flowing N_2.

IRRAS measurements were performed on all films according to the procedures outlined in Section 6.11. XPS measurements were peformed for the DNA layers using the ESCALAB 5 spectrometer described in Section 2.2. SFG measurements were gathered using the broadband SFG setup outlined in Section 2.6, using output powers of no more than 5 μJ and 7 μJ for the VIS and IR beams, respectively. Data were processed according to all three of the methods detailed in Section 2.6.3.

For films that were exposed to wetting and drying cycles, a drop of HPLC-grade water was placed on top of the sample, then allowed to dry in the purified, filtered air of the purge box surrounding the SFG sample stage. Measurements were taken after the drop of water had completely evaporated.

4.4 Results and Discussion

4.4.1 Nucleobase Multilayers

Nucleobase multilayers were examined first, as it was expected that they would provide the simplest spectra and facilitate the assignment of the peaks stemming from the methyl groups

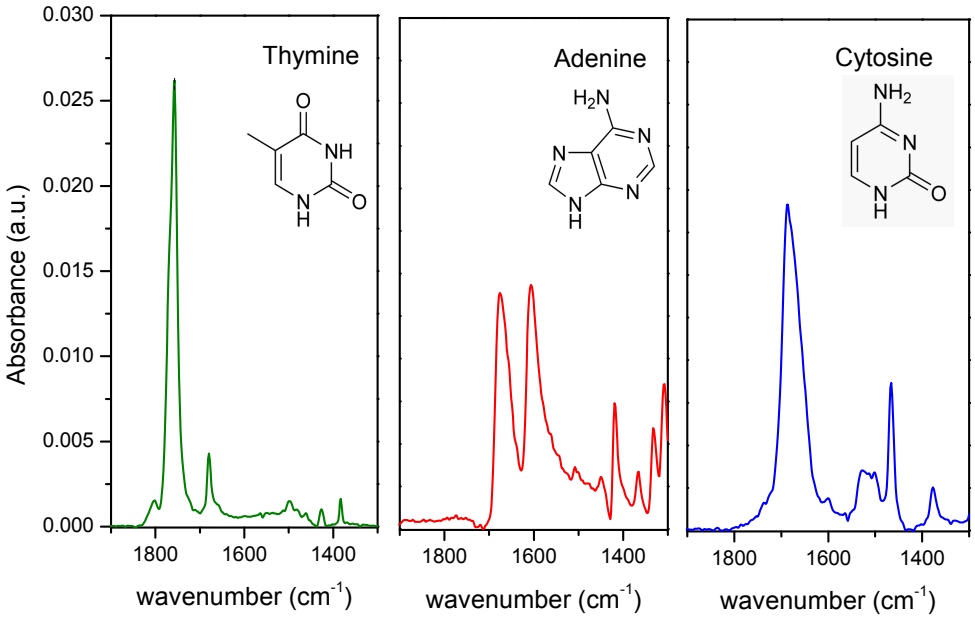

Figure 4.1: IRRAS spectra of thymine, cytosine, and adenine multilayers on gold in the amide I region.

in the bases. Multilayers were chosen instead of monolayers for this purpose as they contain a high nucleobase density and thus provide more signal due to more contributing oscillators. Furthermore, multilayers of DNA nucleobaes can condense on gold substrates into highly ordered structures [36, 140].

Multilayers were first measured with IRRAS in the amide I region in order to verify the sample quality. Results yielded peak positions in agreement with previously published results of different nucleobases [81, 35]. In Fig. 4.1, the spectrum of thymine shows a large peak at $\approx$ 1759cm^{-}1, which is assigned to the vibrations of the C=O at the C2 carbon, while the peak at 1678cm^{-}1 is attributed to the C4=O and C=C vibrations. The major peak in the cytosine spectrum at 1686cm^{-}1 is due to the C2=O vibrations, while the two adenine peaks at 1647 and 1606 cm^{-1} are assigned to NH_2 and N3-C4/C5-C6 stretches, respectively [102]. Examination of adenine and thymine nucleobase multilayers in the CH stretching region between 2800 and 3000 cm^{-1} using IRRAS revealed a sharp peak at around 2940cm^{-}1 for the thymine film, which was assigned to the asymmetric CH_3 stretching vibration [141]. Adenine films showed no such distinguishing characteristics (Fig. 4.2).

In the raw SFG data in the CH region, the thymine multilayer showed a sharp peak at 2935cm^{-1}, while the adenine and cytosine multilayers showed only small, broad peaks which distorted the shape of the non-resonant background (Fig 4.3). Spectra for these films in the Amide I region were also collected, however it was found that peaks from these molecules in the Amide I region, although relatively strong in IR spectroscopy, appear to be only weakly present in SFG spectra. In particular, the C=O stretch at 1700 cm^{-1} for thymine, which is quite prominent and often used as a marker of quality for thymine homo-oligonucleotide films [37, 51], is not significantly Raman active [102], and thus does not appear in the SFG spectra. Upon background suppression, a number of small peaks became visible that were common to all three types of nucleobases, as well as two unique peaks for the thymine multilayer: one large contribution at 2935cm^{-1} and one small contribution at 2905cm^{-1} (Fig. 4.3).

The peaks that are common to all three multilayers could be due to contamination that

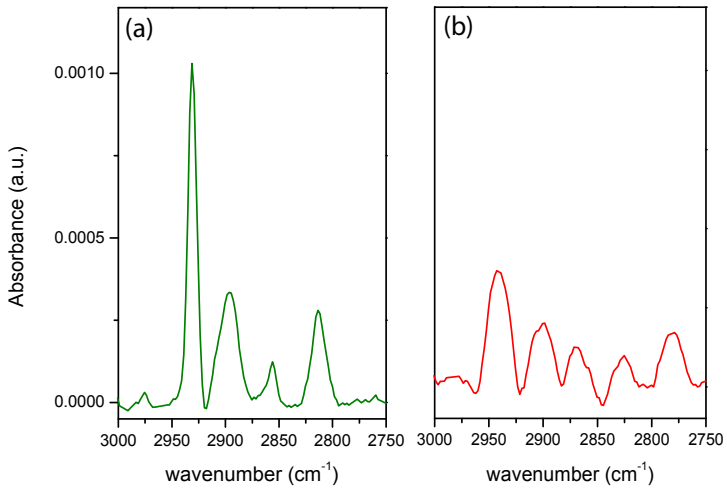

Figure 4.2: IRRAS spectra of thymine and adenine multilayers on gold in the CH region. The thymine film shows a sharp peak at approximately 2940 cm^{-1}, which was assigned to an asymmetric CH_3 stretch. The adenine nucleobase multilayers showed no such strong, sharp contributions, only broader and weaker peaks between 2750 and 3000 cm^{-1}.

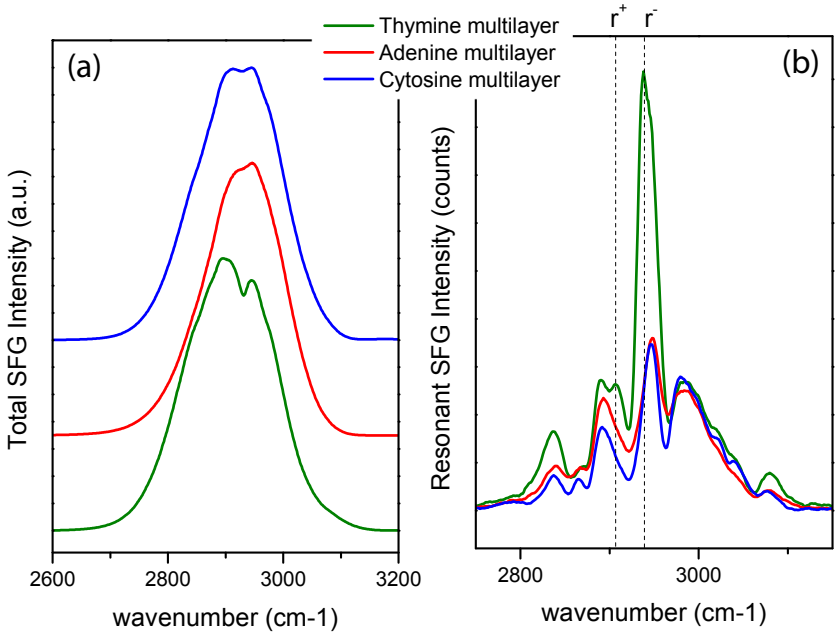

Figure 4.3: SFG spectra of thymine, adenine, and cytosine nucloebase multilayers in the CH stretching region. Data are presented as (a) raw spectra (b) background-suppressed spectra

Table 4.1: Parameters obtained from a fitting of the raw SFG data shown in Fig. 4.5 with Voigt functions using phase as one of the variable parameters. Positions are given in cm^{-1} and phase in degrees. Proposed peak assignments are also given.

ppp			ssp			
Position	Area	Phase	Position	Area	Phase	Assignment
2895	0.26	98	2899	0.06	142	CH_3 sym
2928	0.10	148	2929	0.14	162	CH_3 asym

was present in the deposition solution, or contaminating molecules that adsorbed onto the film during the process of making the films. It is also possible that these peaks are due to overtones of vibrations in the amide region. Each of these nucleobase types shows a number of peaks between 1400 and 1500 cm^{-1} in the IRRAS spectra (Fig. 4.1 which would give overtones in the region between 2800 and 3000 cm^{-1}. However, given that the smaller peaks look nearly identical among the layers, which is unlikely to be the case if these are indeed caused by overtones, as the different structure of the nucleobases should yield unique spectra. Therefore, contamination is the more likely explanation for these peaks.

It is interesting to note the low intensity of the peaks above 3000 cm^{-1}, which is typically the region in which strong ring vibrations are expected [141, 57]. However, other studies on films of nucleobases using SFG have also noted either absent or very weak peaks in this region [57]. This may indicate that the ring vibrations of thymine have either a very small IR cross-section or a very small Raman cross-section, as the SFG signal is the product of both of these [95]. Hommel *et al.* found the major benzene ring vibration at 3070 cm^{-1} decreased significantly when the rings were substituted with methyl groups [141].

The peaks for thymine at 2935 and 2905 cm^{-1} are assigned to the asymmetric and symmetric methyl stretches, respectively. This is in agreement with SFG, IR, and Raman measurements performed on methylated benzene rings at the air/water interface, in which major peaks in the SFG spectra were found at 2980, 2945, and 2915 cm^{-1} and assigned to a symmetric (at 2915 cm^{-1}) and two asymmetric (at 2945 and 2980 cm^{-1}) methyl stretches [141].

Stokes and co-workers [57] examined spin-coated films of thymine nucleobases on glass slides and found a peak with a negative phase at 2943 cm^{-1} and three peaks with positive phases at 2908, 2880, and 2861 cm^{-1}. They assigned these peaks to a methyl asymmetric stretch, a methyl Fermi resonance, a methyl symmetric stretch, and either a second methyl stretch or residual methylene from the deposition solution, respectively. The peak observed in these experiments at 2908 cm^{-1} is quite similar to the peak assigned to a Fermi resonance by Stokes *et al.*, however based on the fact that there are only two clear peaks in these spectra, we believe that an assignment of a symmetric stretch is more accurate. An assignment of a Fermi resonance for this peak would suggest that the symmetric stretch for the methyl vibration in thymine is not visible in either of the polarization combinations tested, which is unlikely.

The highly visible CH_3 asymmetric stretch in the thymine multilayer suggested that this film might have a relatively high degree of order. In order to test this, we examined this film using both ppp- and ssp-polarization combinations. A ppp-polarization combination probes a higher number of $\chi^{(2)}$ components, while an ssp polarization combination probes only those components which are perpendicular to the plane of the sample surface [23]. The spectra are presented in Figure 4.4, with the raw spectra shown in the right panel and the BGS spectra shown in the left.

The large dip in the raw spectra at 2935 cm^{-1} is also visible in the ssp spectra, indicating that these molecules are not lying flat on the gold surface with the methyl group oriented parallel to the substrate. More specific information about the molecules in this film was gathered by fitting the raw spectra using phase as a parameter as described in Section 2.6.3. The results are shown in Fig. 4.5 and the values are listed in Table 4.1. The procedure yielded relatively good fits to the experimental data with values within the expected range.

In ssp polarization, the asymmetric methyl stretch is maximized while the symmetric methyl stretch is near 0. This could be explained by a methyl angle with a preferential alignment more

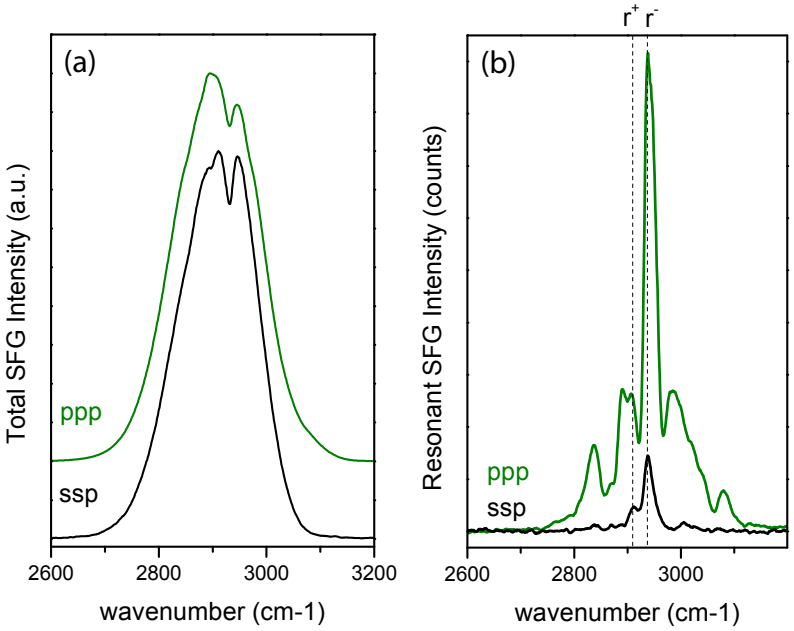

Figure 4.4: SFG spectra of a thymine nucleobase multilayer in ppp and ssp polarization combinations presented as (a) raw spectra and (b) background-suppressed spectra.

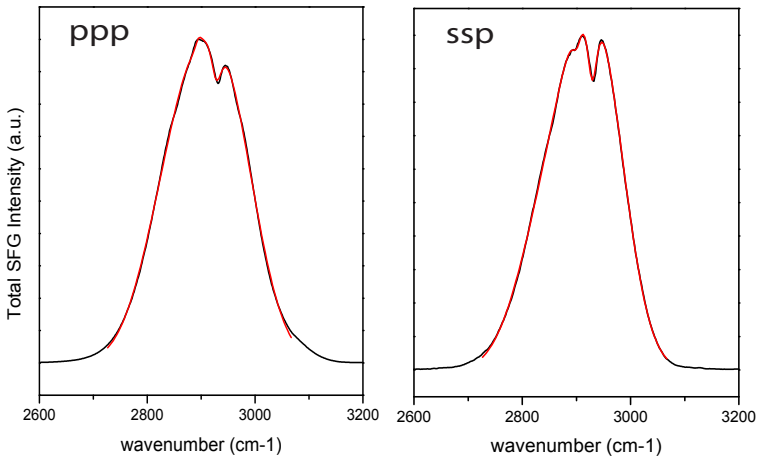

Figure 4.5: The raw SFG spectrum in ppp (left) and ssp (center) polarization combinations of a thymine nucleobase multilayer(black lines)fit using the peak locations determined from the background-suppressed spectrum as fixed parameters and phase, area, and width as variable parameters (red lines).

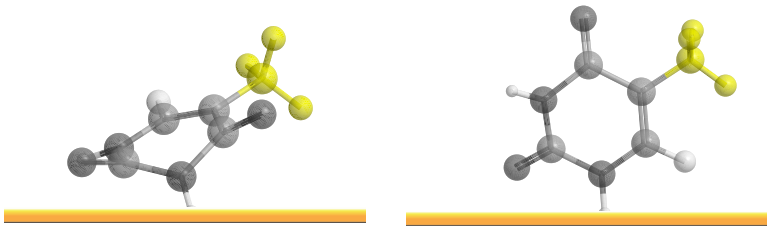

Figure 4.6: Cartoon of a molecule of thymine adsorbed on a gold surface with two potential orientations that would agree with the results presented in this chapter. The methyl group is oriented neither perfectly perpendicular nor perfectly parallel to the substrate, in agreement with previous results.

parallel than perpendicular to the plane of the sample surface. Such and orientation is in agreement with the results of Roelfs and co-workers [36], who examined the adsorption of thymine on gold electrodes using a combination of STM and XPS, and demonstrated that thymine can adsorb on Au(111) in a condensed state in which the molecules are oriented with the plane of the ring perpendicular to the surface and bound by a deprotonated N3 nitrogen to the surface (Fig. 1.4). Other earlier studies done using STM have also suggested an end-on orientation for nucleobases adsorbed on gold [142, 143]. This configuration would place the methyl group at an angle of around 60° relative to the surface plane (Fig. 4.6).

4.4.2 Unmodified DNA Films

Unmodified 6-mer homo-oligonucleotides were investigated using SFG spectroscopy in order to determine which contributions arose from the sugar-phosphate backbone of the DNA molecules. Prior to testing with SFG, the density and overall quality of these films were tested using XPS and IRRAS as described in Chapter 2. Final densities were calculated to be 7×10^{12}, 8.2×10^{12}, and 7.5×10^{12} molecules/cm^2 for thymine, adenine, and cytosine, respectively, according the procedures developed by Petrovykh *et al.* [51]. These densities are in agreement with the current literature, which shows the preference for binding to gold as decreasing from adenine to cytosine to thymine [35]. Adenine is known to resist being rinsed away, while thymine is more easily dislodged from the surface by streaming water. The measured densities in these experiments confirm this trend.

The XPS data themselves showed features typical of DNA monolayers [51]. An example spectra set for the $(dA)_6$ film is shown in Figure 4.7. The C 1s spectra shows two dominant peaks: 1 at 285 eV stemming from carbon with C-C single bonds, and another at 287, which arises from a C=C double bond. The fact that the latter peak is nearly the same intensity as the former is an indication that this film is indeed covered with DNA molecules and not just adventitious carbon contamination, in which C-C bonds are the dominant carbon form. The N 1s signal is strong and shows 2 contributions in a 2:1 ratio which is typical of nitrogen from adenine nucleobases [37]. The P 2p peak is also clearly present, although with a lower intensity due to the lower amount of phosphorous compared to nitrogen in DNA molecules (Fig. 1.4). No S 2p peak is present, as expected for these films.

The SFG spectra generated by these films are shown in Fig. 4.8. Figure 4.8a shows the raw SFG spectra in ppp polarization consisting of the Gaussian-shaped non-resonant background convoluted with the smaller, Lorentzian-shaped resonant contributions appearing as either dips or peaks distorting the Gaussian shape. All three spectra appear to have broad, shallow dips at approximately 2880 and 2930 cm^{-1}, although the higher position of the Gaussian in the cytosine and adenine ssDNA films makes the lower peak appear less prominent. The BGS spectra in ppp polarization are shown in Figure 4.8b and all show two prominent peaks at 2890 and 2940 cm^{-1}, with shoulders at 2870 and 2970 cm^{-1}. In ssp polarization, all spectra show three peaks at 2830, 2860, and 2950 cm^{-1}. In total, all the spectra films of thymine, adenine, and cytosine ssDNA are

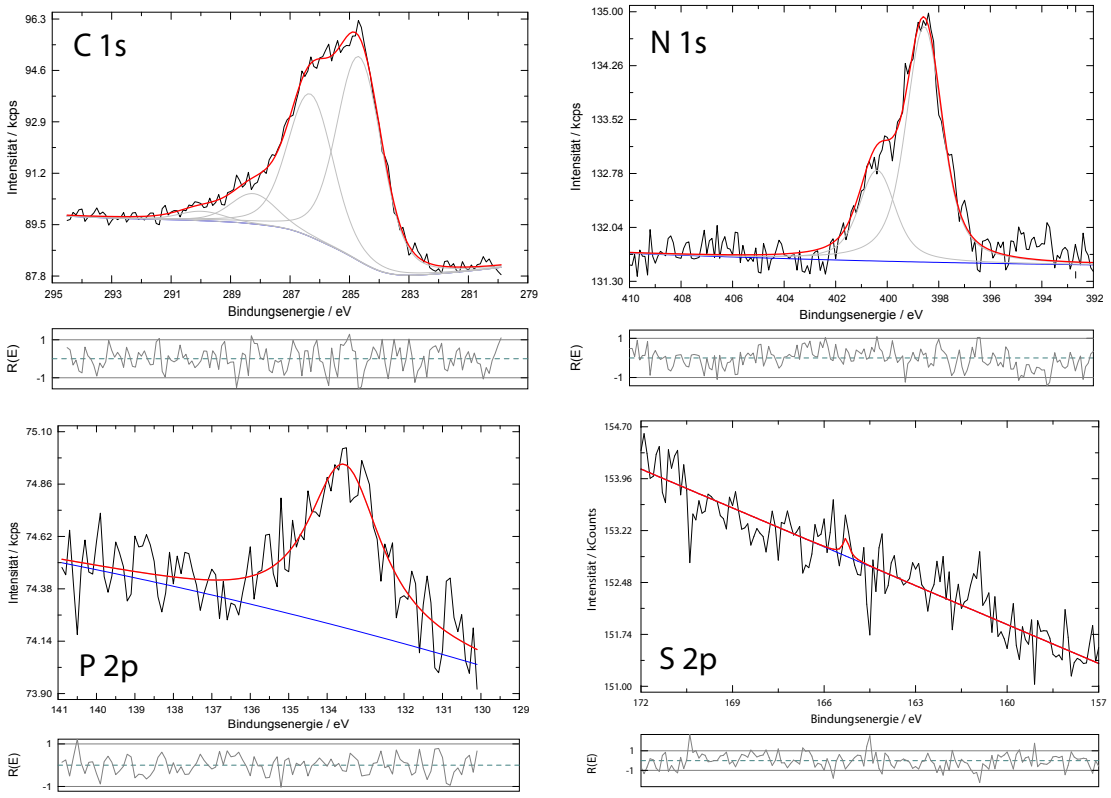

Figure 4.7: XPS C 1s, N 1s, and P 2p spectra from the unmodified adenine ssDNA film. The prominent peak in the C 1s spectrum at 287 eV (C=C bonds) in addition to the peak at 285 eV (C-C bonds) indicating that this film contains a significant amount of DNA rather than just contaminants, which generally contain mostly C-C bonds. The N 1s peak shows a double peak typical of adenine and the clear P 2p peak confirms the amount of DNA on the surface.

very similar, with peaks in the same locations across all the samples. This is especially interesting to note in light of the differing densities of these layers. This may be due to two reasons. First, it is possible that the combination of relatively low molecular densities and a relatively high expected degree of disorder within these films is making it impossible to accurately detect the CH vibrations of these molecules. In the sensitivity experiments presented in Chapter 3, the lower detection limit of the system was found to be below the number of oscillators present in a sparse DNA film. However, it should be noted that the molecules probed in those experiments were in a highly-ordered self-assembled monolayer with the majority of the oscillators pointing in the same direction. When molecules are arranged isotropically, however, the result is a decreased overall resonant signal (see Chapter 2.6.1). In addition, it is possible that the low density of the molecules makes it more likely that the film contains a higher amount of contaminants, which could swamp out the signal from the ssDNA molecules.

It is entirely possible that this is the case for thymine and even cytosine, as C 1s XPS data of these films showed a relatively large peak at 285 eV attributed to contaminants, but the adenine film shows a reasonable density and a good C 1s peak with a large contributions at 287 eV (Fig. 4.7) that indicates that this film is primarily composed of adenine ssDNA. Castner and coworkers [85] examined non-thiolated adenine ssDNA on gold using NEXAFS and showed that

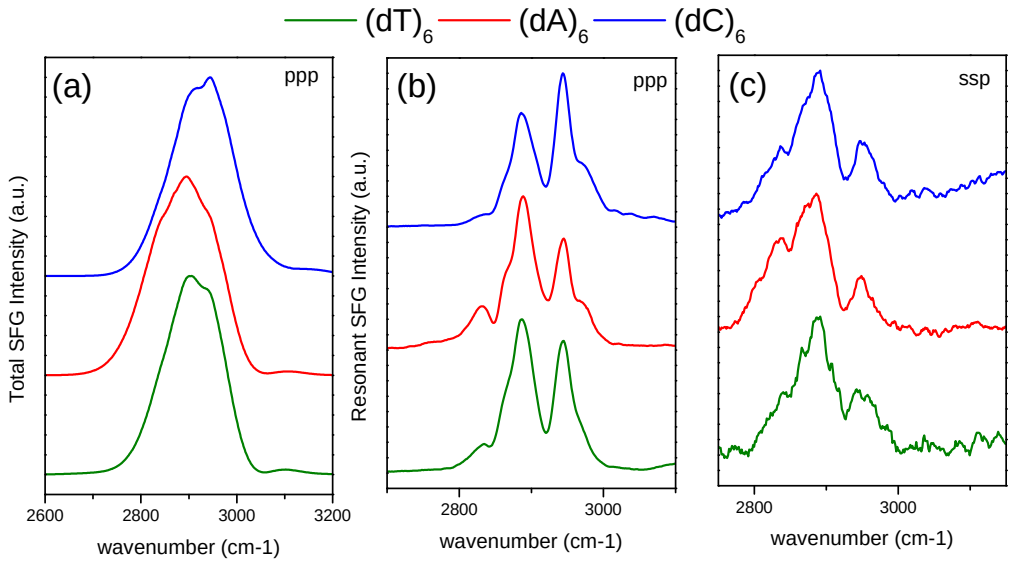

Figure 4.8: SFG spectra of films of unmodified thymine (green), adenine (red), and cytosine (blue) ssDNA, including raw spectra taken in ppp polarization (a), BGS spectra taken in ppp polarization (b), and BGS spectra taken in ssp polarization.

Table 4.2: Parameters obtained from a fitting of the raw SFG data for $(dA)_6$ shown in Fig. 4.8 with Voigt functions using phase as one of the variable parameters. Positions are given in cm^{-1} and phase in degrees. Possible peak assignments are also given.

ppp			ssp			
Position	Area	Phase	Position	Area	Phase	Assignment
-	-	-	2823	0.02	20	-
2868	0.07	20	2857	0.06	142	CH_2 sym
2892	0.16	120	-	-	-	-
2949	0.14	94	2952	0.16	92	CH_2 asym
2973	0.14	64	-	-	-	-

the molecules adsorbed in a configuration in which the adenine rings were perpendicular to the substrate, presumably attached via the nitrogen groups. This would indicate that the methylene oscillators in the backbone cannot be arranged in a completely random fashion and must have some form of preferential order. Therefore, it is most likely that in this film the peaks observed are due to the DNA sugar-phosphate backbone. This would in turn indicate that the similar peaks observed in the thymine and cytosine ssDNA films are also due to the backbone, and that the order in these films must be independent of nucleobase composition. The fact that there is no difference between adenine and cytosine indicate that in these SFG spectra of DNA in air, the methylene backbone vibrations dominate the spectra.

4.4.3 Thiolated DNA Films

Films of thiolated DNA were created in order to examine these molecules in a relatively highly-ordered surface-bound state. The molecules were attached to the surface via a C6-thiol linker connected to the 3′ end of the molecule as shown in Figure 4.9. Very short ssDNA consisting of only 6 nucleobases were chosen as previous results have shown that short DNA molecules form films with higher degrees of order than longer molecules [44]. It was hoped that a higher degree

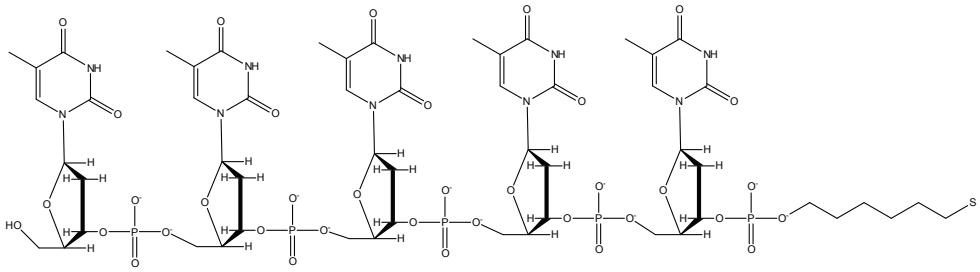

Figure 4.9: The chemical structure of a thiol-modified 5-mer thymine homo-oligonucleotide.

of order would maximize the SFG signal and highlight the differences between DNA films of different nucleobase compositions.

Verification of film quality in the thymine ssDNA layers using XPS revealed a C 1s spectrum typical of DNA, with a large C=C peak at 287 eV (Fig.4.10). The N 1s and P 2p peaks were also strong and yielded a correct ratio of 2, indicating little to know nitrogen-containing contaminants [51]. The S 2p peak showed a strong peak for bound sulfur at 163 eV, and a small peak at 168 eV, indicating that some of the thiolated molecules in this film were oxidized, which may have contributed to a decreased overall order. Adenine and cytosine films were also examined using XPS and gave similar results. The densities of these films were calculated from the fitted XPS data and found to be 6.5×10^{13}, 3.5×10^{13}, and 5.1×10^{13} molecules/cm^2 for the thymine, adenine and cytosine films, respectively. As discussed in Section 1.2.1, the lower density for the adenine ssDNA films is expected, as the high affinity of these molecules for gold causes them to adsorb to the surface via both the sulfur group and the nucleobases [35]. This results in some of the molecules lying with an orientation more horizontal along the surface, taking up more space and preventing the adsorption of further DNA molecules. Thymine, on the other hand, is easily displaced from the gold surface by the thiolated linkers, resulting in more of these molecules standing upright and an overall higher density on the surface [37, 52].

A comparison of the BGS spectra of thymine thiolated ssDNA film and a film of the linker group alone (HS-$(C_2)_6$-OH) is shown in Figure 4.11. The raw data (Fig. 4.11a) show a similar peak at 2930 cm^{-1}. However, the peak at 2880 cm^{-1} is much more prominent in the spectrum of the linker group alone. The BGS spectra (Fig. 4.11b) revealed that most of the peaks in these spectra are in common between the two, including the most prominent peaks at 2880 and 2940 cm^{-1} observed in the raw data. This is unsurprising, as both the C6 linker and the backbone vibrations shown to be dominant in the spectra of unmodified DNA films contain exclusively methylene vibrations. The fact that some of the methylene groups in the DNA backbone are in a different environment should produce small differences in the spectra unless the linker groups are dominating the spectra. This situation was in fact found by Sartenaer and co-workers [58] examining DNA layers on Pt(111) with SFG spectroscopy. However, in these films of DNA on Au(111), from which we expect a slightly greater degree of order, there are two peaks that stand out as distinct in the spectra of $(dT)_6$: one at 2871cm^{-1} and another at 2912cm^{-1}. The peak at 2871cm^{-1} is close to the peak at 2868cm^{-1} was previously observed in the unmodified $(dA)_6$ layer and assigned to a methylene symmetric stretch stemming from the backbone, while the peak at 2912 cm^{-1} was observed in the thymine, adenine, and cytosine thiolated ssDNA spectra and is assigned to a methylene symmetric stretch from the backbone. The other peaks present are assigned to overlapping peaks from the backbone and the C6 linker.

It is clear to see from the data in Figure 4.12 that films of thymine, adenine, and cytosine homo-oligonucleotides adsorbed on gold give largely similar spectra. Given the results presented in Section 4.4.2, this is most likely due to the dominance of the methylene vibrations coming from the sugar-phosphate backbone, and compounded by the presence of the linker group, which are common to all film types and would give peaks in similar locations. It was initially assumed

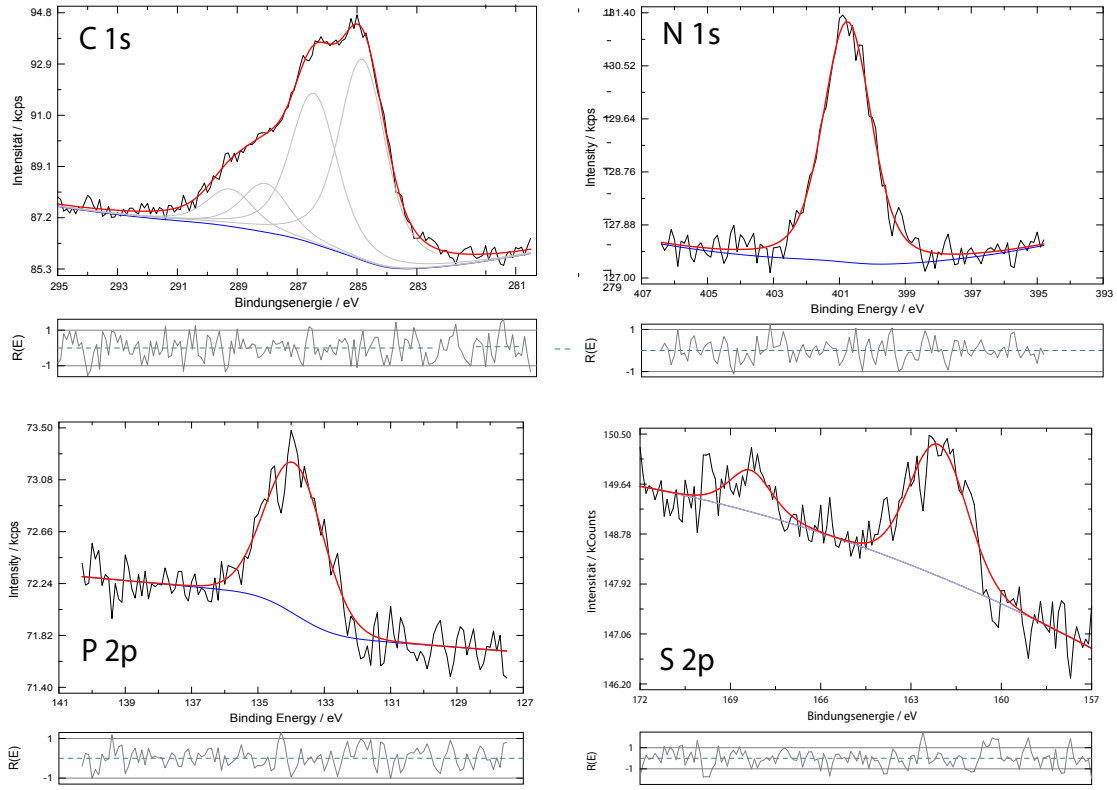

Figure 4.10: XPS C 1s, N1s, P 2p, and S 2P spectra for a 6-nucleobase thymine homo-oligonucleotide film.

that adding a thiol linker, at least to the thymine ssDNA strands, would cause these layers to adopt enough order so that the distinct methyl vibrations from the thymine bases could be seen. However, this proved not to be the case.

The values from a phase fitting of the data for the three types of thiolated ssDNA in ssp and ppp polarizations are given in Table 4.3. As can be seen from these data, the increase in peaks at this location in these two films is due to a combination of a phase change and an intensity increase (in the case of $(dA)_6$-S/Au) in the peak located at 2836 cm^{-1}, as well as a decrease in the intensity of the peak located at 2890 cm^{-1}. If the former peak is assigned to a methylene symmetric stretch coming from both the backbone and the thiol linker, its apparent change in phase in ppp polarization between the adenine and thymine ssDNA could correspond with a change in orientation of the sugar-phosphate backbone. Such a change in both intensity and orientation is also visible in the peak at 2890 cm^{-1} in ssp polarization. For the intensity and phase to change so drastically it would be likely that this is either a CH_2 asymmetric or symmetric stretch, and its 90° phase difference may be yet another indicator of a change in average backbone conformation between the thymine and adenine thiolated ssDNA films.

Nevertheless, the similarities in the overall spectral shapes for each of the three thiolated films suggests that the backbone and linker have similar amounts of overall disordering in each of the three film types. This may indicate that despite the differences in orientation in these films suggested by the XPS data, there is enough flexibility in these DNA chains that the methyl and methylene groups are still somewhat randomly oriented, at least on the level detectable by SFG spectroscopy. Considering the structure of a single-stranded DNA molecule and all the possible configurations it can adopt, this result is imaginable.

Previous work done by Lee and colleagues [39] using NEXAFS spectroscopy to probe the

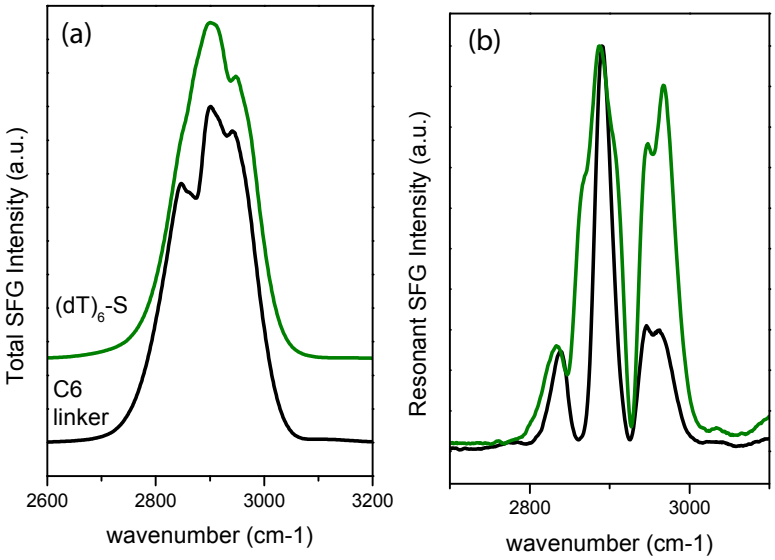

Figure 4.11: Comparison of SFG spectra the C6 linker group alone (black) and a thymine ssDNA film immobilized on gold via the C6 linker group (red) shown as (a) the raw spectra and (b) the background-suppressed spectra. The peaks at 2870 and 2912 cm^{-1} are assigned to methylene stretches from the sugar-phosphate backbone.

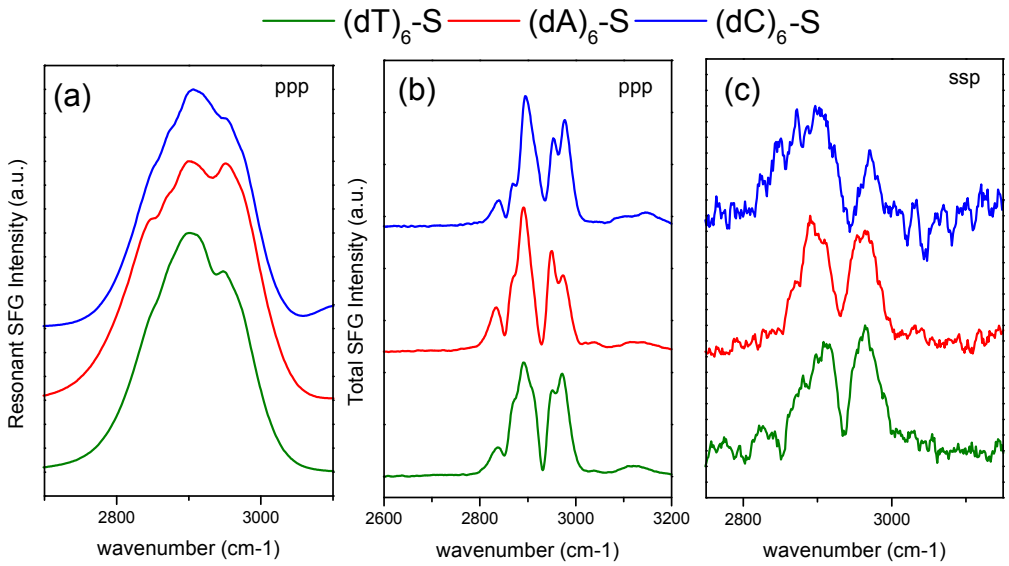

Figure 4.12: SFG spectra of films of thiol-modified thymine (green), adenine (red), and cytosine (blue) ssDNA, including raw spectra taken in ppp polarization (a), BGS spectra taken in ppp polarization (b), and BGS spectra taken in ssp polarization. All spectra were normalized to 1 to facilitate comparison, however all intensities were initially similar.

Table 4.3: Parameters obtained from a fitting of the raw SFG data for $(dT)_6$-S, $(dA)_6$-S, and $(dC)_6$-S ssDNA films shown in Fig. 4.12 with Voigt functions using phase as one of the variable parameters. Positions are given in cm^{-1} and phase in degrees. Possible peak assignments are also given. *Indicates that this peak was located at a position of ± 5 cm^{-1} from the given value.

		$(dT)_6$-S/Au		$(dC)_6$-S/Au		$(dA)_6$-S/Au		
Polarization	Position	Area	Phase	Area	Phase	Area	Phase	Assignment
ppp	2836	0.02	136	0.06	86	0.25	96	
	2868	0.36	109	0.34	112	0.44	111	CH_2 sym
	2890	0.28	104	0.06	119	0.08	93	
	2901	0.05	74	0.05	110	0.05	95	
	2935*	0.17	120	0.17	105	0.24	112	CH_2 asym
ssp	2836	0.31	109	0.26	105	0.21	103	
	2868	0.35	110	0.29	108	0.41	112	CH_2 sym
	2890	0.25	106	0.01	180	0.01	29	
	2901	0.10	100	0.45	109	0.43	110	
	2939*	0.23	109	0.34	110	0.34	113	CH_2 asym

orientation of thiolated thymine ssDNA immobilized on gold. They found a slight degree of orientation of the plane of the nucleobases along the plane of the sample. However, the overall alignment was somewhat weak, suggesting that there was not a high degree of order in these films. This may also be the case in these samples, although even in a situation in which the nucleobases are stacked, it would be quite difficult to get a strong preferential alignment of the methylene groups in the backbone. An irregular orientation of the backbone would in turn affect the orientation of the individual nucleobases in the film, resulting in a disordering of the methyl groups in the thymine nucleobases and giving rise to these results.

In order to verify the hypothesis that these signals were indeed stemming from the backbone, we attempted to induce more order in these systems by exposing them to water and allowing it to evaporate. Previous research has shown that DNA molecules attached at one end to a solid surface can be straightened by exposure to a receding air/water interface [144]. However, in that work the DNA strands were unmodified and straightened along a surface rather than perpendicular to it. It was hypothesized that a degree of ordering could also be induced in dense films of surface-bound DNA, potentially through both the action of the receding air/water interface and the exposure to solution, which should allow the DNA strands to rearrange to a more energetically favorable ordered configuration.

The data of adenine and thymine ssDNA films through two evaporation cycles are shown in Figure 4.13. A control of the same procedure performed on a bare gold substrate is also shown for comparison. The initial films of thymine and adenine (ladled (a) in Fig. 4.13) show the typical shape of an ssDNA film, with a large prominent peak at 2940 cm^{-1} and smaller features between 2860 and 2890 cm^{-1}. The gold control shows broader, less specific peaks, although they are in positions similar to the peaks in the DNA films. This is presumable due to the fact that the primary oscillators in adventitious carbon contamination are also expected to be methylene.

After the first wetting and drying cycle in the ssDNA films (spectra (b) in Fig 4.13), additional peaks around 2860 and 2960 cm^{-1} become prominent. After the second cycle (spectra (c) in Fig 4.13), they are even more so. The position of the Gaussian non-resonant background changes slightly for each of the measurements due to the repositioning of the sample, however the locations and overall shapes of the Lorentzian resonant contributions are highly similar between the adenine and thymine ssDNA, further confirming that the CH vibrations being measured here are from the sugar-phosphate backbone and C6 linker common to both of these molecules. The gold control sample, however, shows perhaps a slight increase in the definition of the peaks above 2900 cm^{-1}, but not the significant increase observed in the DNA films. It is possible that the increase in peak intensity observed is due to some interaction of the DNA strands and contami-

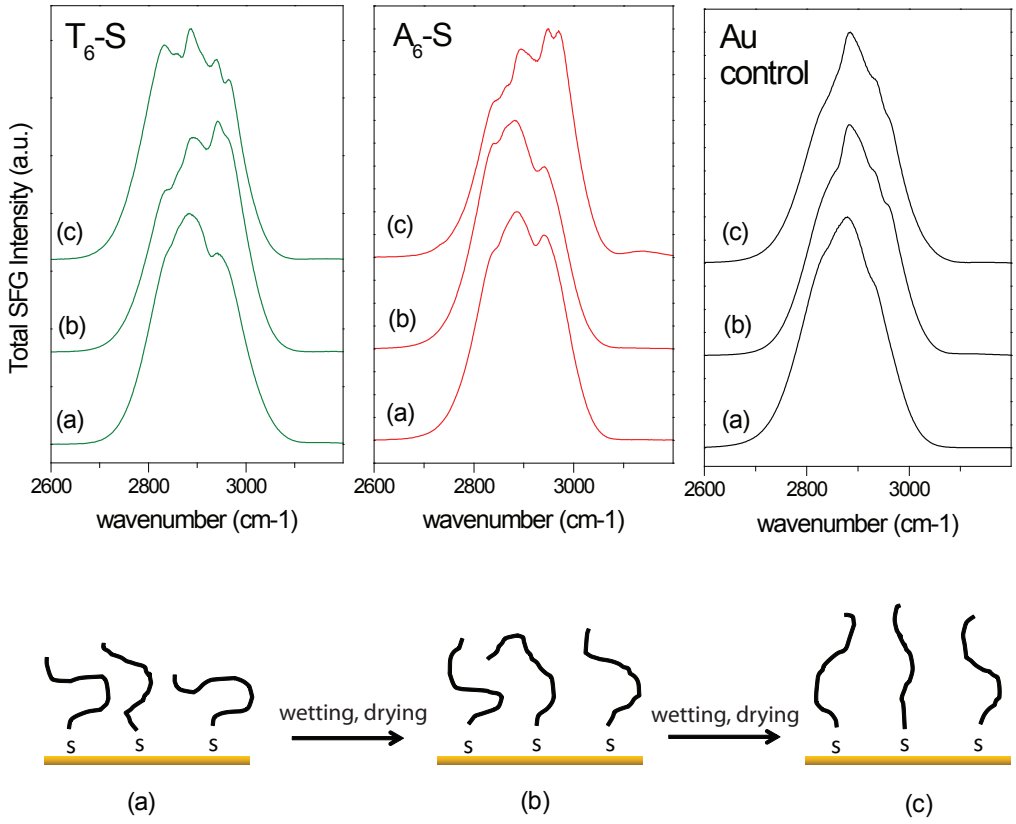

Figure 4.13: Raw spectra of a T_6-S film, a A_6-S film, and a bare gold substrate over repeated wetting and drying. (a) initial films (b) films after 1 wetting and drying cycle (c) films after 2 wetting and drying cycles. The cartoon below offers a graphic description of the hypothesized straightening of the DNA molecules occurring as a result of the wetting and drying in the ssDNA films.

nants, which would explain why it does not occur in the bare Au control. Test on the wetted and dried samples with XPS did indeed show an increase in the peak at 285 eV, indicative of contaminants. However, it was observed through multiple repeats of these experiments with SFG spectroscopy that the positions and relative intensities of these peaks were always similar. If this were indeed caused by contamination, we would expect to see changes in the spectra between samples and between runs, as there are many different types of contaminant molecules which will adsorb to the surface in different ways. This observation further confirms that the changes occurring in the ssDNA layers are due to the presence of DNA molecules and not due to contamination being deposited on the sample during the course of the wetting and drying.

These results show that in air, the SFG spectra of ssDNA films is dominated by the non-specific signals emanating from the sugar-phosphate backbone. However, the fact that there appear to be no nucleobase-specific signals from these films of ssDNA on gold in the CH region may have a positive aspect, as it suggests that this technique could be used to examine overall order in the sugar-phosphate backbone of molecules in DNA films regardless of their nucleobase composition.

4.5 Conclusions

Examination and comparison of films of nucleobase multilayers, unmodified short homo-oligonucleotides (ssDNA), and thiolated short homo-oligonucleotides in air were performed in an effort to track the average orientation of the methyl group among these three types under ambient conditions using a label-free method. Investigation in the CH stretching region revealed clear differences between thymine and the other two the nucleobases which were minimized upon the addition of a sugar-phosphate backbone. It was further found that the addition of a linker group to the DNA molecules in order to improve their overall ordering did not result in the appearance of nucleobase-specific peaks, a fact that was attributed to the dominance of the methylene stretches from the sugar-phosphate backbone and linker group in the SFG spectra in this region. This hypothesis was supported by inducing more order in the films through cycles of wetting and drying, which increased the intensity of the peaks in the ssDNA films, but not in bare gold controls. These clearer peaks were similar in both adenine and thymine ssDNA films, confirming that the primary signal was stemming from the linker and backbone CH groups common to both.

These results demonstrate that while SFG can be used to obtain molecular-level label-free orientation about the methyl groups in thymine, for films of DNA in air it gives information almost exclusively about the methylene groups in the sugar-phosphate backbone and linker groups. This could make it a potentially useful complimentary technique to those such as NEXAFS, which give information about the orientation of the nucleobases. The SFG results presented here suggest that the average orientation and disordering of the backbone or backbone and linker is similar in all three short-chain DNA types tested. This is a reasonable assumption given the fact that DNA molecules are relatively flexible when in a single-strand state, and may suggest that although previous studies with NEXAFS have shown a level of ordering and stacking in the nucleobases of thymine ssDNA immobilized on gold, in the backbone of these molecules there is still a relatively large amount of disorder.

Chapter 5

Surface-Bound DNA *in situ*

5.1 Summary

Understanding the organization and orientation of surface-immobilized single stranded DNA (ssDNA) in aqueous environments is essential for optimizing and further developing the technology based on oligonucleotide binding. In this chapter, SFG spectroscopy was used to compare the structure and orientation of ssDNA films of different nucleobase compositions in air and in water in the CH stretching region. Tests on thiolated ssDNA films of different nucleobase compositions in air versus water revealed a differences in the degree of solvation among these films types. This observation was tied to the different conformations of the DNA strands in the films owing to differing affinities for the gold substrate. Interestingly, the spectra of the different films upon solvation in water appeared to show nucleobase-specific features for DNA containing thymine. Further tests revealed that that this result occurred in both short- and long-chain thymine ssDNA. It was hypothesized that the appearance of these unique thymine peaks was due to a decrease of the dominant backbone and linker group methylene signals upon exposure to water, as the entire DNA chain gained more flexibility in the aqueous environment.

5.2 Background

Many of the most useful techniques for determining information about biological molecules at interfaces on a molecular level and label-free (XPS, NEXAFS, IRRAS, etc.) are performed either under ultra-high vacuum (UHV) conditions, or in air. However, the ability to characterize ssDNA films in aqueous environment is important because it allows for the examination of these films *in situ* —the conditions under which they are actually used. Furthermore, the ability to directly compare results obtained *in situ* and *ex situ* can provide a way to determine whether the results obtained in air or under ultrahigh vacuum conditions are applicable in aqueous environments. In this chapter, information obtained from the proof-of-principle experiments shown in Chapter 3 and the understanding of ssDNA films in air presented in Chater 4 were applied to gather knowledge about the changes that these films undergo when exposed to *in situ* conditions. The goal of these experiments was to determine how these films changed in water versus in air and correlate these changes to the current understanding of these systems.

DNA is a flexible molecule with the potential to adopt multiple conformations depending on the local microenvironment (see Chapter 1). This raised the question of how much variability would be present in the spectral shapes of thymine ssDNA upon exposure to liquid. A high degree of change among the spectra across multiple experiments would indicate a high degree of sensitivity of these films to external conditions upon rearrangement in liquid, while a low degree of change would indicate that the changes occurring upon exposure to liquid were largely due to molecular properties.

Pure water was chosen as the liquid environment for these experiments, as it was expected that the lack of any screening charges would maximize electrostatic repulsion between the strands and thus cause the greatest degree of order, increasing the chances of obtaining a clear SFG sig-

nal. Furthermore, pure water has a much lower experiment-to-experiment variability than buffer solution, which must be made fresh for each experimental run and thus will be slightly different each time. Experiments in standard 1M NaCl-TE buffer were also performed with variable results, so for clarity of presentation only those data obtained from samples in water are presented and discussed. Adenine and thymine molecules were also tested as controls for the CH region, as they contain all the same oscillators as the thymine ssDNA in the backbone and linker, but differ in base-specific CH groups.

5.3 Experimental Details

Short-chain (6-mer), thiol-modified thymine, adenine, and cytosine homo-oligonucleotides were chosen for these experiments. Experiments were conducted at least 6 times, although tests with background suppression were performed only twice. The films for some of these experiments were made in the 1 M PBS solution described in Section 2.1.3, although the larger part was made in the 1 M TE-$CaCl_2$ buffer, as it was found that higher DNA densities were achievable using this method.

Characterization and assessment of film quality was performed for all of the films using IRRAS and XPS. Although the quality did vary to some extent, it was found that all layers had densities of $>2.0 \times 10^{13}$, which is considered good surface coverage in the literature [37, 51]. SFG measurements were made as described in Chapter 2 and the data were processed according to the procedures outlined in Section 2.6.3.

5.4 Results and Discussion

5.4.1 Structure Changes in Water

The ability of a solution to penetrate or not penetrate a thin film is of importance in such areas as protein adsorption [125, 145], molecular rearrangement upon exposure to stimuli such as temperature [10], and the effectiveness of hybridization in DNA films [146, 38, 62]. Zolk *et al.* [125] examined the solubility of oligo(ethylene glycol)-terminated self-assembled monolayers (OEG SAMs) in polar and non-polar solvents. They found that they could detect solvation of only the upper in H_2O versus the solvation of the entire layer in CCl_4 by examining the appearance of peaks attributed to Gauche defects in the SAMs.

Fitted SFG data typical of what was observed for nearly all of the experiments is shown in Figure 5.1. The densities for these films were 1.9×10^{13}, 2.0×10^{13}, and 2.3×10^{13} molecules/cm^2 for the adenine, cytosine, and thymine layers, respectively.

The somewhat drastic decrease in overall signal in the thymine ssDNA layers is in contrast to the work by Zolk *et al.*, who observed no such loss in overall signal [125]. This may be due to the difference in molecular density between ssDNA and OEG layers. OEG molecules have the ability to arrange themselves in relatively highly-ordered, densely-packed SAMs [145]. In molecular simulations of solvated OEG SAMs, Zhang and co-workers noted a reduced flexibility of these molecules which they attributed to the high packing density [145]. This may explain the retention in overall signal strength in the work by Zolk and colleagues: although the films in H_2O and CCl_4 were acquiring Gauche defects upon exposure to liquid, the density of the SAM was still high enough to restrict the mobility of these molecules, enforcing a particular conformation to some degree and resulting in a higher SFG signal.

Conversely, the formation of highly-ordered layers by DNA molecules is hindered by the strong electrostatic charge of the sugar-phosphate backbone as well as the greater size of these molecules [137, 43]. The density of the molecules for the thymine ssDNA film presented in Figure 5.1 translates to 0.23 molecules/nm^2, which is conceivably enough space for movement considering an idealized surface-bound 6-mer ssDNA strand 1 nm in diameter and 1.8 nm high at its fullest extension [137]. This relatively large amount of space surrounding the molecule could allow the sugar-phosphate backbone enough freedom of movement in the liquid environment to be continuously moving and changing position, resulting in a lower SFG signal due to the non-

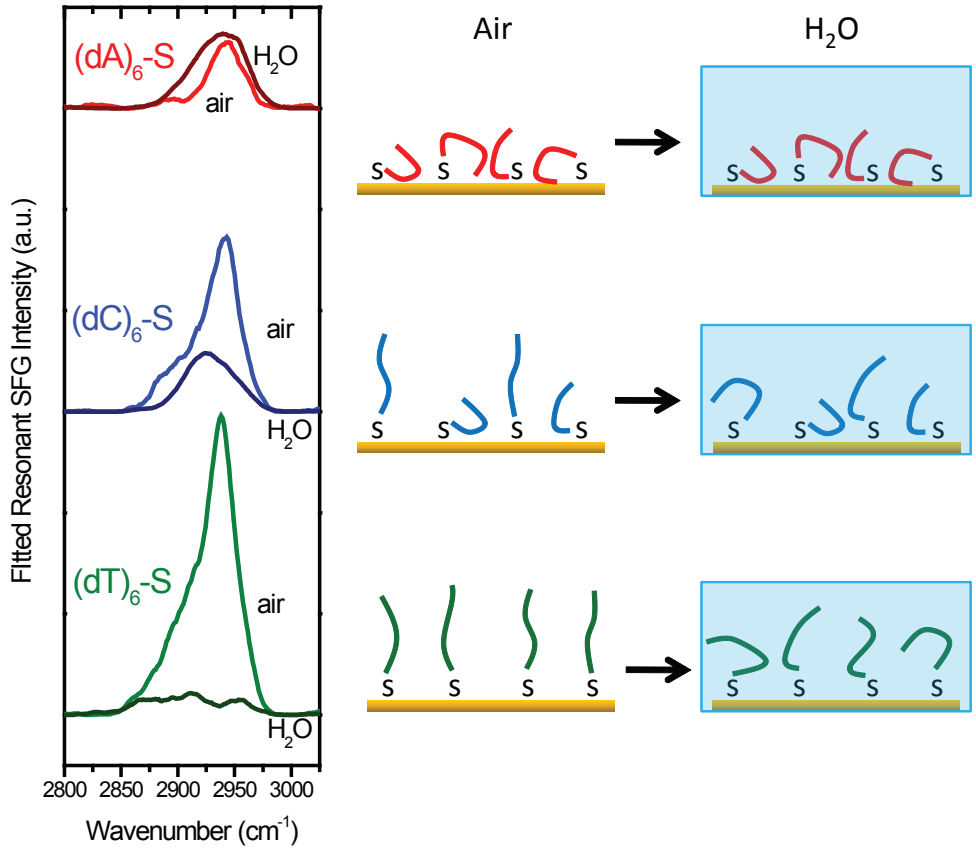

Figure 5.1: SFG spectra of thymine, adenine, and cytosine ssDNA layers in air and in water

alignment of the CH moieties as well as an increase in destructive interference from oscillators pointing in opposite directions.

The fact that the adenine ssDNA does not lose intensity as drastically as the thymine ssDNA in solution can be explained by the expected arrangement of these molecules with respect to the gold substrate. Adenine has been shown to have a significantly higher affinity for gold than thymine, resulting in a preferential attachment of these nucleobases to the gold [35, 34]. It is therefore likely that the adenine strands in this experiment are attached to the substrate not only through the thiol linker groups, but also to some extent through the nucleobases themselves. This is also in agreement with the results presented in Chapter 4 from a separate experiment. If this were indeed the case, it would mean that these strands have less mobility in solution than thymine strands, and we would expect to see less change when they are exposed to solution, as is the case. The fact that the peak is broadening is likely due to a slight increase in the dispersion of the beam caused by passing through the CaF_2 prism and the thin water film.

The cytosine film appears to lose more intensity than the adenine film, but less than the thymine film. This is consistent with the fact that this type of nucleobase has an affinity for gold between that of adenine and that of thymine [35]. It would therefore be expected that there would be an intermediate number of nucleotides in the ssDNA film bound to the surface, and thus an intermediate amount of DNA strands with high mobility to result in a decreased signal intensity. This is consistent with what is observed in Figure 5.1.

These results show that the structure changes in films of ssDNA exposed to water appear to be nucleobase-dependent, and largely related to affinity of the individual nucleobases comprising the DNA strand for the gold substrate. Films of thymine ssDNA, a nucleobase with a

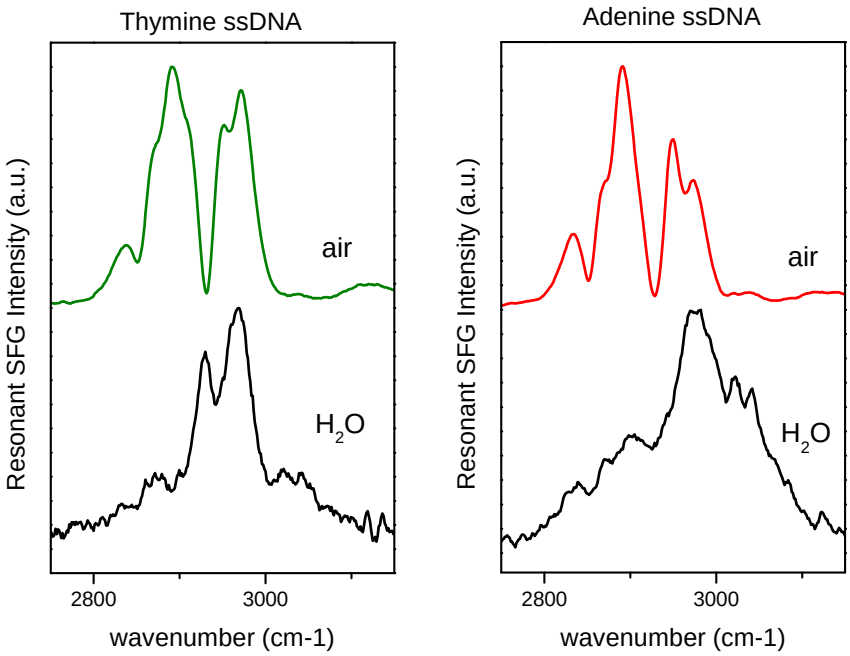

Figure 5.2: Raw (upper curves) and BGS (lower curves) SFG spectra of thymine (left panel) and adenine (right panel) ssDNA layers in air and in water

low affinity for gold, showed the most drastic changes, consistent with these molecules having a higher mobility on account of being bound to the substrate primarily through the thiol linker. Films of adenine ssDNA, a nucleobase with a high affinity for gold, showed little changes, likely due to the fact that these molecules are bound to the surface not only through the thiol groups, but also through a number of the nucleobases themselves. This would result in a lower mobility of these molecules upon exposure to solution. Films of cytosine ssDNA, a nucleobase with an intermediate affinity for gold, showed changes in spectra intermediate between thymine and adenine ssDNA films, in agreement with previous studies showing this type of nucleobase to have an affinity for gold between that of adenine and cytosine [35].

5.4.2 Nucleobase-Dependent Orientation in Water

Despite the low overall intensity of the ssDNA layers in water, the signal stemming from the CH groups in the solvated chains is still above the level of noise and can be further brought out by background suppression. The BGS data for the $(dT)_6$ and $(dA)_6$ thiolated films analyzed in air in Chapter 4, with corresponding densities of 9.5×10^{13} and 6.5×10^{13} molecules/cm^2, respectively.

Figure 5.2 shows a comparison of BGS data for thymine and adenine ssDNA films in air and H_2O. It is clear from the spectra that although these films appear quite similar when measured in air, upon exposure to solution they show distinct differences. Thymine shows two distinct peaks at 2927 and 2960 cm^{-1}, while adenine has one particularly prominent peak at 2975 cm^{-1}. Both adenine and thymine ssDNA films show smaller peaks at 2870 cm^{-1} as well as at 3020 and 3040 cm^{-1}, although these are barely above the noise level in these spectra. This is similar to the peaks seen above 3000 cm^{-1} in the spectra of the nucleobase multilayers (Fig. 4.3, although the peaks observed here are much sharper.

Upon phase-fitting (Table 5.1), it can be seen that the two most prominent peaks in the thymine ssDNA spectra in ppp polarization are both shifted 30 cm^{-1} higher than the methyl peaks observed in the thymine nucleobase multilayers (Table 4.1). Previous studies using IR

Table 5.1: Parameters obtained from a fitting of the raw SFG data for a thymine ssDNA film in H_2O with Voigt functions using phase as one of the variable parameters. Positions are given in cm^{-1} and phase in degrees. Proposed peak assignments are also given.

ppp			ssp			
Position	Area	Phase	Position	Area	Phase	Assignment
2927	0.28	98	2942	0.49	107	CH_3 sym
2960	0.05	180	2981	0.06	151	CH_3 asym/CH_2

spectroscopy to examine poly(vinyl methyl either) showed a blue shift of approximately 20 cm^{-1} in the methyl groups of these polymers as they moved from a dehydrated to a hydrated state [147]. It may be that what is visible in this BGS spectrum of thymine ssDNA in air are the methyl asymmetric and symmetric stretches of the thymine bases. This would be consistent with the appearance of the peaks above 3000 cm^{-1}, also assigned to the bases. It is conceivable that they would appear when the dominating signals from the backbone and linker groups are decreased due to the flexibility afforded them by the liquid environment. The bases themselves, however, are planar molecules with significantly less flexibility, and could therefore remain in their more energetically favorable stacked state with less mobility than the linker and backbone, or even arrange into a more highly ordered stacked state, as this is generally the most energetically favorable arrangement for these nucleobases [41].

Comparison of the thymine spectrum to the adenine spectrum in H_2O in Figure 5.2 shows that unlike the thymine spectrum, the adenine spectrum consists of really only one prominent peak. The location of the most prominent peak in this spectrum, located at 2975 cm^{-1}, is again approximately 30 cm^{-1} higher than the most prominent peak in the spectrum of the adenine nucleobase multilayer, located at 2945 cm^{-1}. Furthermore, the shape of this spectrum is quite similar to the shape of the spectrum from the adenine nucleobase multilayer shown in Figure 4.3. These observations suggest that this spectrum, like the spectrum of the thymine ssDNA film in H_2O, is dominated by the nucleobases.

An alternative explanation could be that a peak at approximately 2965 cm^{-1} is due to the backbone and linker groups in their hydrated state. This would be a likely explanation for the spectrum of the adenine ssDNA film, given that the intensity of the SFG signal from this film did not decrease as drastically as that of the thymine film. To further test this, we examined a $(dC)_6S$/Au film in a hydrated state. The background-subtracted SFG spectra for the three film types in air and in H_2O are shown in Figure 5.3. The spectra for the three film types in air are all similar in shape, with a main peak at approximately 2935 cm^{-1} and slightly differing peaks between 2860 and 2890 cm^{-1}, in agreement with the spectra in air shown in Chapter 4. In water, however, differences in the spectral shapes in the thymine and adenine ssDNA layers become apparent, similar to what was observed in the BGS spectra shown in Figure 5.2, with the thymine films showing two clear peaks and the adenine just one. The cytosine spectrum in water also shows just one major contribution, more similar to the adenine film than to the thymine film. The positions of the peaks in these spectra are slightly different than the peak positions shown in Figure 5.2. This is likely due to the phase of these peaks, which is a contributing factor in the background-subtracted spectra and not in the BGS spectra (see Section 2.6.3), and thus may cause an apparent shift in one spectral set versus the other.

An assignment of the single peak observed in the adenine and cytosine spectra to a hydrated state of the methylene backbone and linker groups would explain the similarity of the spectral shape between these two films, and would further indicate that the only the peak at 2927 cm^{-1} is due to the thymine bases, with the second expected peak at 2960 cm^{-1} either not present due to a more highly aligned conformation or present but strongly overlapping with the hydrated backbone/linker peak. However, given that the spectrum of the cytosine nucleobase multilayer appeared very similar to the adenine nucleobase multilayer, it could still be the case that what is observed in the cytosine spectrum is also a nucleobase-specific shape. Yet regardless of which of the two presented peak assignments is ultimately correct, these results still show that nucleobase-specific contributions, at least in the case of thymine homo-oligonucleotides, are

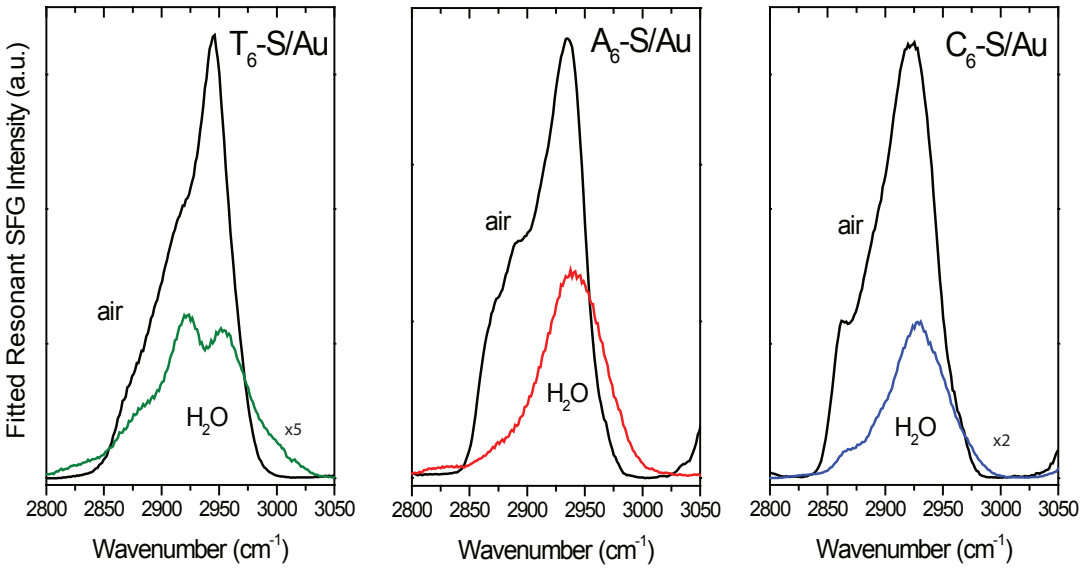

Figure 5.3: SFG spectra of thymine, adenine, and cytosine ssDNA layers in air and in water

present in the SFG spectra of hydrated ssDNA films.

In order to further test if the unique peaks observed in the thymine ssDNA layers were due to the short length of these molecules, which would be expected to form more ordered, stacked structures, or rather due to more to type of nucleobase, a longer thiolated thymine ssDNA film, $(dT)_{25}S/Au$, was tested. A comparison of the raw spectra for the short $(dT)_6S/Au$ film, the longer $(dT)_{25}S/Au$ film, and the $(dA)_6S/Au$ film in both air and H_2O are shown in Figure 5.4.

In air, the $(dT)_{25}S/Au$ film appears similar to the $(dT)_6$ and $(dA)_6S/Au$ films, with the major peak appearing at 2935 cm^{-1}, although further on the right side of the Gaussian than in the $(dT)_6S/Au$ and $(dA)_6S/Au$ films due to the position of the $(dT)_{25}S/Au$ sample during the time of measurement. When exposed to solution, however, the $(dT)_{25}S/Au$ film displays a spectral shape nearly identical to that of the $(dT)_6S/Au$ film, with two clear peaks: one at 2927 cm^{-1} and another at 2960 cm^{-1}. The $(dA)_6S/Au$ film, in contrast, displays only on broad peak at 2970 cm^{-1}. These results indicate that the nucleobase composition of the thymine film is more of a factor in the determination of the spectral shape in solution than the length of the DNA molecule.

Since it was hypothesized that the loss of signal in these layers was due to a loss of order in the sugar-phosphate backbone upon exposure to water, the question arose of whether the order induced by the repeated wetting and drying of these films presented in Chapter 4 would cause the film to retain some of its ordered structure. To test this, films of $(dT)_6$-S/Au that had been repeatedly wetted and dried were placed in H_2O and measured. The resulting raw spectra are shown in Figure 5.5.

The raw spectrum of the wetted and dried thymine film in air shows a spectral shape similar to those observed in Figure 4.13, with four clear peaks between 2860 and 2960 cm^{-1}, attributed to an increase in order in the sugar-phosphate backbone and linker groups. This apparent increase in order in air, however, does not seem to be retained when the film is exposed to water, as the spectrum of the wetted and dried film in water is highly similar to those of the $(dT)_6$-S/Au and $(dT)_{25}$-S/Au films in water.

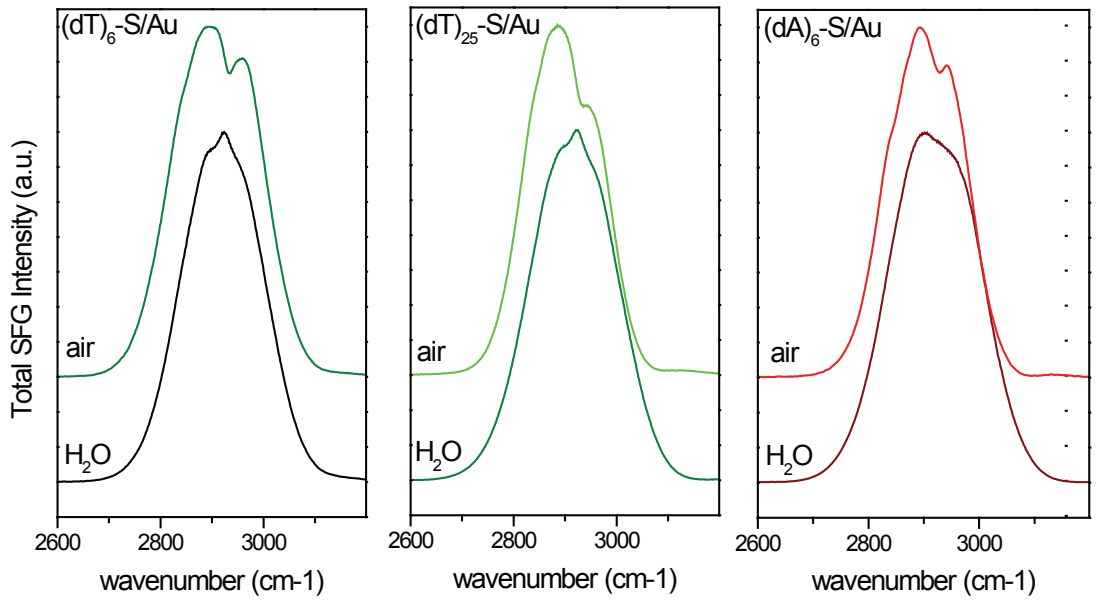

Figure 5.4: Raw SFG spectra of a $(dT)_6S/Au$, $(dT)_{25}S/Au$, and a $(dA)_6S/Au$ ssDNA layer in air and in water. The spectral shapes of all three films in air appear similar, however in water the two thymine films have similar shapes while the adenine film appears different, indicating that nucleobase type is the important factor in determining the spectral shape in solution.

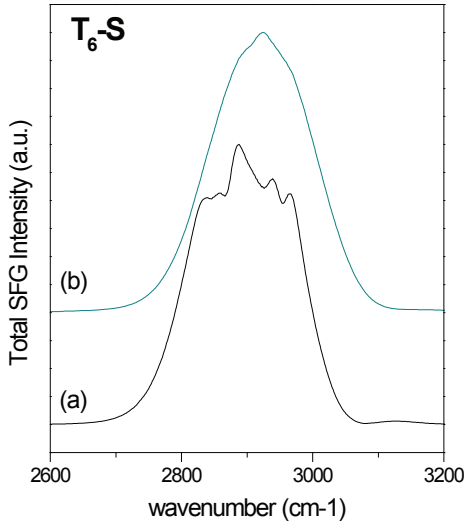

Figure 5.5: Raw SFG spectra of a $(dT)_6$-S/Au after two wetting and drying cycles (a) in air, showing the characteristic peaks of a DNA film with induced order and (b) in H_2O. In H_2O, the film still loses its ordered structure and adopts the spectral shape of a typical thiolated thymine film in water.

5.5 Conclusions

These data demonstrate the application of SFG spectroscopy to films of ssDNA immobilized on gold for comparison between air and aqueous environments. Tests on the solubility of thiolated ssDNA films of different types in water showed a significant decrease in the intensity of the thymine ssDNA films, less of a decrease in the cytosine films, and the least decrease in the adenine films. This was correlated to the preference of these different nucleobases for the gold substrate: the adenine ssDNA molecules are known to bind to the gold through not only the thiol linker but also through the high-affinity nucleobases, making drastic orientational and conformational changes in solution less likely, whereas the thymine molecule are known to adsorb to the gold primarily through the thiol linker alone, making it easier for these molecules to become more randomized upon exposure to the solution. Such a randomization could lead to a more isotropic environment for the CH groups in the sugar-phosphate backbone, resulting in a reduced SFG signal from these oscillators. A closer examination of these films in water revealed nucleobase-specific contributions from thymine ssDNA films which appeared to be independent of the length of the molecule, with both the $(dT)_6$ and $(dT)_{25}$ thiolated films showing similar spectra in water.

These results show that there are significant differences in the structure of ssDNA films *in situ* versus *ex situ*, and that SFG spectroscopy can be a useful technique for comparing the two. Furthermore, they show that the sugar-phosphate backbone and linker groups in the DNA strands have a significant degree of flexibility and a much more random orientation in liquid than in air. Such information could be useful for those seeking to connect *ex situ* orientational information to *in situ* performance of systems involving DNA immobilized on surfaces.

Chapter 6

Surface-Bound DNA Hybridization

6.1 Summary

Understanding hybridization and the structure of hybrids formed by DNA immobilized on solid surfaces is important for the further development of biotechnology based on these systems. In order to further this understanding, a combination of X-ray photoelectron spectroscopy (XPS), high-resolution XPS (HRXPS), near-edge X-ray absorption fine structure spectroscopy (NEXAFS), and sum-frequency-generation (SFG) spectroscopy was used to monitor two types of ssDNA films on Au(111) before and after hybridization. First, hybridization in films of different types was tested. Thiolated thymine d(T) homo-oligonucleotides and thymine-adenine d(A-T) block-oligonucleotides were chosen, as they represent two common types of ssDNA used for immobilization on gold substrates. In accordance with previous work, hybridization of the shorter and more densely packed thiolated ssDNA films produced fewer (if any) hybrids, whereas the longer and less densely packed layers exhibited a larger hybridization yield. These effects were less pronounced in the case of the d(A-T) films where the hybridization yield of the less densely packed monolayers was significantly lower. This was presumably due to the formation of inter- and intramolecular hybrids during the immobilization step of these self-complimentary d(A-T) probe molecules, resulting in the formation of fewer additional hybrids upon exposure to the target molecules. In all ssDNA films displaying a reasonable number of hybrids present, significant orientational changes were observed and could be monitored in detail. Second, films of surface-bound homo-oligonucleotides on gold were hybridized with a complementary strand and subjected to rinses using various volumes of water in preparation for *ex situ* spectroscopic analysis. It was found again through a combination of XPS, HRXPS, NEXAFS and SFG spectroscopy that lightly rinsed films contained relatively well-ordered DNA hybrids with mostly upright orientation relative to the surface, while films rinsed with a greater volume of water showed a decreased number of hybrids. For these films a significant disruption of their intactness and upright order in both target and probe DNA strands was observed, with the latter adopting a preferably horizontal orientation relative to the substrate. These results demonstrate the significant effects that rinsing with water can have on a hybridized DNA film and illustrate the importance of taking into account preparation procedures when interpreting *ex situ* spectroscopic data of such systems. Furthermore, the work presented in this chapter demonstrates the usefulness of the combined use of XPS, HRXPS, NEXAFS, and SFG spectroscopy for gaining information about surface-bound DNA hybrids.

6.2 Effects of Density and Film Type

6.2.1 Background

Reliable and efficient recognition of complex biomolecules is one of the major challenges of modern biology and medicine. Important in this regard are systems of surface-bound single-stranded oligonucleotides (ssDNA). Such systems can be used in multiple applications, including

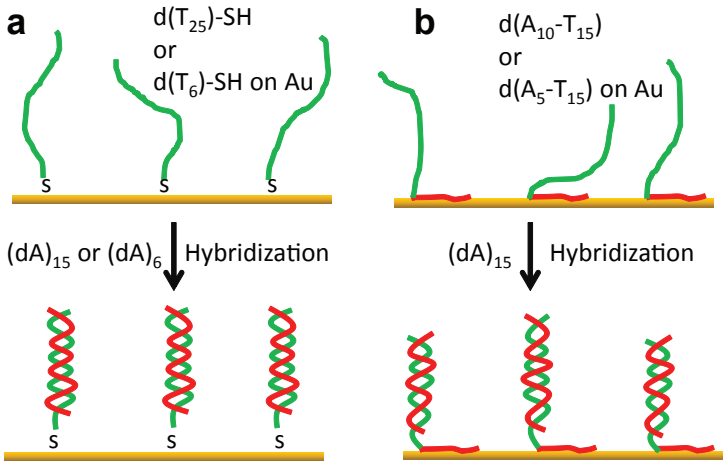

Figure 6.1: Schematical illustration of the experiments. Primary films of thiolated thymine homo-oligonucleotides a) and thymine-adenine diblock-oligonucleotides b) hybridized with the suitable adenine homo-oligonucleotides. The red and green colour codes are used for the thymine- and adenine-based oligonucleotides, respectively.

the detection of target nucleotides by hybridization [14], the functionalization of nanoparticles for use in specialized drug delivery systems [29], and directing the settlement of cells on surfaces [7]. As hybridization is the critical event in most applications of these systems, it is desirable to thoroughly understand this process in order to both optimize it and further its application to new areas and technologies.

In order to help achieve these goals, we examined the effects of hybridization in thiolated thymine and d(A-T) block types of ssDNA films (see Section 1.2.2) using XPS, high-resolution XPS (HRXPS), NEXAFS spectroscopy, and SFG spectroscopy. The goal of our study was threefold: first, to assess the extent of hybridization using these techniques; second, to gain molecular-level information on the orientational and conformational changes that occur as the result of the formation of hybrids and third, to determine the advantages and limitations of the techniques applied in the present study in terms of their usefulness for detecting hybrids and the changes due to their formation in the given types of systems.

6.2.2 Experimental Details

Two thiolated d(T) homo-oligonucleotides of different lengths (a 6-nucleobase strand, 5´-HS-$(CH_2)_6$-$d(T)_6$-3´ abbreviated to $(dT)_6$-SH, and a 25-nucleobase strand, and 5´-HS-$(CH_2)_6$-$(dT)_{25}$-3´ abbreviated to $(dT)_25$-SH) as well as two different d(A-T) block-oligonucleotides of different lengths (a 20-nucleobase strand, 5´-$d(A)_5$-$d(T)_{15}$-3´ abbreviated to d(A5-T15), and a 25-nucleobase strand, 5´-$d(A)_{10}$-$d(T)_{15}$-3´, abbreviated to $d(A_10\text{-}T_15)$), as well as $(dA)_6$ and $(dA)_{15}$ target sequences, were used as received as described in Section 2.1.3. In both cases, varying the lengths of the probes was intended to affect initial film parameters such as packing density and orientation of the film constituents, as well as hybridization dynamics. The idea of the experiments is schematically shown in Figure 6.1, along with the assumed adsorption geometry of the ssDNA molecules comprising the initial unhybridized ssDNA films.

After rinsing, samples for examination prior to hybridization were dried under flowing N_2 while samples intended for treatment with the hybridization step were placed in a 3microM solution of either $(dA)_6$ [for $(dT)_6$-SH films] or $(dA)_{15}$ [for $(dT)_{25}$-SH, $d(A_5\text{-}T_{15})$ and $d(A_{10}\text{-}T_{15})$ films)]. After hybridization, samples were rinsed with 1M NaCl buffer for 1 min, briefly dipped in deionized water to remove excess salts, and finally dried under flowing N2 according to previ-

ously described procedures [74]. It should be noted that treatments of these types of films in order to prepare them for *ex situ* measurements, in particular rinsing with pure water, even though very gentle in our case, are known to affect the stability of any hybrids present [74, 37]. Therefore, the state of these films as measured (i.e. after the hybridization step, including dipping and drying) may vary to some extent from what would be observed for these films *in situ*. Furthermore, the term "hybridization" is used here to refer to any degree of base-pair association of the probe and target molecules which remains after the above cleaning procedure.

The unhybridized ssDNA films and those after the hybridization step were either characterized immediately or stored under an inert gas atmosphere in glass containers until the experiments at the synchrotron (see below). The films were characterized by XPS, HRXPS, NEXAFS spectroscopy, and SFG spectroscopy as described in Chapter 2. All experiments were performed at room temperature. The XPS, HRXPS, and NEXAFS measurements were carried out under UHV conditions at a base pressure better than 1.5×10^{-9} mbar. The spectra acquisition time was selected in such a way that no noticeable damage by the primary X-rays occurred during the measurements [104, 85]. The SFG experiments were performed in air using a ppp polarization combination.

6.2.3 Results

6.2.3.1 XPS

XPS data were only used for determination of the packing density of the unhybridized ssDNA films according to the procedure suggested by Petrovykh *et al.* [51]. The packing densities of the $(dT)_6$-S/Au, $(dT)_{25}$-S/Au, $d(A_5\text{-}T_{15})$/Au and $d(A_{10}\text{-}T_{15})$/Au films were estimated to be 4.1×10^{13}, 2.0×10^{13}, 1.6×10^{13}, and 9.2×10^{12} molecules/cm^2, respectively, based on previously published procedures [60]. Note that above and in the following, the specifications $(dT)_6$-S/Au and $(dT)_{25}$-S/Au are used for the films prepared from $(dT)_6$-SH and $(dT)_{25}$-SH, respectively, in view of the abstraction of the hydrogen atom upon adsorption.

6.2.3.2 HRXPS

C 1s and N 1s HRXPS spectra of the ssDNA films before and after hybridization are presented in Figures 6.2 and 6.3, with the samples after the hybridization step denoted by either :A_6 or :A_{15} (we use the abbreviations T_n-S, A_nT_m, and A_n in the spectroscopic figures instead of $(dT)_n$-SH, $d(A_n\text{-}T_m)$/Au, and $d(A)_n$, respectively, in the text).

The HRXPS spectra exhibit the characteristic emissions of ssDNA films [39, 87, 74, 64, 81, 44, 37, 82, 83, 51, 60]. In particular, the C 1s spectra in Figure 6.2 show a characteristic pattern of at least four emissions at BEs of 285.0, 286.65, 288.0, and 289.3 eV, with the former peak being dominant [39, 81, 82, 83]. The N 1s spectra in Figure 6.3 exhibit the characteristic features of the adenine and thymine nucleotides (see below).

The C 1s, O 1s, and P 2p spectra of all unhybridized ssDNA films are quite similar to one another, independent of the exact nucleotide composition and the use of either a thiol linker group or a $(dA)_n$ anchor. This is in agreement with previous results, at least regarding the nucleotide composition [81, 37, 83]. However, what is probably even more important in the context of the current study - these spectra, apart from the total intensity changes, do not change significantly after the hybridization step. This means that the acquisition of C 1s, O 1s or P 2p XPS spectra is not suitable to measuring changes resulting from the formation of hybrids these films.

In contrast to the abovementioned data, the N 1s HRXPS spectra in Figure 6.3 are quite specific with respect to the exact nucleotide composition of the unhybridized ssDNA films, which is in accordance with previous observations [81, 37, 83]. The spectra of $(dT)_6$-S/Au and $(dT)_{25}$-S/Au films are dominated by a strong emission at a BE of 400.5 eV accompanied by a weak shoulder at a BE of 398.5 eV. The emission is ascribed to the thymine moieties in the upright $(dT)_n$ strands while the shoulder is believed to be mostly related to the thymine moieties which are in direct contact with the substrate [44]. These features have 93% and 7% of the total intensity, respectively. The N 1s spectrum of the reference adenine $(dA)_15$/Au film exhibits two emissions at BEs of 398.7 and 400.5 eV with the characteristic intensity ratio of 2:1 [81, 37, 83]. These energies are slightly lower

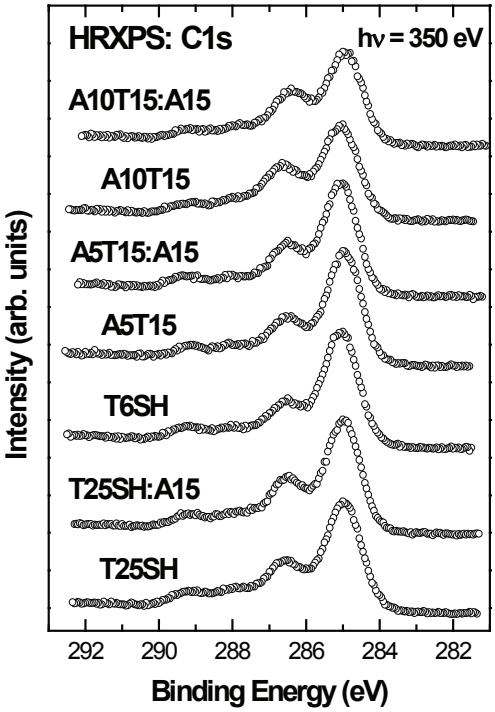

Figure 6.2: C 1s HRXPS spectra of the ssNDA templates before and after the hybridization step.

than the analogous values for the upright adenine homo-oligonucleotides (399.0 and 400.8 eV, respectively) [83], which is probably related to the stronger screening of the photoemission hole by the electrons in the gold substrate in the case of the horizontal adsorption geometry which has previously been measured for similar systems [148]. Note that it is currently assumed that the N 1s spectral feature of adenine is not affected by interaction with the gold surface, unlike what is apparent in the thymine spectra [37]. There are however still some debates on this subject [83].

The N 1s spectra of the d(A_5-T_{15})/Au and d(A_{10}-T_{15})/Au films are, in accordance with the molecular composition, a superposition of the spectra of the d(A) and d(T) portions of the oligonucleotides. These spectra as well as the spectra of the hybridized films (see below) were decomposed into the individual contributions related to the $(dT)_n$ and $(dA)_n$ fractions, taken, as described in the previous paragraph, the one-peak spectrum of $(dT)_n$ and the two-peak spectrum of $(dA)_n$ as the principal components. Significantly, the relative spectral weights of the adenine and thymine components in the d(A_5-T_{15})/Au and d(A_{10}-T_{15})/Au films, which are 1:5 and 2:3.3, respectively, correspond roughly to the molecular composition, which would be not the case if a significant part of the thymine block were in direct contact with the substrate. As mentioned above and reported in the literature [37], this configuration would result in a higher intensity of the emission at 398.5 eV in the N 1s spectrum of thymine, which would coincide with the strongest peak in the spectrum of adenine. Subsequently, a much higher spectral weight of adenine (compared to the molecular composition) would be recorded in the spectra of the d(A_5-T_{15})/Au and d(A_{10}-T_{15})/Au films, which is definitely not the case. On the contrary, a higher weight of thymine (compared to the molecular composition) is observed for d(A_5-T_{15})/Au, which can be tentatively explained by the attenuation of the adenine-related signal by the thymine block "overlayer". This effect is less pronounced for the more loosely packed d(A_{10}-T_{15})/Au film.

The N 1s spectra of the $(dT)_{25}$-S/Au, d(A_5-T_{15})/Au, and d(A_{10}-T_{15})/Au films change after the hybridization step, exhibiting an increase in the peak at 398.7 eV associated with the adenine nucleobase (the most intense peak in the characteristic doublet). This suggests an increased number of the d(A) nucleotides present in the film after the hybridization step, as would be expected.

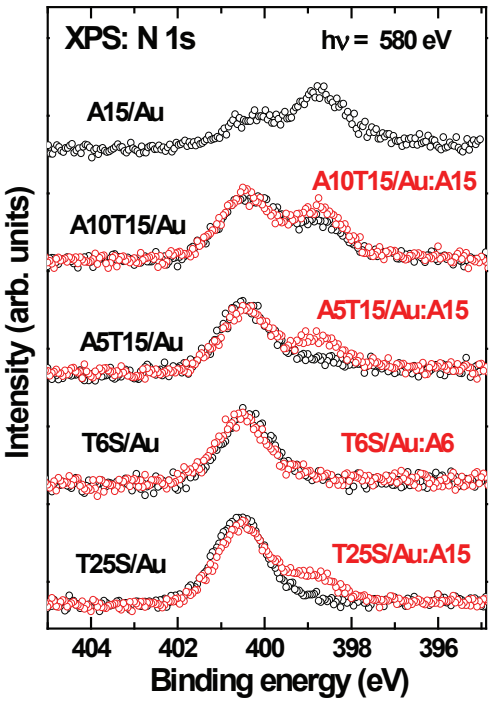

Figure 6.3: N 1s HRXPS spectra of the ssNDA templates before black) and after red) the hybridization step.

In contrast, almost no change was observed in the case of $(dT)_6$-S/Au, indicating that there were no additional adenine nucleotides present in this film after hybridization and the cleaning procedure.

In order to obtain an estimate of the percentage of the target $(dA)_6$ or $(dA)_{15}$ strands in these films, we performed a decomposition of the N 1s HRXPS spectra of the DNA monolayers after the hybridization step, taking the spectra of pristine $(dT)_6$-S/Au, $(dT)_{25}$-S/Au, and $(dA)_{15}$/Au as references, and correcting for the initial branching of the individual components and molecular composition. The resulting estimates for the hybridization degree are 31.5%, 4%, 26%, and 11% for $(dT)_{25}$-S/Au, $(dT)_6$-S/Au, $d(T_{15}\text{-}A_5)$/Au, and $d(T_{15}\text{-}A_{10})$/Au, respectively.

6.2.3.3 NEXAFS spectroscopy

The N K-edge NEXAFS spectra of the unhybridized films are quite specific with respect to the nucleotide composition of the DNA moieties. These spectra (55°), along with the analogous spectra acquired after hybridization, are presented in Figure 6.4, while the respective difference spectra ("90°" - "20°") are depicted in Figure 6.5.

The N K-edge spectra of the primary and reference films in Figure 6.4 show the shape typically obtained from ssDNA films [39, 44, 83, 148] and exhibit the characteristic π*-like resonances of the respective nucleobases in the pre-edge region, viz. t1 and t2 for thymine and a1 and a2 for adenine. The t1 and t2 resonances of thymine at 401.1 and 402.0 eV correspond to the N1s LUMO and N1s LUMO+1 transitions, respectively; these transitions involve all nitrogen atoms of this particular base [149]. Similar, the a1 and a2 resonances of adenine at 399.4 and 401.3 eV correspond to the N1s LUMO and N1s LUMO+2 transitions, respectively; these transitions involve all nitrogen atoms of adenine [149]. Both t1/t2 and a1/a2 pairs exhibit the characteristic intensity branching between the individual components [149]. Whereas the π* resonance features in the spectra of $(dT)_6$-S/Au and $(dA)_{15}$/Au are exclusively representative of either thymine or

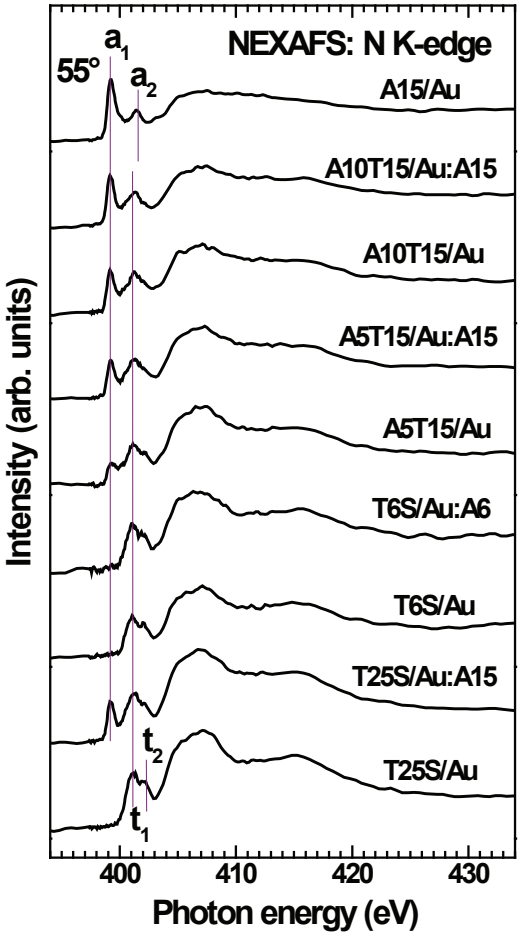

Figure 6.4: N K-edge NEXAFS spectra of the ssNDA templates and reference A_{15} film before and after the hybridization step. The spectra were acquired at an X-ray incidence angle of 55°. The positions of the most pronounced, π*-like absorption resonances of thymine (t1 and t2) and adenine (a1 and a2) are marked by the vertical gray solid lines.

adenine, the spectra of d(T_{15}-A_5)/Au and d(T_{15}-A_{10})/Au contain a superposition of the above features. In accordance with the molecular composition, the contribution of the adenine-related features is larger in the spectrum of d(T_{15}-A_{10})/Au as compared to d(T_{15}-A_5)/Au. Interestingly, the spectrum of $(dT)_6$-S/Au does not exhibit an additional feature at 399.0 eV, which, as mentioned above, has been previously observed for such films and attributed to the thymine bases which are in direct contact with the gold substrate [44, 83]. Significantly, no analogous shift in the resonance position has so far been observed for adenine ssDNA films, as follows from the inspection of the spectra of $(dA)_{15}$/Au.

Along with the conclusions mentioned above, information on the orientational order and molecular orientation in the probe films can be derived by monitoring linear dichroism effects in X-ray absorption, as previously stated. The 90°-20° difference spectra of the unhybridized ssDNA templates and reference $(dA)_{15}$/Au film in Figure 6.5 exhibit either negative or positive peaks at the positions of the characteristic absorption resonances of the thymine and adenine bases, which implies the presence of a certain orientational order in the target films. Considering that the respective molecular orbitals have π* character, i.e. are oriented perpendicular to the planes of the nucleobases, the negative sign of the difference peaks (indicating a higher absorption intensity at the grazing incidence) suggests that the nucleobases are preferentially orientated parallel to the

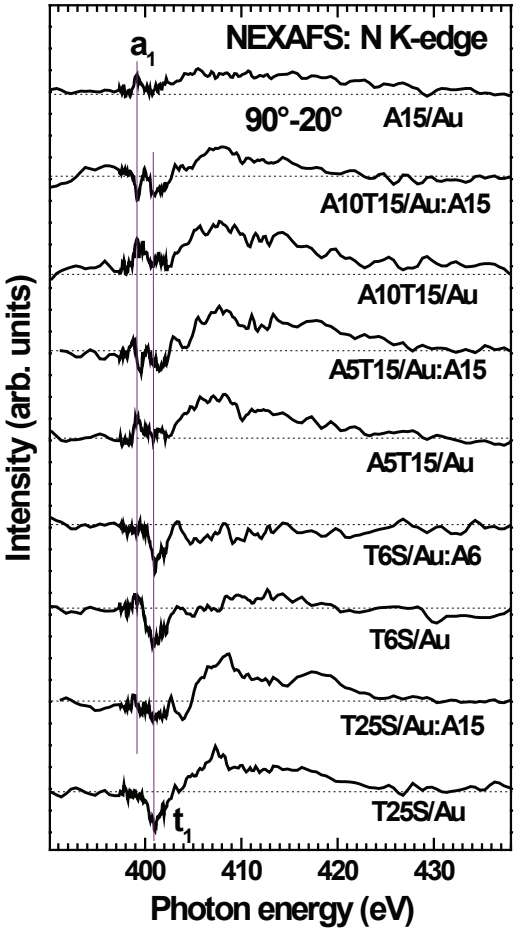

Figure 6.5: N K-edge NEXAFS difference (90˚-20˚) spectra of the ssNDA templates and reference A15 film before and after the hybridization step. The positions of the most pronounced, π*-like absorption resonances of thymine (t1) and adenine (a1) are marked by the vertical gray solid lines. The horizontal dashed lines correspond to zero for the individual spectra.

substrate surface, i.e. the ssDNA strands are standing upright. Vice versa, the positive sign of the difference peaks (indicating a higher absorption intensity at the normal incidence) suggests that the nucleobases are preferably orientated perpendicular to the substrate surface, i.e. the ssDNA strands are laying on the substrate. The latter is clearly the case for $(dA)_{15}/Au$, where a positive peak is observed at the position of the a1 resonance. So, the $(dA)_{15}$ strands are predominantly oriented parallel to the Au substrate, which could be expected on the basis of available literature data [37, 148]. In contrast, the distinct negative peak at the positions of the most intense t1 resonance for $(dT)_6$-S/Au and $(dT)_{25}$-S/Au suggests a predominant upright orientation of the ssDNA strands in these films, which, again, is in accordance with the literature [39, 44, 83, 148].

Similar to the case of $(dA)_{15}/Au$, the difference spectra of $d(A_5\text{-}T_{15})/Au$ and $d(A_{10}\text{-}T_{15})/Au$ exhibit a positive peak at the position of the a1 resonance and only a very weak (if any) negative peak at the position of the t1 resonance. This means that the $(dA)_n$ anchor blocks of the $d(A_5\text{-}T_{15})$ and $d(A_{10}\text{-}T_{15})$ oligonucleotides are predominantly oriented parallel to the gold substrate, most likely in the direct contact with it, whereas the $(dT)_{15}$ stems are mostly disordered, with probably only a weak tendency toward upright orientation. The reason for such a disorder could be a weak intra- molecular hybridization between the complimentary $(dA)_n$ and $(dT)_{15}$ blocks of these

molecules occurring after deposition, or partial inter-molecular hybridization occurring in solution prior to deposition [37]. However, it can be concluded from the lack of the 399.0 eV feature associated with the direct contact of thymine with the substrate (see above) in the 55° spectra, that after deposition only adenine is bound to the Au substrate, in agreement with the findings of previous studies [35]. Presumably, at the level of the single molecule, there is a partial coordination of the $(dT)_{15}$ with the horizontally oriented $(dA)_n$ anchor block, with the remainder of the $(dT)_{15}$ stem existing as a loose end. As a result, on average, no pronounced upright alignment of the $(dT)_{15}$ strands is observed.

Consistent with the N 1s HRXPS spectra, N K-edge NEXAFS spectra of $(dT)_{25}$-S/Au, d(A_5-T_{15})/Au, and d(A_{10}-T_{15})/Au in Figure 6.4 changed significantly after the hybridization step, whereas the spectrum of $(dT)_6$-S/Au remains unchanged, which suggested that in the latter case hybrids either did not form or were so weak that they were cleaved by the short dipping utilizing in the present study. For the other systems of this study, the formation of stable hybrids did occur to some extent. Whereas a quantitative evaluation of the hybridization degree for these systems is questionable to the problem with normalization and lack of the necessary reference data, at least qualitative estimate can be performed. From the N K-edge NEXAFS spectra it can be concluded that the changes after hybridization are most pronounced for $(dT)_{25}$-S/Au suggesting, in accordance with the XPS data, a relatively large hybridization degree for this film. In the case of d(A_5-T_{15})/Au and d(A_{10}-T_{15})/Au, the changes are smaller but more pronounced for the former film, once more in full agreement with the HRXPS results.

The hybridization step is accompanied by pronounced changes in the orientation of the individual nucleotides in the initial ssDNA films (Figure 6.5). In particular, much smaller linear dichroism is observed at the position of the t1 resonance in the case of $(dT)_{25}$-S:$(dA)_{15}$ while there is almost no dichroism at the position of the a1 resonance. This suggests a partial orientational disordering of the initially better ordered $(dT)_{25}$-S/Au film. In the case of both d(A_5-T_{15})/Au and d(A_{10}-T_{15})/Au, the positive peak at the position of the a1 resonance in the difference spectra disappears after the hybridization step, whereas the distinct negative peaks at the position of the a1 and t1 resonances appear. This indicates that both the thymine and a reasonable part of the adenine portions of the d(A_5-T_{15})/Au:d$(A)_{15}$ and d(A_{10}-T_{15})/Au:d$(A)_{15}$ complexes are predominantly oriented perpendicular to the substrate in these films. Whereas, in view of the given hybridization degree (26%), the dichroic contributions from the laying $(dA)_n$ anchor blocks and the "standing" $(dA)_{15}$ hybridized targets should be comparable, a possible partial quenching of the resonance intensity in the case of the $(dA)_n$ anchor blocks, which are in a direct contact with the substrate, and attenuation of the respective PEY signal by the $(dT)_{15}$: $(dA)_{15}$ overlayer makes the contribution of the standing $(dA)_{15}$ hybridized targets stronger, resulting in the joint negative peak at the position of the a1 resonance.

6.2.3.4 SFG Spectroscopy

SFG spectroscopy probes vibrations of molecules at interfaces and is particularly useful for the study of orientation and conformation of functional groups in organic monolayers, including DNA, down to submonolayer coverages [58, 84, 101, 26, 150]. The data presented in Figure 6.6a show the SFG signal in the spectral region where the CH-stretching vibrations are located (between 2800 and 3000cm^{-1}).

The signal is a convolution of a Gaussian-like non-resonant background emanating from electronic transitions in the Au substrate and vibrational resonant contributions from the ssDNA film. Due to the complexity of these spectra it is useful to plot the resonant contributions without the non-resonant signal in order to follow the changes that occur upon hybridization. The corresponding absolute value of the resonant signals obtained after fitting the spectra in Figure 6.6a using Equation 2.9 are shown in Figure 6.6b. Note that all spectra are normalized to the non-resonant background and can be directly compared.

A slightly higher overall intensity of the resonant signal is observed for the unhybridized thiolated films, of which $(dT)_{25}$-S/Au shows a slightly higher intensity than $(dT)_6$-S/Au. Assuming that both films have similar order and surface density, one would expect a 25-fold increase in intensity for the $(dT)_{25}$-S/Au film in comparison to the $(dT)_6$-S/Au film as the SFG intensity is proportional to the square of the total number of C H oscillators [43]. Even taking into account the

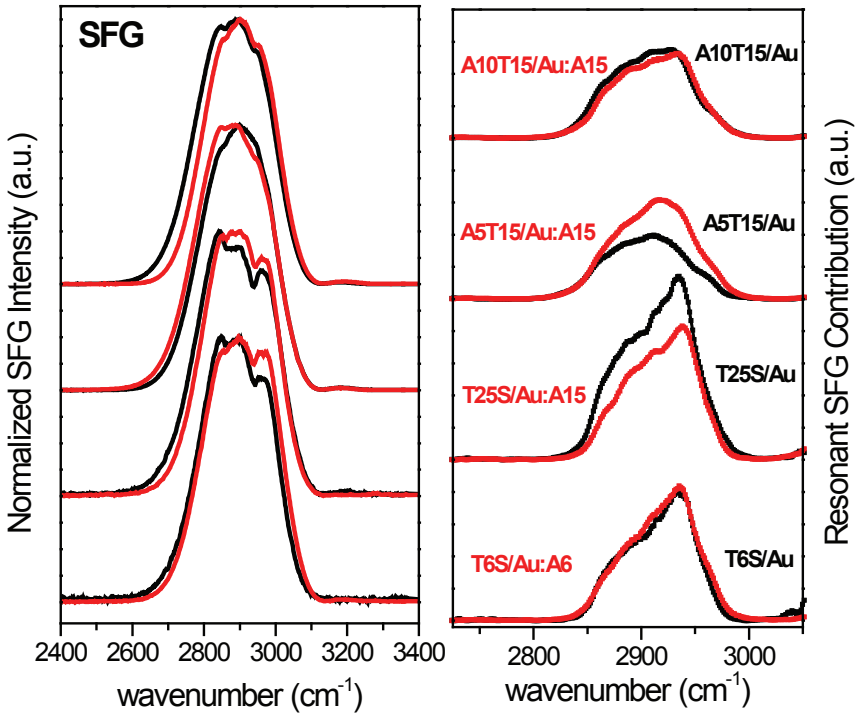

Figure 6.6: SFG spectra of hybridized (gray lines) and unhybridized (black lines) oligonucleotides films. (a) Raw spectra containing both non-resonant (overall Gaussian shape) and resonant contributions. (b) Background-subtracted spectra divided by the Gaussian non-resonant contribution showing only the resonant contributions shifted by 180°. The spectra appear as a sum of multiple overlapping resonant contributions with widths of 30 cm^{-1}.

50% lower surface coverage for the $(dT)_{25}$-S/Au film, one would still expect more than a 4-fold signal increase. As order and SFG intensity are closely related, the fact that the intensity is not increased to this degree is an indicator of lower orientational order in the $(dT)_{25}$-S/Au film than in the $(dT)_6$-S/Au one, in agreement with previous studies [44].

After the hybridization step, the overall intensity of the SFG signal decreased in the case of $(dT)_{25}$-S/Au, while for $(dT)_6$-S/Au it remained the same. A lack of change in the resonant contributions in the SFG spectra of $(dT)_6$-S/Au confirms what was observed with both NEXAFS and HRXPS, i.e. that little to no bound $d(A)_6$ target molecules are present in the final film and no significant changes in the film structure have occurred. For $(dT)_{25}$-S/Au, however, there is a noticeable decrease in the intensity of the resonant contributions with respect to the non-resonant background, indicating, in agreement with the NEXAFS results, a decrease in overall order.

For the block-oligonucleotides, the spectral shapes of the resonant contribution are different than in the thiolated films. This difference may be related to two factors: first, the lack of a C6 linker group, and second, the presence of the horizontally-oriented $(dA)_n$ block anchoring the entire strand to the gold substrate. The spectrum of the lower-density $d(A_{10}\text{-}T_{15})$/Au film exhibited little change upon hybridization, while that of the higher-density $d(A_5\text{-}T_{15})$/Au template showed a noticeable increase in intensity. As was the case for $(dT)_6$-S/Au, the lack of change in the spectra of $d(A_{10}\text{-}T_{15})$/Au indicates little change in these films after the hybridization step. This would suggest fewer hybrids present in this film relative to $d(A_5\text{-}T_{15})$/Au, in agreement with the HRXPS and NEXAFS results.

6.2.4 Discussion

As reported in previous work [44] and found here, short-chain thiolated d(T) homo-oligonucleotides form more dense and better ordered films on gold substrates than long-chain molecules of the same type, presumably due to the specific character of the inter-molecular interaction in ssDNA monolayers [44, 83]. In agreement with this tendency, the packing densities of $(dT)_6$-S/Au and $(dT)_{25}$-S/Au were estimated to be 4.1×10^{13} and 2.0×10^{13} molecules/cm^2, respectively. In the case of the block-oligonucleotides, the packing density was controlled by varying the length of the d(A) block [74, 37]. These molecules are assumed to adsorb in an L-shape geometry, with the d(A) block serving as the anchor group oriented parallel to the substrate surface and the d(T) block protruding upright into the ambient [37]. Whereas such a bonding mode was verified in the present work, the L-shape geometry seems to be a course description only since no preferential upright orientation was found for these films. This may be due to either intra-molecular coordination of the d(T) blocks with the complimentary d(An) blocks, the inter-molecular association of separate d(T_{15}-A_m) molecules, or, most likely, some combination of the above factors [74, 37]. However, even with this relatively complex adsorption geometry, the packing density of the ssDNA molecules can be altered in a controlled manner by varying the length of the d(A) block. Indeed, the packing densities in d(A_5-T_{15})/Au and d(A_{10}-T_{15})/Au in this study were estimated at 1.6×10^{13} and 9.2×10^{12} molecules/cm^2, respectively.

The shorter $(dT)_6$-S/Au film exhibited only a very small (4%) hybridization degree compared to the $(dT)_{25}$-S/Au film (31.5%) and showed, accordingly, no noticeable change in the orientation of the ssDNA strands after the hybridization step. High packing densities and short chain lengths have been previously correlated with lower hybridization efficiencies [148, 62] tentatively explainable by electrostatic repulsion and steric constraints, i.e. by the lack of intermolecular free space necessary for the entrance of the target strands into the ssDNA template [104, 151]. The respective entrance channels are not necessarily static but can open dynamically through changes in the orientation and conformation of the film constituents, which can be both spontaneous and induced by the interaction with the target ssDNA strands. These changes are, however, hardly possible in the case of the dense packing observed for the $(dT)_6$-S/Au film.

Furthermore, the shorter chain length of the $(dT)_6$-SH species means that there are overall fewer nucleotides available for hybridization, making the binding of target molecules in this film even less stable [148]. In addition, the presence of fewer nucleotides to participate in hybridization also means that this film is more likely to be disrupted by the deionized-water dipping procedure. As mentioned previously, these procedures were necessary to remove excess salts before spectroscopic analysis. Removing salts from ssDNA films results in a lack of screening charges [74]. As a consequence, the negatively charged backbone of the complementary DNA strands are able to repel each other more strongly, potentially overcoming the forces holding the strands together. As there are fewer of these bonds to begin with in the short-chain $(dT)_6$-S/Au film, this process is more likely to happen as compared to $(dT)_{25}$-S/Au, resulting in some cases in a disruption and/or dehybridization of some of the hybrids initially present. Recent work by Schreiner *et al.* using SPR has shown that nearly 100% of hybrids can be disrupted by rinsing even in a dilute (0.001 M) NaOH solution [74], however in those studies the samples were rinsed for 4 minutes with no shorter rinsing times tested [103]. Although the dipping procedure used in this work is likely affecting the hybrids to some extent, the presence of increased adenine-specific spectral signatures in both the NEXAFS and HRXPS spectra confirm that there are hybrids still present.

Multiple *in situ* studies systematically examining the relationship between hybridization efficiency and density in such films have shown the optimal number of nucleotides per unit area for hybridization to be 5×10^{12} molecules/cm^2 [74, 104, 103]. However, in the most loosely packed d(A_{10}-T_{15})/Au film (9.2×10^{12} molecules/cm^2) used in this work, the hybridization yield is noticeable lower (11%) than in the more densely packed $(dT)_{25}$-S/Au and d(A_5-T_{15})/Au films (2.0×10^{13} and 1.6×10^{13} molecules/cm^2) with 31.5% and 26% hybridization degree, respectively. Previous experiments performed by Schreiner *et al.* [74]. observed a higher degree of hybridization in d(A_{10}-T_{15})/Au than d(A_5-T_{15})/Au, presumably due to the larger intermolecular spacing in these films.

As mentioned above, the self-complementary d(A_n-T_{15}) probe sequences can form intramolecular hybrids during the immobilization step. In previous work, a rinsing step with NaOH

(or urea) was included to destabilize any intermolecular associations, allowing for more effective hybridization to take place [74, 37]. Note that such a NaOH rinsing step was not included in our preparation protocol. Therefore, in the case of d(A_{10}-T_{15})/Au, the intra-molecular hybrids were likely to be present, effectively reducing the estimated hybridization yield. The 11% estimate of the yield for the d(A_{10}-T_{15})/Au films was reduced by the presence of such dimeric hybrids in two ways: by overestimating the density of available probes and by suppressing the ability to capture solution targets.

Most importantly, as follows from both the NEXAFS and SFG data, the hybridization step in all ssDNA films with a reasonable degree of hybridization was accompanied by changes in the molecular orientation. In the case of $(dT)_{25}$-S/Au, the film became more disordered, although a definite orientational order persisted. This could be explained by the fact that the $(dT)_{25}$ strand can only be partially hybridized by a $(dA)_{15}$ strand, either in different positions in the $(dT)_{25}$ strand or by only a partial penetration of the target DNA strands into this film, with hybridization occurring mainly on the unbound end of the $(dT)_{25}$-S molecules. In work examining the kinetics of hybridization in similar 25-mer thiol-moldified ssDNA films on Au, Peterson and co-workers found that the rate of hybridization for the unbound ends of the probe molecules was much greater than for the portions of the molecules closer to the thiol linker, presumably due to electrostatic effects [148]. Such partial and/or end-hybridization in these films would result in the presence of either more distorted films or longer and more flexible strands, which would decrease the overall degree of order in the film. In the case of d(A_5-T_{15})/Au, where the number of nucleotides in the target and probe strands matched, the NEXAFS and SFG data both showed an increase in order upon hybridization. This would be consistent with the concept of the d(A_5-T_{15}) molecules gaining a greater degree of upright orientation following the cleavage of the weak intra-molecular hybridization of the $(dT)_{15}$ blockstem with the horizontally-oriented $(dA)_5$ surface-binding block. This was also shown to occur in the d(A_{10}-T_{15})/Au films, although to a lesser extent, presumably due to the higher degree of intramolecular coordination between the $(dT)_{15}$ and $(dA)_5$ blocks. It is interesting to note, however, that the changes observed for the $(dT)_{25}$-S/Au film (decrease in order) and the d(A_5-T_{15}) template (increase in order) are completely opposite despite the similar densities and hybridization yields of these films. This leads to the conclusion that observation of orientational changes in these films is important, as hybridization does not always lead to a greater degree of order.

6.3 Effects of Rinsing

6.3.1 Background

In the previous experiment, the combination of XPS, HRXPS, NEXAFS, and SFG spectroscopy proved useful in obtaining molecular-level information on surface-bound DNA hybrids. The use of other types of spectroscopy has also proven to be advantageous in obtaining molecular-level information about surface-bound DNA systems [83, 84, 35, 87, 44, 74, 82, 26]. Among these techniques, those which operate under *ex situ* conditions have been shown to yield valuable information about the composition and molecular density of DNA films [51, 60], the orientation of the molecules [83, 87, 44, 85], and changes that can occur between *ex situ* and *in situ* conditions [152, 84, 125]. However, for all of these techniques the question of sample preparation is essential, as the relatively high amount of salt necessary for successful DNA deposition and/or hybridization must be removed to some degree in order to be able to perform *ex situ* measurements accurately [37, 74]. It is known that such salt removal by solutions containing little to no salt results in the destabilization of surface-bound hybrids [74]. In this work, we provide evidence that such treatment can have the further effect of significantly disrupting the intactness of the remaining hybrids and orientation of the surface-bound DNA probe molecules.

6.3.2 Materials and Methods

Thiol-modified, HPLC-purified thymine homo-oligonucleotides [oligo(dT)] were purchased from Sigma-Aldrich. The thiol linkers were deprotected using DTT by the vendor and used as-

received. Films of these molecules immobilized on gold (T25S/Au) were prepared in 1M $CaCl_2$ solutions containing 10μM TRIS and 1μM EDTA ($CaCl_2$-TE) according to previously described procedures [74], followed by hybridization with adenine poly(A_{25}) for 8 hours in 1M TE-NaCl buffer (T25S/Au:A25).

After hybridization, samples first rinsed for 1 minute under flowing 1M NaCl buffer, then were rinsed with 0.5 mL, 1 mL, or 2 mL of Milli-Q water (resistivity $>$ 18.2 MΩ-cm). The samples were held vertically and the water was directed at the surface at an angle of 45° by a pipette. The flow rate was the same for all rinses, and thus the amount of time that the sample was in contact with water roughly doubled from the 0.5 mL to 1 mL to 2 mL rinses. After rinsing, the samples were dried under flowing N_2. It was not possible to measure films with no rinsing due to the heavy layer of salt encrusting such layers. The final atomic percent of Na present was found to be 6.97% for the films rinsed with 0.5 mL and 3.97% for the films rinsed with 2 mL. It should be noted that this amount is still relatively high despite the goal of the rinsing procedure to remove residual salt, and may mean that this type of preparation technique would not be useful for spectroscopic analysis particularly sensitive to the presence of salt, such as ToF-SIMs.

As in the previous experiment, samples were characterized with HRXPS, NEXAFS spectroscopy, IRRAS, and SFG spectroscopy. The experimental conditions and the way the spectra were measured were identical to those of Ref [74]. The density of the initial unhybridized T25S/Au film was found to be 6.3×10^{13} molecules/cm^2 by a standard XPS characterization procedure [51, 60].

6.3.3 Results and Discussion

The top panel of Fig. 6.7 shows the N 1s HRXPS spectra obtained for the unhybridized film and the three rinsed hybridized films; the spectra are decomposed into their adenine and thymine spectral components. The spectrum of the unhybridized film exhibits only the thymine component, which is a single emission at 400.8 eV. This emission is characteristic of thymine which is not in direct contact with the gold substrate. The emission for thymine chemisorbed directly on Au, located at ~400.3 eV [44], was not observed, suggesting an upright orientation of the T25S moieties in this film.

The spectra of the hybridized films contain both thymine and adenine components. The latter consists of two peaks at 399.5 and 400.5 eV with an intensity ratio of 1:2 [83, 37, 81]. These peaks are most prominent in the film rinsed with 0.5 mL of water, indicating that this layer contains a comparatively high amount of hybrids, as expected. The relative intensity of the adenine component decreases as the volume of the rinsing water increases, contributing 38%, 32%, and 23% of the total N 1s intensity for the films rinsed with 0.5 mL, 1 mL, and 2 mL, respectively (Fig. 6.7, bottom panel). This is in agreement with recent results from Opdahl *et al.* [74], who systematically investigated the destabilization of surface-bound hybrids upon rinsing using SPR. Normalizing the above values for the relative intensities of the adenine and thymine components to the amount of the nitrogen atoms in both bases yields the percentage of adenine target strands per thymine probe strand. These values are given in Table 6.1, along with the efficient thicknesses of the films derived from the attenuation of the Au4f signal in the HRXPS data. The overall percentage of the adenine strands is relatively low for all the films, including the one that was only rinsed with 0.5 mL of water. This can be tentatively explained by the relatively high packing density of the initial T25S/Au film (6.3×10^{13} molecules/cm^2), which would cause a greater degree of steric hindrance to the incoming target molecules and impede the hybridization process to some extent [63, 87, 62]. It was, however, not the goal of the present study to maximize the hybridization degree, but rather to monitor the effects of the post-hybridization treatment on the molecular structure of the T25S/Au:A25 films. In this regard, the tendency is clear: the overall percentage of the adenine strands decreases continuously with the increasing volume of water used for the rinse, suggesting a destabilization of the hybrids and a gradual washing away of the A25 target moieties over the course of this procedure.

This behavior is only partly reflected in the effective thickness (Table 6.1) which, as expected, increases to some extent after hybridization, but does not exhibit a continuous decrease with increasing rinsing water volume. Possible reasons for this discrepancy may be (i) a limited accuracy of the absolute intensities derived from the synchrotron-based HRXPS spectra or (ii)

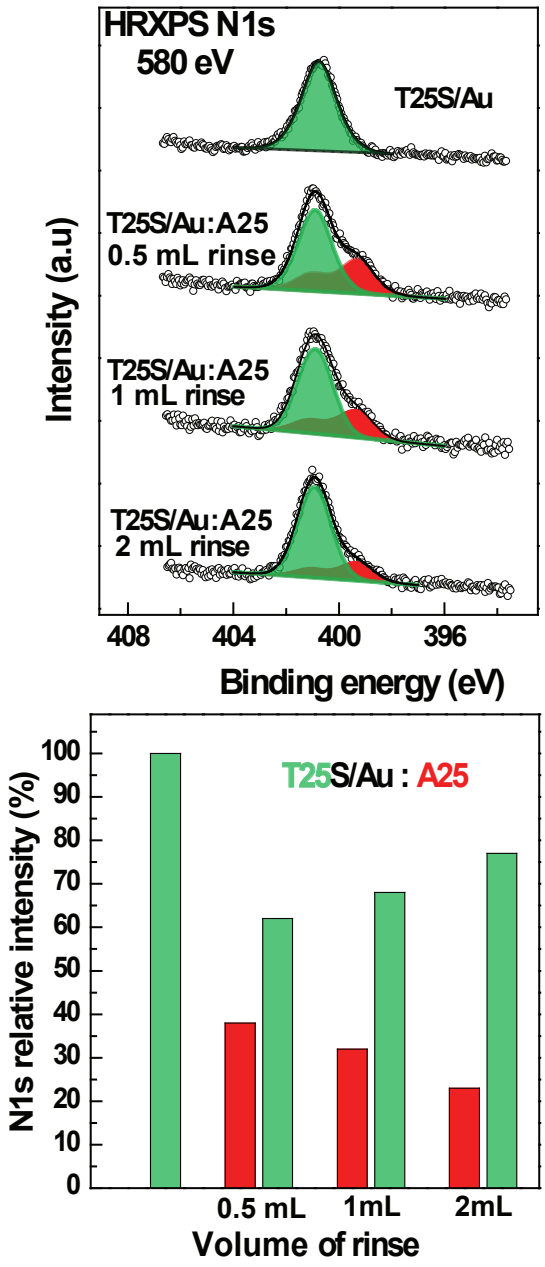

Figure 6.7: Top panel: N 1s HRXPS spectra of T25S/Au before and after hybridization with poly(dA_{25}) and subsequent light, medium, or heavy rinsing with water. The spectra are decomposed into the components related to thymine (green) and adenine (red). Bottom panel: relative intensities of these components.

Sample	Thickness (nm)	Percentage of adenine strands (%)
T25S/Au	4.10	n.a.
T25S/Au:A25 0.5 mL Rinse	4.32	24.5
T25S/Au:A25 1 mL Rinse	4.20	18.8
T25S/Au:A25 2 mL Rinse	4.30	12.0

Table 6.1: Thickness and percentage of adenine target strands per thymine probe strand calculated from the HRXPS data.

drastic structural transformations occurring over the course of rinsing (see below). This is, however, a good example how non-specific experimental data can result in erroneous conclusions when dealing with systems as complex as ssDNA and dsDNA films.

Both specific information on the chemical composition and, more importantly, structural changes occurring in the films over the course of rinsing were monitored using NEXAFS spectroscopy [83, 44, 40]. In Fig. 6.8, the N K-edge NEXAFS spectra of the unhybridized and hybridized films are shown. The spectra obtained at the so-called magic angle (55°, top panel) are only representative of the electronic structure of the target films [153] and exhibit specific characteristic resonances, the most pronounced of which are two merged π*-like absorption resonances from thymine at 401.1 and 402.0 eV (corresponding to the N1s→LUMO and N1s→LUMO+1 transitions, respectively)[154] and a sharp π*-like resonance from adenine at 399.4 eV (corresponding to the N1s→LUMO transition) [154]. The intensities of these features indicate the amount of each nucleobase present. Accordingly, the NEXAFS spectra confirm the HRXPS results, showing only a thymine signal for the unhybridized film, both thymine and adenine signals for the hybridized film, and a decreasing amount of adenine signal with increasing rinsing volume.

The 90°-20° spectra in Fig. 6.8 (bottom panel) give information about the orientation of the molecules in the film. Qualitatively, this orientation is given by the sign and amplitude of the difference peak at the position of a certain absorption resonance. Considering that the molecular orbitals associated with the most pronounced absorption resonances in Fig. 6.8 have π* character, i.e. are oriented perpendicular to the planes of the nucleobases, the negative or positive signs of the difference peaks indicates that the nucleobases are preferably orientated parallel or perpendicular to the substrate surface, respectively. This corresponds to the preferentially upright or horizontal orientations of the DNA strands, respectively. Accordingly, the spectrum of the pristine unhybridized T25S/Au shows a reasonable (for this length)[44] degree of upright orientation for the T25S strands, as evidenced by the pronounced downward peak at the position of the most prominent π* resonances of thymine. The difference spectrum of the hybridized film rinsed with 0.5 mL of water exhibits an even stronger downward peak at the position of the latter resonances and the pronounced downward peak at the position of the most prominent π* resonance of adenine. This indicates a comparable if not slightly greater degree of upright orientation of the T25S strands, in addition to uprightly oriented A25 moieties: exactly what would be expected from a film containing upright, relatively well-formed, intact hybrids as shown in Fig. 6.9.

In contrast, the spectrum of the hybridized film subjected to the 1 mL rinse shows only a very small difference peak for T25S and a small but pronounced positive difference peak for A25. The former is due to a significant loss in order of the T25S probe strands in this film in comparison to the film rinsed with 0.5 mL. The latter observation shows that the A25 target moieties in the film are also disordered, but possess a slightly preferable horizontal orientation, which is only possible if these moieties are partly relocated to the film-ambient interface (Fig. 6.9).

Surprisingly, the spectrum of the hybridized film treated with the 2 mL rinse shows a strong downward difference peak for T25S similar to those observed in the pristine T25S/Au and 0.5 mL-rinsed T25S/Au:A25, whereas the difference peak for A25 looks very similar to that of the film subjected to the 1 mL rinse, with an upward orientation and only a slightly smaller intensity (Fig. 6.8). The former finding indicates that the T25S probe moieties have regained their initial upright orientation characteristic of the molecules in the non-hybridized film (Fig. 6.9). The latter observation shows a low degree of order for the A25 target molecules, with a very slight preference of the horizontal orientation. Considering that the 2 mL rinse is associated with the

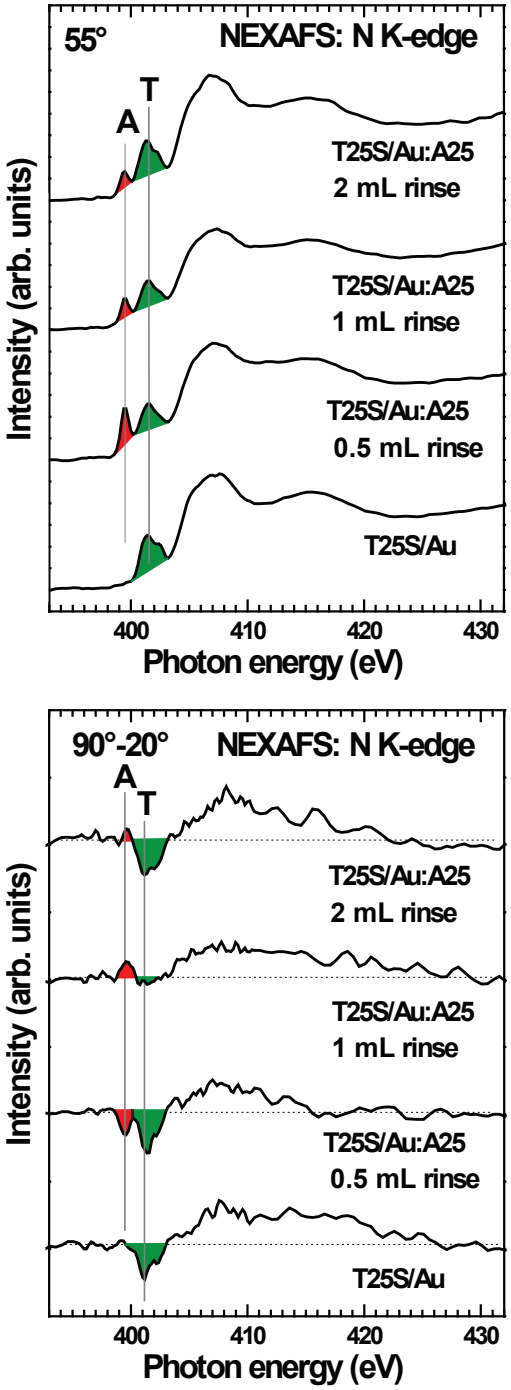

Figure 6.8: N K-edge NEXAFS spectra of T25S/Au before and after hybridization with A25 followed by rinsing with various volumes of water. The spectra in top panel were acquired at an X-ray incidence angle of 55° while the bottom panel shows the difference between spectra acquired at 90° and 20°. The horizontal dashed lines in the bottom panel correspond to zero for the individual spectra. The most pronounced π*-like absorption resonances and difference peaks of thymine (T) and adenine (A) are highlighted by green and red, respectively. Their positions are marked by the thin vertical solid lines.

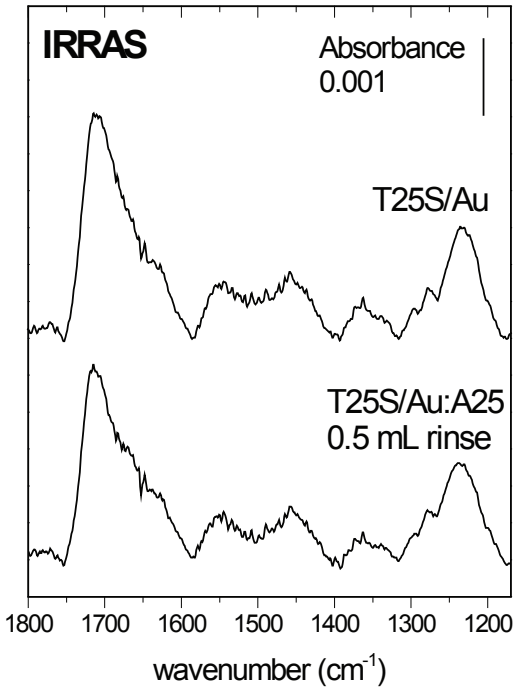

Figure 6.9: IRRAS spectra of a pristine T25S/Au film and a hybridized film after rinsing with 0.5 mL of water. The pristine film shows a spectrum typical for this type of films, with a major peak at 1700 cm^{-1}. The spectrum of the film after hybridized does not show significant changes, likely due to the low hybridization efficiency.

desorption of a significant part (more than 50%) of the A25 species from the hybridized film, we can tentatively assume that the reattainment of the preferable upright orientation is related to the almost complete removal of the A25 species from the body of the T25S/Au film and to the almost complete relocation of the residual A25 species to the film-ambient interface (Fig. 6.9). The observed improvement in the orientational order could be caused by the directionality of the applied rinsing water, which may be causing the DNA strands to orient themselves along the direction of the stream. A further factor may be the more effective removal of screening charges, which would allow the electrostatic repulsion between the DNA strands to be more effective. This should allow the strands to separate from each other more by gaining an upright and ordered conformation.

It should be noted that while Figure 6.9 shows one possible option for the orientation of the adenine target strands after the rinsing procedures, other orientations may also be possible. For instance, depending on the direction of the unzipping of the hybrids upon disruption by the rinse, some of the adenine strands may end up trapped within the bulk of the film closer to the substrate than the surface. This could also result in the horizontal orientation of the adenine components observed in the NEXAFS data. However, such a configuration would be more likely for the film rinsed with 1 mL of water, as the greater degree of order observed in the thymine bases in the sample rinsed with 2 mL would likely be difficult to achieve with adenine strands present within the film itself.

SFG spectroscopy was applied in the CH region in order to gain an understanding in the amount of order present in the CH groups in the sugar-phosphate backbone of the DNA molecules. The background-subtracted spectra are shown in Figure 6.10 The unhybridized T25S/Au film shows a spectral shape characteristic of a well-formed thiolated thymine ssDNA films (see Chapter 4), with a major peak at 2935 cm^{-1} and very minor contributions between 2860 and 2890 cm^{-1}. Upon hybridization and rinsing with 0.5 mL of water, the overall intensity of the

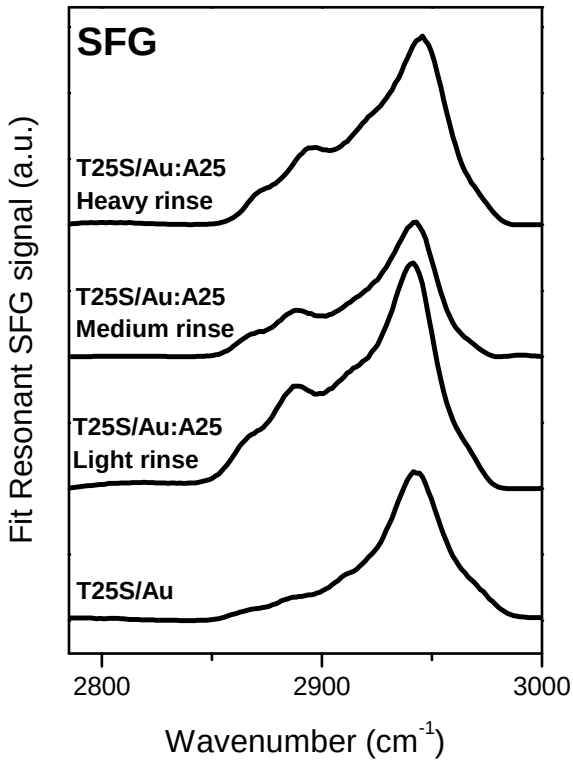

Figure 6.10: SFG spectra of T25S/Au before and after hybridization with A25 followed by rinsing with 0.5, 1, or 2 mL of water. The lightly rinsed hybridized film shows an increase in the intensity of all peaks, consistent with an increase in order observed using NEXAFS spectroscopy. This intensity decreases when the film is rinsed with 1 mL of water and is regained upon rinsing with 2 mL, again in agreement with the NEXAFS data.

peaks increases, indicating an increase in order in this film. This is in agreement with the observations made upon wetting and drying presented in Chapter 4, the data presented in Figure 6.6 for films undergoing hybridization, as well as the NEXAFS data shown in Figure 6.8. Upon rinsing with 1 mL of water, this intensity is decreased, again in agreement with the NEXAFS data. The overall intensity of the resonant peaks is again increased when the film is rinsed with 2 mL of water, supporting the hypothesis of the molecules regaining some degree of their initial upright orientation upon rinsing with this volume of water.

In addition to the HRXPS and NEXAFS spectroscopy, we applied IRRAS to the characterization of the unhybridized and hybridized films (Fig. 6.11). The initial unhybridized T25S/Au showed, in accordance with the HRXPS and NEXAFS results, an IRRAS spectrum typical of a well-formed thymine ssDNA monolayer [83, 37, 60] with a strong C=O peak at 1707 cm^{-1}. It is interesting to note that the hybridized film did not show a mode around 1600 cm^{-1} typical for adenine [37, 60]. This result has been reproduced several times, along with parallel XPS experiments confirming the presence of adenine in the films. In fact, besides a slight increase of the shoulders around 1670 cm^{-1} and 1650 cm^{-1} for the hybridized film, we did observe significant changes in other frequency regions. We believe that this issue of the IR spectrum of adenine-based DNA warrants further investigation. However, such an analysis lies beyond the scope of the present work.

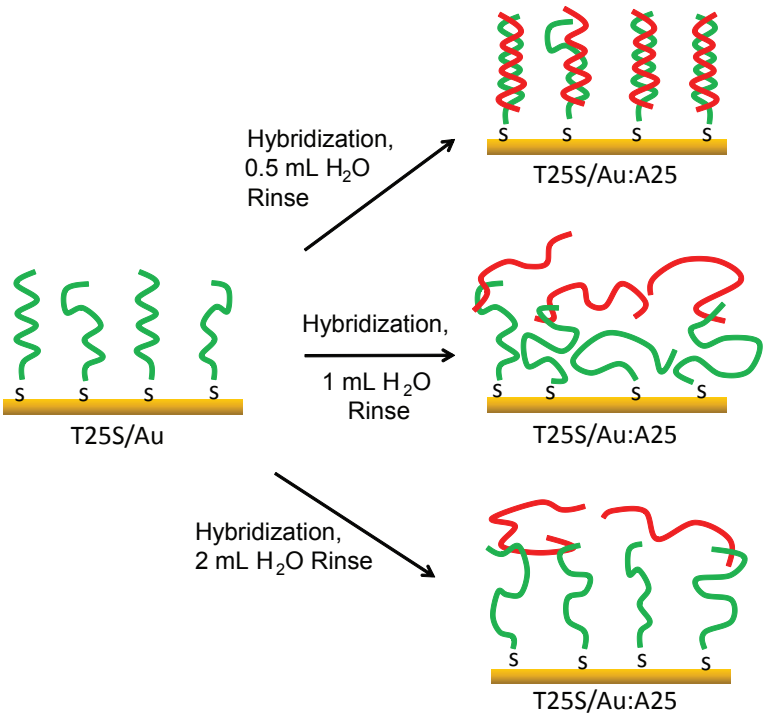

Figure 6.11: Illustration of the effects of varying degrees of rinsing on the extent of residual hybridization and orientational order in the target DNA films. For simplicity, we show all ssDNA moieties participating in the hybridization, whereas in reality only approximately 25% of the DNA strands were hybridized.

6.4 Conclusions

The complementary spectroscopic techniques of XPS, HRXPS, NEXAFS spectroscopy, and SFG spectroscopy were used to monitor the effects of hybridization in ssDNA films of different types (thiolated d(T) homo-oligonucleotides and d(A-T) block-oligonucleotides) and packing densities (from 9.2×10^{12} to 4.1×10^{13} molecules/cm^2) as well as to gather information about the effects of preparation for *ex situ* analysis on surface-bound hybrids.

Whereas XPS provided information on the packing density in the films, HRXPS was used to gather information on their composition. According to the experimental data, in the shorter and most densely packed $(dT)_6$-S/Au only very few (if any) hybrids were present after the cleaning procedure. At comparable packing densities, the films comprised of d(A_n-T_n) ssDNA were found to have hybridization yields similar to the thiolated films. However, increasing the length of the adenine block in the d(A_n-T_n) ssDNA led to a lower surface density and hybridization yield. The latter effect was presumably due to the creation of inter- and intramolecular hybrids during the immobilization step, substantially lowering the binding of the target molecules. There are, however, some indications that this intra-molecular coordination can be avoided by a rinsing step with NaOH or urea [74]. The combination of NEXAFS and SFG spectroscopy was found to be particular useful since it gives insight into the orientation of the ssDNA species before and after hybridization. As mentioned above, it was found that the assumed initial L-shape bonding geometry of d(A_n-T_n) species was partly distorted by the mutual coordination of the adenine and thymine blocks, which was lifted to some extent after the hybridization step, resulting in a better upright alignment of the thymine stems. In contrast, the $(dT)_{25}$-S/Au film displayed partial disordering of the primary chains in the thiolated $(dT)_n$ ssDNA after hybridization, possibly due to partial hybridization and/or the use of a mismatched $(dA)_{15}$ target.

The process of salt removal by water rinsing to prepare DNA films for *ex situ* spectro-

scopic analysis was found to affect significantly not only the number but also the orientation of surface-bound DNA molecules as well as the intactness of the residual hybrids. In our model experiments, hybridized T25S/Au:A25 DNA films treated with a 0.5 mL rinse showed mostly well-ordered, upright, and intact A:T hybrids, while hybridized films treated with a 1 mL, or 2 mL rinse displayed a progressive disruption of the hybrids with the removal of a part of the target DNA strands and relocation of the remaining strands to the film-ambient interface. These processes were accompanied by initial disordering of the film and subsequent reattainment of the orientational order for the probe strands.

These results demonstrate the usefulness of NEXAFS, HRXPS, and SFG spectroscopy in the examination of ssDNA films before and after hybridization. Furthermore, they show the importance of correlating hybridization yields and surface densities with other film parameters such as orientation and conformation, as well as the effects of preparation procedures, in order to obtain a full picture of the changes that occur in these films upon hybridization.

Chapter 7

Further Biological Applications

7.1 Summary

The ability to probe an interface beneath a layer of living cells *in situ* without the need for labeling and fixation has the potential to unlock some of the key questions in cell biology and biointerfacial phenomena. In order to test the usefulness of SFG spectroscopy for this purpose, fixed fibronectin-coated gold surfaces with and without adherent embryonic fibroblasts were probed. The SFG spectra were compared to infrared reflection-absorption spectroscopy (IRRAS) data in the CH stretching region. Noticeable differences were observed in the IRRAS spectra of the samples, while SFG spectra of the same samples were largely similar. These results suggest that cells with their overall random distribution of CH groups do not contribute to the SFG spectra, resulting in similar spectral features related to the fibronectin coating regardless of whether or not cells are adhered on it. Furthermore, SFG spectra of cells adhered directly on gold were found to have features similar to those of cells adhered on fibronectin covered gold. Additional experiments with living cells in vitro treated with the high powered lasers used in these experiments did not result in any visible radiation damages to the cells. These results demonstrate the feasibility of using SFG spectroscopy as an experimental tool to characterize the extracellular matrix (ECM) layer adjacent to a gold substrate beneath a layer of cells, and also suggest that this technique could be operated to examine the ECM *in vitro*. In order to further test this hypothesis, SFG spectroscopy was used to probe alkanethiol self-assembled monolayers (SAMs) buried underneath a layer erythrocytes (ECs) *in situ*. SFG spectra with and without ECs show the spectral signatures typical of these SAMs, indicating that the signal was being generated solely by the SAM and was not influenced by the presence of cells. These results could have important implications for the characterization of surfaces in biomedical, environmental and industrial applications.

7.2 Background

Mammalian cells and bacteria express a hydrated polymeric matrix to form biofilms. Formation of these sessile communities -and in the case of bacteria- their inherent resistance to antimicrobial agents is at the root of many persistent and chronic infections [155, 156]. Extracellular matrix (ECM) components like fibronectin, laminin and collagen play a vital role in cell and tissue morphogenesis [157]. These components provide different adhesion motifs for various cell types as well as instructive cues for cell differentiation. ECM components can also act as storage compartments for otherwise diffusible growth factors [158]. The ECM role in stem cell niches5-8 and the cellular microenvironment, especially with regard to tumor development [159, 160, 161], are currently areas of active research. Yet despite great advances in our understanding of the ECM in recent years, many questions remain about the interactions of ECM components with both artificial and natural cell substrates, the orientation and conformation of those components, and the temporal composition and chemical structure of the ECM during cell adhesion and differentiation.

Techniques currently employed to investigate cell adhesion and ECM composition in vitro include fluorescence microscopy [161] and a combination of confocal reflectance microscopy with coherent anti-Stokes Raman scattering (CARS) microscopy [162], both of which can be used to visualize the arrangement of the ECM. Additionally, attenuated total reflectance infrared (ATR-IR) spectroscopy has been used to track conformational changes in proteins at depths of approximately 1-2 μm [163, 164, 165, 166]. However, the development of more techniques capable of characterizing the ECM could prove useful in investigations such as the in vitro deposition of ECM during wound healing and variations in the ECM during tumor development, especially if those techniques have surface specificity sufficient enough to be able to distinguish between cellular contributions and the ECM itself.

In recent years the surface specific non-linear optical technique of sum-frequency generation spectroscopy (SFG) has emerged as a complementary experimental technique to characterize biological molecules at interfaces [167, 168, 169, 170, 171, 100, 172, 173, 174, 175]. SFG relies on the generation of signals through a second order non-linear optical process which can only occur when inversion symmetry is broken. This suppresses spectral contribution from bulk phases making SFG spectroscopy inherently surface specific and suitable for the investigation of "buried" liquid-solid interfaces [176]. SFG spectroscopy has recently been applied to characterize biological samples such as model peptides [170, 171], and amino acids [100], bovine serum albumin (BSA) [172], immunoglobulin G (IgG) [169], collagen [173], fibrinogen [174], urea orientation at protein surfaces [175], and heat-shock proteins (HSP) [169]. Here we introduce SFG as a useful complementary technique to current linear spectroscopy methods for studying the ECM.

7.3 Probing the Extracellular Matrix with SFG Spectroscopy

7.3.1 Experimental Details

Fresh wafers of polycrystalline gold on silicon were UV-sterilized for 2 hours immediately prior to deposition. Gold was chosen because is causes a strong enhancement of the SFG signal, allowing for the specific detection of the break in symmetry between gold and another substance. Fibronectin (FN) (Sigma-Aldrich, St. Louis, MO) at 50 μg/mL was adsorbed onto the gold wafers. The thickness of the fibronectin layer, measured by ellipsometry, was 53 nm. Rat embryonic fibroblast (REF) cells (kindly provided by Prof. B. Geiger, Weizmann Institute, Israel) in DMEM (Gibco BRL, supplemented with l-glutamine and 1% FBS) media were seeded at 25,000 cells per cm2 on the gold wafers and allowed to adhere for 3-4 hours under standard cell culture conditions. Remaining fibronectin-covered gold wafers were incubated in media with no cells. Following the incubation period, the samples were fixed in a 1:1 mixture of acetone and methanol at -20°C for 10 minutes and dried in air. Three replicates per condition were prepared.

7.3.2 Results

Figure 7.1 shows FTIR spectra, SFG spectra, and light microscopy images of gold wafers covered with fibronectin (red squares) and gold wafers covered with REF cells on fibronectin (blue circles) in the CH stretching region. The FTIR spectra (Fig. 7.1a) differ substantially between the fibronectin samples and the sample containing both fibronectin and REF cells both in intensity and peak positions. This is likely due to fact that the IR light is passing through more components in the cells containing CH groups, resulting in an increased number of spectral contributions.

In the SFG spectra (Fig. 7.1b), however, the positions of the peaks remain the same with only a slight difference in relative peak intensity between the fibronectin samples and the samples containing REF cells and fibronectin. This can only be the case when the same molecules are being probed in the SFG spectra, independent whether or not REF cells are present. The selection rules of SFG dictate that a signal cannot be produced in a material in which the molecules possess an overall random (centrosymmetric) arrangement. The similarities observed in the CH stretching region SFG spectra for the samples with cells and those without cells, therefore, may indicate that the CH groups within the cells possess enough of a centrosymmetric arrangement to avoid contributing to the SFG spectra. This then suggests that SFG is capable of directly probing the

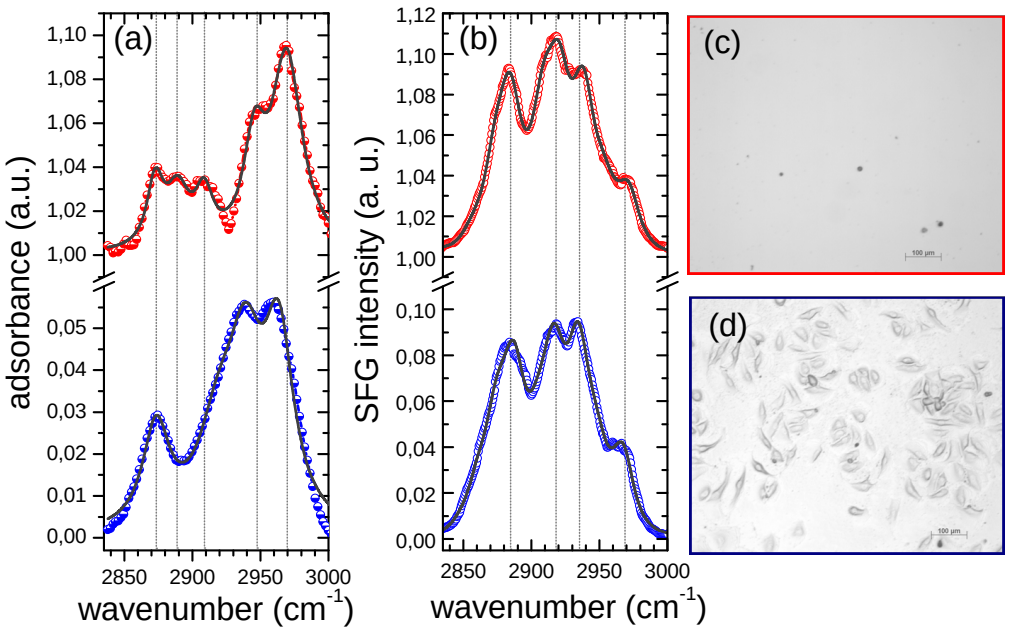

Figure 7.1: FTIR spectra (a), SFG spectra (b), optical microscopy image of fibronectin on gold (red squares) (c), and fibroblasts adhered on fibronectincovered gold (blue circles) (d) in the CH stretching region. Spectra are offset for clarity. The gray lines are corresponding fits to the data, and the dotted vertical lines are guide to the eyes for the peak positions. The FTIR spectra differ substantially between samples covered with fibronectin and fibroblasts on fibronectin. The SFG spectra, however, show similar peak positions with only slight changes in relative peak intensities.

layer between solid surfaces and REF cells, and could prove a useful technique for detecting ECM components through a layer of cells.

Figure 7.2 shows SFG spectra of a bare gold substrate exposed to the media used in the cell experiments (squares), of REF cells adhered on fibronectin covered gold substrates (circles) and cells on bare gold (triangles). The small features in the spectrum of bare gold are due to contaminants in the media and bear no resemblance to the spectra of REF cells on FN or REF cells on gold. It can therefore be concluded that the SFG signals observed stem from FN or other cell related materials, rather than from contaminants in the cell media. Furthermore, the spectral contributions for the cells on bare gold and on fibronectin covered gold differ in relative peak intensities, yet are comparable in all peak positions. The differences may be due to the fact that the composition of the ECM under the cells on bare gold differs from FN.

In order to test the influence of laser light treatment on the cells, in vitro experiments were performed. Figure 7.3 shows the light microscopy image of living cells adhered on a fibronectin coated gold wafer after 30 minutes of 20 μJ femtosecond light pulses (2900 cm^{-1}) simultaneously with 7 μJ nanosecond light pulses at 800 nm both with a repetition rate of 1000 Hz. For the duration of the experiment the cells were kept in CO_2 independent media (Gibco BRL, Catalogue No. 1805-054 supplemented with L-glutamine and 1% FBS). After 30 minutes of light treatment there was no visible irradiation damage. Observations after 16 hours of incubation of the irradiated samples under standard cell culture conditions indicated cell adhesion and proliferation attributable to a healthy population. It can therefore be concluded that the influence of SFG radiation on these REF cells was negligible, indicating that in vitro measurements of cells with SFG spectroscopy are possible. Further development of this technique could also include the creation

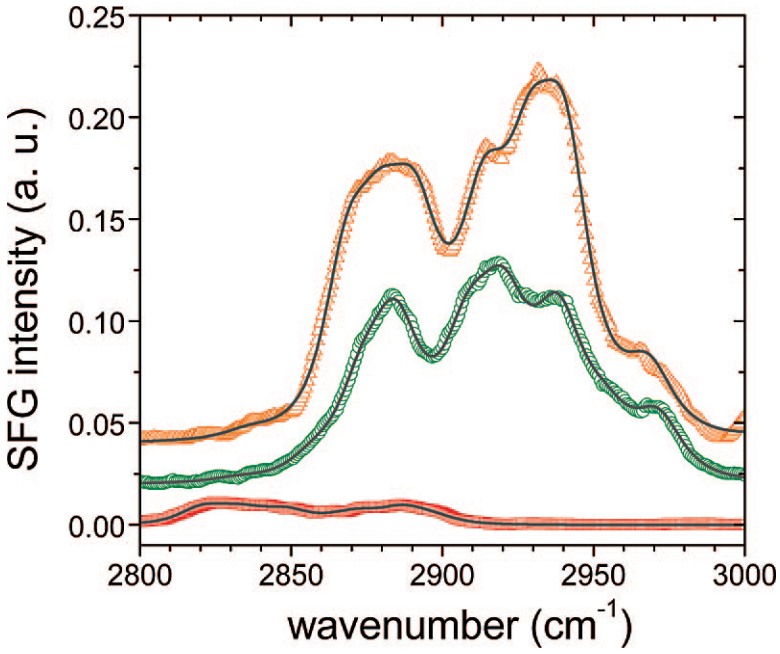

Figure 7.2: SFG spectra of a gold wafer exposed to phosphate-buffered saline alone (red squares), cells on fibronectin-coated gold (green circles), and fibroblasts adhered directly on gold (orange triangles). The SFG spectrum of cells on gold (triangles) shows spectral contributions similar in location to those of the fibronectin spectra, with significant alterations in relative peak intensities.

of spectral library of relevant ECM molecules, especially in the lower wavelength region (fingerprint region), in order to more conclusively determine the composition, and potentially the ordering of the ECM under a cellular layer.

7.4 Tests on Living Erythrocytes

7.4.1 Background

The *in situ* monitoring of the interphase between a substrate and the cellular layer is of great interest as it allows determination of changes in surface properties upon cell adhesion. Typically, this is accomplished by labeling and fixing the cell samples, which may result in their disruption and in the loss of valuable information. In this work we show that the surface specificity of vibrational sum-frequency-generation (SFG) spectroscopy permits the *in situ* characterization of an interfacial layer through living cells, without the need for fixation or labeling. SFG spectroscopy has proven well-suited to probing various interfaces [96, 99]. In recent years, this technique has been applied to the *in situ* investigation of biomolecules [177], including peptides [100, 178], proteins [179], and DNA [84, 26]. These results will be useful for those seeking to apply this system to investigate layers under living cells with high surface specificity.

7.4.2 Experimental Details

In order to test the ability of this technique to probe a substrate through living cells, a well-characterized self-assembled monolayer (SAM) was probed underneath a layer erythrocytes (ECs). Highly-ordered SAMs of deuterated dodecanethiol ($CD_3(CD_2)_{11}$-SH, *d*-DDT) were chosen, as they have a distinctive spectral signature in the CD stretching vibrational region (2000 to

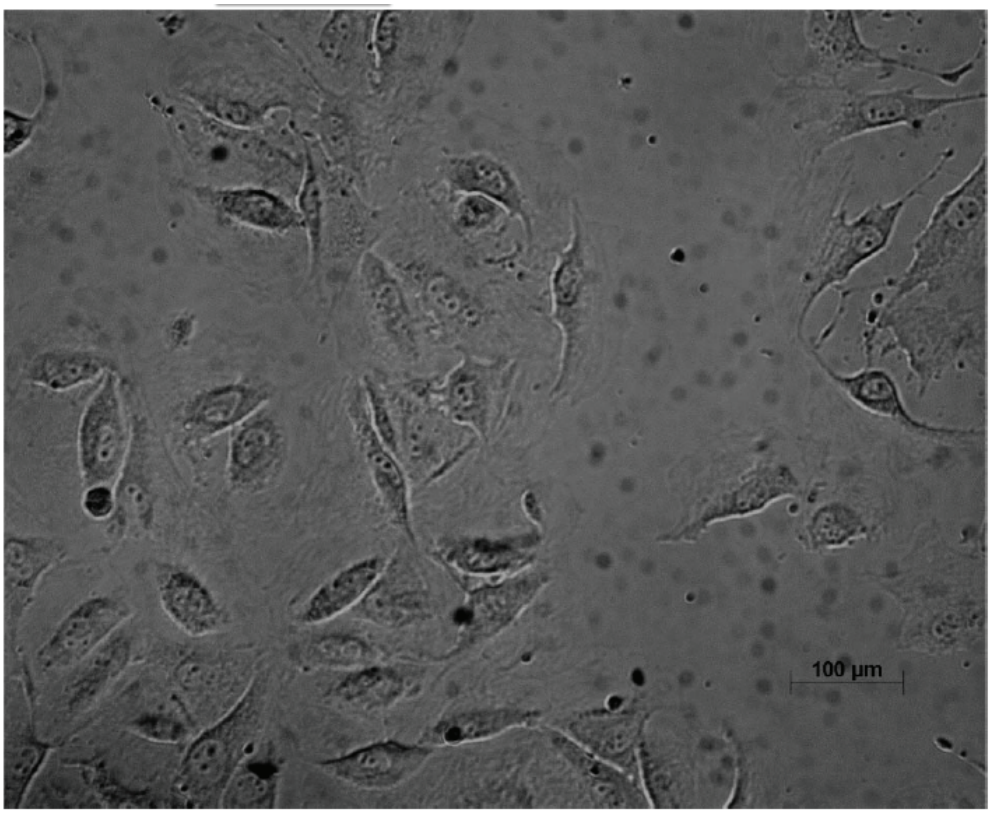

Figure 7.3: Optical microscopy image of fibroblasts adhered on fibronectin-covered gold after 30 min of irradiation with 20 μJ femtosecond light pulses. No visible irradiation damage is observable.

2300 cm^{-1}). These deuterated layers give little to no signal in the CH stretching region (2800 to 3000 cm^{-1}), allowing us to detect any contribution from the cells or cellular debris. In addition, we investigated undeuterated dodecanethiol ($CH_3(CH_2)_{11}$-SH, DDT) in the CH region to confirm that the typical spectral signatures of an alkanethiol SAM remained unchanged even in the presence of cells.

Living ECs were selected as the biological barrier since they contain the majority of molecule types encountered in most biological systems. These cells are known to have no direct interaction with the surface offered to them and will lay flat on it if given enough time to settle [180]. ECs do not deposit extracellular matrix (ECM) of their own or modify surface chemistry, allowing them to act as biological barriers without altering surface properties [181]. Additionally, these cells contain a large amount of hemoglobin, which make them optically dense in comparison to most other thin biological layers. If these cells pose no obstacle to the generated SFG signal, many biological barriers, either pro- or eukaryotic, become eligible for use with this technique.

A crudely purified solution of ECs in phosphate-buffered saline (PBS) was placed in between the SAM substrate and an optically transparent prism. All samples were measured using a femtosecond broadband SFG spectrometer in *ppp* polarization. Spectra were acquired in 2.5 s, background-subtracted and normalized to the non-resonant background.

7.4.3 Results

First, the presence of the *d*-DDT was confirmed by measurement in the CD stretching region (2000-2300 cm^{-1}) (Fig. 7.4). CD stretches of *d*-DDT SAMs were probed in air, sterile PBS, and PBS with ECs. In Figure 7.4A the Gaussian-like envelope reflects the spectral profile of the

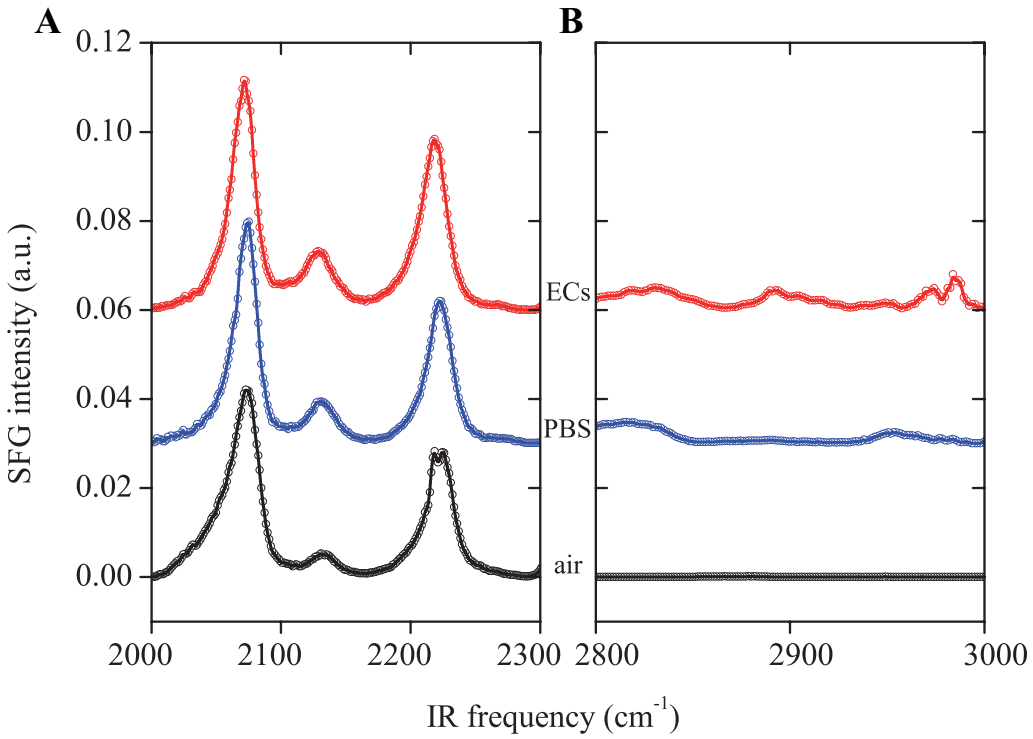

Figure 7.4: SFG spectra of a *d*-DDT SAM recorded in air (*black*), sterile PBS (*blue*), and media containing ECs (*red*). (**A**) Spectra containing non-resonant contributions in the CD (2000–2300 cm^{-1}) region. (**B**) Processed spectra showing only resonant contributions in the CD spectral region. The CD peaks remain unchanged upon addition of ECs.

femtosecond IR pulse, whereas the resonant peaks appear as *dips* in the spectra with a phase difference of π. These peaks at 2072, 2133, and 2222 cm^{-1} are established to be CD stretching vibrations of the terminal deuterated methyl group (CD_3) in the *d*-DDT SAM [182].

The lack of deuterated methylene (CD_2) vibrations in the spectrum is related to the presence of an inversion center in between these groups within the alkane chain and indicates the absence of kinks or gauche defects. Figure 7.4B shows the resonant contributions after data processing of the spectra shown in Figure 7.4A. The lack of appearance of new CD_2 peaks due to gauche defects in the film indicates that the film quality is not significantly affected by the presence of ions, cells, or cellular debris. A more thorough analysis of the ratio between the asymmetric and symmetric CD_3 stretching vibrations yielded values of 0.55, 0.63 and 0.77 for air, PBS and PBS with ECs, respectively. This translates to a calculated tilting angle variation [138] of about 2°, indicating a negligible reorientation of the terminal CD_3 headgroup.

Measurements in the CD spectral region show that the *d*-DDT SAM can be detected through a cellular layer, however, this region does not have contributions from cellular components. To verify whether we can detect signatures of the alkanethiol SAM even in the CH region, we further compared resonant SFG spectra of deuterated and undeuterated SAMs both in air, PBS, and PBS with ECs (Fig. 7.5). The lower and upper curves correspond to the measurement of *d*-DDT and DDT SAMs, respectively.

The spectrum of the *d*-DDT SAM, taken in air is a flat line, as one would expect, whereas the DDT spectrum in air shows the features typical of an alkanethiol SAM in the CH region. The same holds true for the PBS spectra with the exception of very weak features in the *d*-DDT SFG spectra which are attributable to a slight hydrocarbon contamination of the PBS solution.

Most interestingly, the spectrum with the ECs on top of the *d*-DDT SAM also does not show any significant spectral contributions other than those which are comparable in intensity with the PBS spectra. The two peaks at higher wavenumbers are related to fitting artifacts of the initial

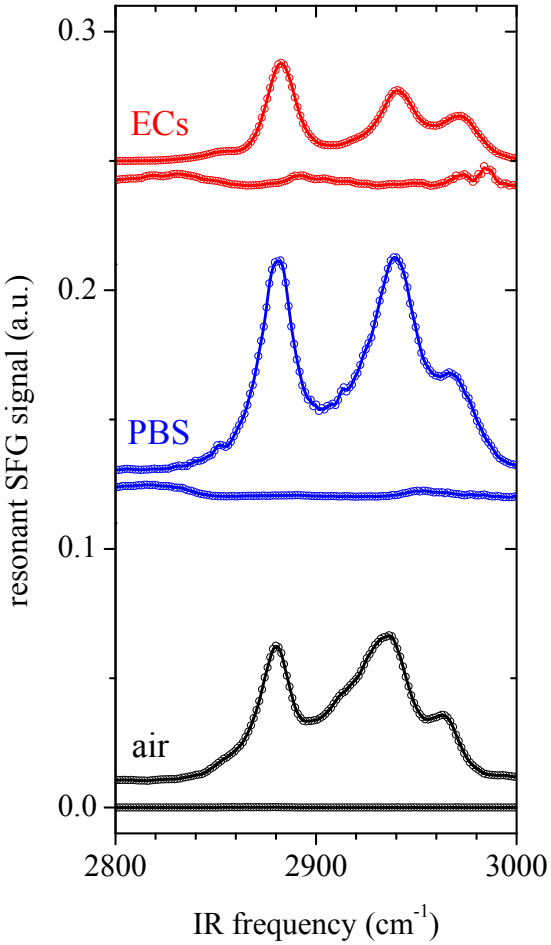

Figure 7.5: Resonant SFG spectra of *d*-DDT (*lower curve*) and DDT SAMs (*upper curve*) recorded in air (*black*), sterile PBS (*blue*), and PBS containing ECs (*red*). The CH peaks of the DDT SAMs show the typical spectral features upon addition of ECs, and only weak CH signatures show up in the presence of PBS and ECs.

broadband spectra, as the IR frequency was at the edge of the Gaussian-like envelope. This is also supported by the fact that these signatures are not observed in the DDT spectra, which show only the typical features of the SAM. If the cellular structures were contributing to the spectra, one would expect to see additional peaks appearing in the CH region, which are not observed. All the contributions from these structures cancel out since on average there is no broken inversion symmetry thus not fulfilling the SFG selection rules.

The lack of other spectral contributions is surprising considering the fact that the crudely purified EC solution used in these experiments contains not only whole cells, but also many small CH-containing debris, including sugars, peptides, and membrane fragments. It could be argued that this debris would give rise to an SFG signal due to the build up of a locally ordered layer at the interface driven by the amphiphilic character of these molecules. This might be the source of the very weak signals detected in the CH region, however, the peak intensities are one to two orders of magnitude lower than the signal generated by the SAM. These results show that SFG spectroscopy is able to probe buried interfaces even through a cellular layer.

7.5 Conclusions

SFG spectroscopy has been employed to study the ECM under a layer of fibroblast cells adhered on a solid support. No differences were observed in the SFG spectra of samples with cells and those without cells, indicating that SFG spectroscopy is capable of probing the layer in between a solid substrate and cells. Spectra of cells adhered on bare gold showed features similar (but not identical) to spectral features of cells adhered on fibronectin-coated gold. Tests on live fibroblast cells irradiated with SFG laser pulses revealed that these cells were not visibly adversely affected by the treatment, indicating that this technique could potentially be applied to *in vitro* measurements of the ECM under living cells. This was further explored by investigating interfaces under a layer of living cells without labeling or fixation. It was found that SFG spectroscopy could accurately detect a dodecanethiol SAM through a dense layer of erythrocytes, with no apparent contribution from the cells themselves. Further test on deuterated SAMs showed that the signal stemming from the erythrocytes was indeed negligible, a result which was hypothesized to be due to the inherent internal disorder of the cells. These results demonstrate that SFG spectroscopy is able to penetrate through biological barriers as long as they are optically transparent, and lays the groundwork for the use of this technique in diverse systems including the growth and development of biofilms *in situ*, the corrosive activity of bacteria and fungi on metal surfaces, or the interaction of cells with nanopatterned surfaces.

Chapter 8

Conclusions and Outlook

In this work, a basis for the *in situ* investigation of biological molecules on surfaces using sum-frequency-generation spectroscopy was presented. This was accomplished by first verifying the suitability of this technique to measure under the necessary conditions. As the density of biological molecules on surfaces is often relatively low, sensitivity measurements were performed to quantify the lower detection limit, which was found to be approximately 2×10^{13} oscillators/cm^2. Proof-of-principle measurements on hydrophilic and hydrophobic alkanethiol SAMs in air and in water were performed to confirm the accurate detection of the changes occurring in these films between *in situ* and *ex situ* conditions. These tests found no changes in the spectra of hydrophobic layers upon exposure to water, as was expected due to the lack of interaction between the water molecules and the surfaces of the film, and a significant change in the hydrophilic films upon exposure to water, also as was expected due to the hydrogen bonding of the water molecules with the surface of the film.

Biological systems on solid surfaces can be highly complex, and so in order to gain the clearest possible understanding of these systems, DNA was chosen due to its relative simplicity among biomolecules. In order to gain label-free, molecular-level information about DNA molecules immobilized on solid surfaces using SFG spectroscopy (aim [i] of this work), a bottom-up approach was used: examination of first the nucleobases alone, followed by unmodified DNA strands, and finally thiolated DNA strands on gold substrates. It was found that while CH_3 contributions from the methyl groups unique to thymine were clear in the dense nucleobase multilayers, these distinct signatures were not detectable in films of ssDNA. Observations that in these films the composition of the DNA strands (whether adenine, thymine, or cytosine) produced highly similar spectra, indicating that the methylene vibrations of the sugar-phosphate backbone and, in the case of the thiolated ssDNA, the linker group attaching the DNA strand to thiol moiety, were dominating the spectra. The lack of differences between the ssDNA types further suggested a similar degree of partial order in these films. It was found that this order could be improved by repeated wetting and drying of the samples, most likely due to the temporary introduction of a liquid environment gave the DNA strands freedom to rearrange into a more energetically favorable state before re-drying. The fact that SFG spectroscopy only detects signals from the sugar-phosphate backbone in films of ssDNA make make this technique useful for examining DNA strands regardless of their nucleobase composition, as well as for use as a complimentary method to those which only probe the bases, such as NEXAFS.

Comparison of results from ssDNA films in air to ssDNA films in water was performed in order to obtain an understanding of how these films change when exposed to liquid (aim [ii] of this work). Results revealed that thymine films appeared to lose the most overall SFG intensity, followed by cytosine films, and finally adenine films. This was tied to a known increase in preference for attachment to gold from thymine to cytosine to adenine, resulting in adenine films in which more of the molecules are attached via both the thiol linker and some of the nucleobases and thymine films in which the molecules are attached primarily through the thiol linker alone. Cytosine films fall somewhere in between. In the thymine ssDNA films the molecules lost the most order upon exposure to water due to the increased flexibility afforded them by being attached through only the thiol linker, while in adenine ssDNA films the molecules had less flex-

ibility due to being attached to the substrate through multiple points, and thus showed less of a loss of order when examined in water. Interestingly, closer examination of the spectra in water revealed unique signatures for thymine ssDNA films, suggesting that under these *in situ* conditions the increased flexibility of the backbone resulted in a suppression of the methylene signal strong enough to reveal nucleobase-specific signatures for this particular base. Such a phenomenon was found to occur regardless of the length of the DNA chain, with both 6- and 25-base thymine ssDNA strands showing similar spectra in water, as well as in films that had previously undergone repeated wetting and drying to induce order.

To further the understanding of the more complex system of hybridized DNA on surfaces, specifically about the level of order in these systems before and after hybridization (aim [iii] of this work), various DNA films were compared before and after hybridization using the complimentary techniques of high-resolution XPS and NEXAFS spectroscopy, in addition to SFG spectroscopy. It was found that HRXPS could be used to quantify the amount of target molecules in the film post-hybridization, while SFG and NEXAFS spectroscopy contributed information on the overall degree of order in the film. A film of shorter, more densely-packed thiolated thymine ssDNA showed nearly no hybridization, which was attributed to both the fact that the target molecules could not penetrate easily into this film and the fact that the smaller number of bases available for hybridization made any hybrids that did form inherently unstable. A significant number of target molecules was found in the less densely packed film made of longer ssDNA molecules. However, through NEXAFS and SFG it was found that the degree of order in these films decreased, contrary to the concept of an increasing molecular order upon hybridization known for DNA molecules in solution. This finding was attributed to the formation of incomplete or imperfect hybrids in this film, as well as a disruption of these hybrids due to the processing procedures necessary for analysis via these three spectroscopic techniques. Further tests on the extent of the effects caused by these preparation procedures revealed that even light processing for *ex situ* spectroscopic analysis can have a significant effect on both the ordering and number of surface-bound hybrids.

Finally, the knowledge obtained from the examination of these relatively simple biomolecular systems of DNA was applied to the complex system of cells on surfaces (aim [iv] of this work). Tests on fibronectin-coated gold surfaces with and without an overlayer of fixed cells were performed with SFG spectroscopy. It was found that the SFG signal was not altered by the layer of cells, suggesting that it was possible to "see through" this cellular layer with SFG spectroscopy, probing just the extracellular matrix beneath. The ability to probe through a layer of living cells was tested using non-adherent erythrocytes over self-assembled monolayers. Results showed a clear signal from the surface-bound SAM with little to no signal generated by cells, demonstrating that this technique can also be used through a living cellular layer.

Although the use of SFG spectroscopy for obtaining these insights has proven useful, there are nevertheless some limitations which could render this technique less suitable than others for some types of investigations. First, SFG in the CH region has been shown to be quite non-specific. This is unsurprising as many contaminants have CH oscillators similar to what can be found in samples, especially biomolecules. However, it still makes the interpretation of data in this region difficult. Furthermore, spectroscopic analysis in other regions such as the amide I were found to have very low, if any, signal. This is most likely due to the fact that the IR peaks found in this region have a very small Raman cross sections, however it limits the use of SFG spectroscopy for detecting these generally highly informative bands. It may also be the case that the significant decrease signal for ssDNA films in liquid (as seen in Chapter 5) will make it difficult to obtain further accurate information about these types of films *in situ*. Although it could also be the case that the disappearance of the dominant methylene backbone signals proves useful for researchers attempting to study such things as intercalation of drugs between nucleobases.

Future directions for this work could include further investigations of DNA in different types of buffer solutions, such as those made with monovalent versus divalent cations. The findings presented here could also be useful for the *in situ* versus *ex situ* analysis of applied DNA films, such as those created by dip-pen nanolithography or microcontact printing. Such an analysis may reveal differences in the solubility of films made in different ways, suggesting a greater hybridization potential in one over another. Films of other biological molecules with distinctly different CH moieties could also be measured, such as arginine, leucine, alanine, and glycine syn-

thetic peptides, in air and solution. This could reveal more about the differences in ordering in these types of biomolecular systems on surfaces as researchers seek to optimize them as specialized diagnostic tools. Such investigations would further bridge the gap between *in situ* and *ex situ* measurements, allowing for a more accurate comparison between the two.

The presentation of clear and accurate reference spectra for DNA in solution in this work could also make possible the acquisition of dynamic measurements in solution. The fs SFG system used here has a current time resolution scale on the order of seconds, and so could be used to monitor phenomena such as the change in order during hybridization and melting of DNA on surfaces in real time. A similar dynamic real-time approach could also be used to examine changes in molecular ordering during the formation or breakdown of the extracellular matrix under a layer of cells, knowledge which could prove exceptionally valuable in the understanding of processes in such areas as cancer and tissue development.

Yet no matter the future directions, the results presented here provide new knowledge about biological molecules, particularly DNA, on solid surfaces *in situ* and can help pave the way for future investigations of these systems using SFG spectroscopy.

Bibliography

[1] D. G. Castner and B. D. Ratner, "Biomedical surface science: foundations to frontiers," *Surface Science*, vol. 500, pp. 28–60, Mar. 2002.

[2] B. Kasemo, "Biological surface science," *Surface Science*, vol. 500, pp. 656–677, Mar. 2002.

[3] P. Harder, M. Grunze, R. Dahint, and D. Heidelberg, "Molecular conformation in oligo (ethylene glycol) -terminated self-assembled monolayers on gold and silver surfaces determines their ability to resist protein adsorption," *Journal of Physical Chemistry B*, vol. 102, no. 97, pp. 426–436, 1998.

[4] R. G. Chapman, E. Ostuni, L. Yan, and G. M. Whitesides, "Preparation of mixed self-assembled monolayers (SAMs) that resist adsorption of proteins using the reaction of amines with a SAM that presents interchain carboxylic anhydride groups," *Langmuir*, vol. 16, pp. 6927–6936, 2000.

[5] Q. Liu, L. Wang, A. G. Frutos, A. E. Condon, R. M. Corn, and L. M. Smith, "DNA computing on surfaces," *Nature*, vol. 403, pp. 175–179, Jan. 2000.

[6] W. C. E. Schofield, J. McGettrick, T. J. Bradley, J. P. S. Badyal, and S. Przyborski, "Rewritable DNA microarrays," *Journal of the American Chemical Society*, vol. 128, pp. 2280–5, Feb. 2006.

[7] S. C. Hsiao, B. J. Shum, H. Onoe, E. S. Douglas, Z. J. Gartner, R. a. Mathies, C. R. Bertozzi, and M. B. Francis, "Direct cell surface modification with DNA for the capture of primary cells and the investigation of myotube formation on defined patterns," *Langmuir*, vol. 25, pp. 6985–91, June 2009.

[8] E. S. Douglas, R. a. Chandra, C. R. Bertozzi, R. a. Mathies, and M. B. Francis, "Self-assembled cellular microarrays patterned using DNA barcodes," *Lab on a Chip*, vol. 7, pp. 1442–8, Nov. 2007.

[9] M. A. Cooperstein and H. E. Canavan, "Biological cell detachment from poly(N-isopropyl acrylamide) and its applications," *Langmuir*, vol. 26, pp. 7695–707, June 2010.

[10] V. Kurz, M. Grunze, and P. Koelsch, "In situ characterization of thermo-responsive poly (N-Isopropylacrylamide) films with sum-frequency generation spectroscopy," *ChemPhysChem*, vol. 11, pp. 1425 – 1429, 2010.

[11] A. Q. Emili and G. Cagney, "Large-scale functional analysis using peptide or protein arrays," *Nature Biotechnology*, vol. 18, pp. 393–7, Apr. 2000.

[12] S. F. Kingsmore, "Multiplexed protein measurement: technologies and applications of protein and antibody arrays," *Nature Reviews Drug Discovery*, vol. 5, pp. 310–20, Apr. 2006.

[13] B. B. Haab, "Antibody arrays in cancer research," *Molecular & Cellular Proteomics*, vol. 4, pp. 377–83, Apr. 2005.

[14] D. J. Lockhart and E. a. Winzeler, "Genomics, gene expression and DNA arrays," *Nature*, vol. 405, pp. 827–836, June 2000.

[15] M. J. Heller, "DNA microarray technology: devices, systems, and applications," *Annual Review of Biomedical Engineering*, vol. 4, pp. 129–53, Jan. 2002.

[16] N. Fusetani, "Biofouling and antifouling," *Natural Product Reports*, vol. 21, pp. 94–104, Feb. 2004.

[17] B. Carpentier and O. Cerf, "Biofilms and their consequences, with particular reference to hygiene in the food industry," *The Journal of Applied Bacteriology*, vol. 75, pp. 499–511, Dec. 1993.

[18] M. Heydt, A. Rosenhahn, M. Grunze, M. Pettitt, M. E. Callow, and J. A. Callow, "Digital in-line holography as a three-dimensional tool to study motile marine organisms during their exploration of surfaces," *The Journal of Adhesion*, vol. 83, pp. 417–430, May 2007.

[19] S. Schilp, A. Kueller, A. Rosenhahn, M. Grunze, M. E. Pettitt, M. E. Callow, and J. a. Callow, "Settlement and adhesion of algal cells to hexa(ethylene glycol)-containing self-assembled monolayers with systematically changed wetting properties," *Biointerphases*, vol. 2, pp. 143–50, Dec. 2007.

[20] A. Rosenhahn, S. Schilp, H. J. Kreuzer, and M. Grunze, "The role of "inert" surface chemistry in marine biofouling prevention," *Physical chemistry chemical physics : PCCP*, vol. 12, pp. 4273–4, May 2010.

[21] G. C. Kumar and S. K. Anand, "Significance of microbial biofilms in food industry: a review," *International Journal of Food Microbiology*, vol. 42, pp. 9–27, 1998.

[22] P. Thevenot, W. Hu, and L. Tang, "Surface chemistry influences implant biocompatibility," *Current Topics in Medicinal Chemistry*, vol. 8, pp. 270–280, 2008.

[23] G. L. Richmond, "Molecular bonding and interactions at aqueous surfaces as probed by vibrational sum frequency spectroscopy," *Chemical Reviews*, vol. 102, pp. 2693–724, Aug. 2002.

[24] F. M. Geiger, "Second harmonic generation, sum frequency generation, and chi(3): dissecting environmental interfaces with a nonlinear optical Swiss Army knife," *Annual Review of Physical Chemistry*, vol. 60, pp. 61–83, Jan. 2009.

[25] N. C. Seeman, "DNA in a material world," *Nature*, vol. 421, pp. 427–31, Jan. 2003.

[26] S. R. Walter and F. M. Geiger, "DNA on Stage: Showcasing Oligonucleotides at Surfaces and Interfaces with Second Harmonic and Vibrational Sum Frequency Generation," *The Journal of Physical Chemistry Letters*, vol. 1, pp. 9–15, Jan. 2010.

[27] P. W. K. Rothemund, "Folding DNA to create nanoscale shapes and patterns.," *Nature*, vol. 440, pp. 297–302, Mar. 2006.

[28] S. Cosnier and P. Mailley, "Recent advances in DNA sensors," *The Analyst*, vol. 133, pp. 984–91, Aug. 2008.

[29] C. A. Mirkin, R. L. Letsinger, R. C. Mucic, and J. J. Storhoff, "A DNA-based method for rationally assembling nanoparticles into macroscopic materials," *Nature*, vol. 382, pp. 607–609, 1996.

[30] J. J. Storhoff and C. a. Mirkin, "Programmed materials synthesis with DNA," *Chemical Reviews*, vol. 99, pp. 1849–1862, July 1999.

[31] N. L. Rosi and C. a. Mirkin, "Nanostructures in biodiagnostics," *Chemical Reviews*, vol. 105, pp. 1547–62, Apr. 2005.

[32] L. M. Adleman, "Molecular computation of solutions to combinatorial problems," *Science*, vol. 266, pp. 1021–1024, Nov. 1994.

[33] R. a. Chandra, E. S. Douglas, R. a. Mathies, C. R. Bertozzi, and M. B. Francis, "Programmable cell adhesion encoded by DNA hybridization," *Angewandte Chemie (International ed. in English)*, vol. 45, pp. 896–901, Jan. 2006.

[34] J. J. Storhoff, R. Elghanian, C. a. Mirkin, and R. L. Letsinger, "Sequence-Dependent Stability of DNA-Modified Gold Nanoparticles," *Langmuir*, vol. 18, pp. 6666–6670, Aug. 2002.

[35] H. Kimura-Suda, D. Y. Petrovykh, M. J. Tarlov, and L. J. Whitman, "Base-dependent competitive adsorption of single-stranded DNA on gold," *Journal of the American Chemical Society*, vol. 125, pp. 9014–5, July 2003.

[36] B. Roelfs, E. Bunge, C. Schröter, T. Solomun, H. Meyer, R. J. Nichols, and H. Baumgärtel, "Adsorption of thymine on gold single-crystal electrodes," *The Journal of Physical Chemistry B*, vol. 101, pp. 754–765, Jan. 1997.

[37] A. Opdahl, D. Y. Petrovykh, H. Kimura-Suda, M. J. Tarlov, and L. J. Whitman, "Independent control of grafting density and conformation of single-stranded DNA brushes," *Proceedings of the National Academy of Sciences of the United States of America*, vol. 104, pp. 9–14, Jan. 2007.

[38] P. Gong, C.-y. Lee, L. J. Gamble, D. G. Castner, D. W. Grainger, L. J. A. Chem, and G. M. Harbers, "Surface coverage and structure of mixed DNA/alkylthiol monolayers on gold: characterization by XPS, NEXAFS, and fluorescence intensity measurements.," *Analytical chemistry*, vol. 78, pp. 3326–3334, May 2006.

[39] C.-Y. Lee, L. J. Gamble, D. W. Grainger, and D. G. Castner, "Mixed DNA/oligo(ethylene glycol) functionalized gold surfaces improve DNA hybridization in complex media," *Biointerphases*, vol. 1, pp. 82–92, June 2006.

[40] S. M. Schreiner, A. L. Hatch, D. F. Shudy, D. R. Howard, C. Howell, J. Zhao, P. Koelsch, M. Zharnikov, D. Y. Petrovykh, and A. Opdahl, "Impact of DNA-Surface Interactions on the Stability of DNA Hybrids," *Analytical Chemistry*, vol. 83, pp. 4288–95, June 2011.

[41] W. Saenger, *Principles of Nucleic Acid Structure (Springer Advanced Texts in Chemistry)*. Springer, 1983.

[42] J. Rubin, T. Brennan, and M. Sundaralingam, "Crystal and molecular structure of a naturally occurring dinucleoside monophosphate. Uridylyl-(3'-5')-adenosine hemihydrate. Conformational rigidity of the nucleotide unit and models for polynucleotide chain folding," *Biochemistry*, vol. 11, pp. 3112–3128, Aug. 1972.

[43] A. Vainrub and B. M. Pettitt, "Sensitive quantitative nucleic acid detection using oligonucleotide microarrays.," *Journal of the American Chemical Society*, vol. 125, pp. 7798–9, July 2003.

[44] D. Y. Petrovykh, A. Opdahl, H. Kimura-Suda, J. M. Sullivan, M. J. Tarlov, F. J. Himpsel, L. J. Whitman, and V. Pérez-Dieste, "Nucleobase orientation and ordering in films of single-stranded DNA on gold," *Journal of the American Chemical Society*, vol. 128, pp. 2–3, Jan. 2006.

[45] J. B. Mills, E. Vacano, and P. J. Hagerman, "Flexibility of single-stranded DNA: use of gapped duplex helices to determine the persistence lengths of poly(dT) and poly(dA)," *Journal of Molecular Biology*, vol. 285, pp. 245–57, Jan. 1999.

[46] B. Tinland, A. Pluen, J. Sturm, and G. Weill, "Persistence Length of Single-Stranded DNA," *Macromolecules*, vol. 30, pp. 5763–5765, Sept. 1997.

[47] M. Murphy, I. Rasnik, W. Cheng, T. M. Lohman, and T. Ha, "Probing single-stranded DNA conformational flexibility using fluorescence spectroscopy," *Biophysical Journal*, vol. 86, pp. 2530–2537, Apr. 2004.

[48] W. J. Parak, T. Pellegrino, C. M. Micheel, D. Gerion, S. C. Williams, and a. P. Alivisatos, "Conformation of oligonucleotides attached to gold nanocrystals probed by gel electrophoresis," *Nano Letters*, vol. 3, pp. 33–36, Jan. 2003.

[49] D. Zanchet, C. M. Micheel, W. J. Parak, D. Gerion, and a. P. Alivisatos, "Electrophoretic Isolation of Discrete Au Nanocrystal/DNA Conjugates," *Nano Letters*, vol. 1, pp. 32–35, Jan. 2001.

[50] V. Singh, M. Zharnikov, A. Gulino, and T. Gupta, "DNA immobilization, delivery and cleavage on solid supports," *Journal of Materials Chemistry*, vol. 21, pp. 10602–10618, May 2011.

[51] D. Y. Petrovykh, H. Kimura-Suda, M. J. Tarlov, and L. J. Whitman, "Quantitative characterization of DNA films by X-ray photoelectron spectroscopy," *Langmuir*, vol. 20, pp. 429–440, Jan. 2004.

[52] L. K. Wolf, Y. Gao, and R. M. Georgiadis, "Sequence-dependent DNA immobilization: specific versus nonspecific contributions," *Langmuir*, vol. 20, pp. 3357–61, Apr. 2004.

[53] W. Yang, O. Auciello, J. E. Butler, W. Cai, J. A. Carlisle, J. E. Gerbi, D. M. Gruen, T. Knickerbocker, T. L. Lasseter, J. N. Russell, L. M. Smith, and R. J. Hamers, "DNA-modified nanocrystalline diamond thin-films as stable, biologically active substrates," *Nature Materials*, vol. 1, pp. 253–7, Dec. 2002.

[54] T. Knickerbocker, T. Strother, M. P. Schwartz, J. N. Russell, J. Butler, L. M. Smith, and R. J. Hamers, "DNA-Modified Diamond Surfaces," *Langmuir*, vol. 19, pp. 1938–1942, Mar. 2003.

[55] T. Strother, "Covalent attachment of oligodeoxyribonucleotides to amine-modified Si (001) surfaces," *Nucleic Acids Research*, vol. 28, pp. 3535–3541, Sept. 2000.

[56] T. Böcking, K. A. Kilian, K. Gaus, and J. J. Gooding, "Single-step DNA immobilization on antifouling self-assembled monolayers covalently bound to silicon (111)," *Langmuir*, vol. 22, pp. 3494–6, Apr. 2006.

[57] G. Y. Stokes, J. M. Gibbs-davis, F. C. Boman, B. R. Stepp, A. G. Condie, S. T. Nguyen, and F. M. Geiger, "Making sense of DNA," *Journal of the American Chemical Society*, vol. 129, pp. 7492–7493, 2007.

[58] Y. Sartenaer, G. Tourillon, L. Dreesen, D. Lis, A. a. Mani, P. a. Thiry, and A. Peremans, "Sum-frequency generation spectroscopy of DNA monolayers.," *Biosensors and Bioelectronics*, vol. 22, pp. 2179–83, Apr. 2007.

[59] B. Sun, P. E. Colavita, H. Kim, M. Lockett, M. S. Marcus, L. M. Smith, and R. J. Hamers, "Covalent photochemical functionalization of amorphous carbon thin films for integrated real-time biosensing," *Langmuir*, vol. 22, pp. 9598–605, Nov. 2006.

[60] D. Y. Petrovykh, H. Kimura-Suda, L. J. Whitman, and M. J. Tarlov, "Quantitative analysis and characterization of DNA immobilized on gold," *Journal of the American Chemical Society*, vol. 125, pp. 5219–26, Apr. 2003.

[61] C. Frontali, E. Dore, A. Ferrauto, E. Gratton, A. Bettini, M. R. Pozzan, and E. Valdevit, "An absolute method for the determination of the persistence length of native DNA from electron micrographs," *Biopolymers*, vol. 18, pp. 1353–73, June 1979.

[62] A. W. Peterson, R. J. Heaton, and R. M. Georgiadis, "The effect of surface probe density on DNA hybridization," *Nucleic Acids Research*, vol. 29, pp. 5163–8, Dec. 2001.

[63] M. F. Hagan and A. K. Chakraborty, "Hybridization dynamics of surface immobilized DNA," *The Journal of Chemical Physics*, vol. 120, pp. 4958–68, Mar. 2004.

[64] T. M. Herne and M. J. Tarlov, "Characterization of DNA Probes Immobilized on Gold Surfaces," *Journal of the American Chemical Society*, vol. 119, pp. 8916–8920, Sept. 1997.

[65] A. W. Peterson, L. K. Wolf, and R. M. Georgiadis, "Hybridization of mismatched or partially matched DNA at surfaces important in both fundamental and applied research in chemistry," *Journal of the American Chemical Society*, vol. 682, no. 15, pp. 14601–14607, 2002.

[66] T. Livache, E. Maillart, N. Lassalle, P. Mailley, B. Corso, P. Guedon, A. Roget, and Y. Levy, "Polypyrrole based DNA hybridization assays: study of label free detection processes versus fluorescence on microchips," *Journal of Pharmaceutical and Biomedical Analysis*, vol. 32, pp. 687–696, 2003.

[67] L. Moiseev, M. S. Unlü, A. K. Swan, B. B. Goldberg, and C. R. Cantor, "DNA conformation on surfaces measured by fluorescence self-interference," *Proceedings of the National Academy of Sciences of the United States of America*, vol. 103, pp. 2623–8, Feb. 2006.

[68] L. M. Demers, C. a. Mirkin, R. C. Mucic, R. a. Reynolds, R. L. Letsinger, R. Elghanian, and G. Viswanadham, "A fluorescence-based method for determining the surface coverage and hybridization efficiency of thiol-capped oligonucleotides bound to gold thin films and nanoparticles," *Analytical Chemistry*, vol. 72, pp. 5535–41, Nov. 2000.

[69] L. a. Chrisey, G. U. Lee, and C. E. O'Ferrall, "Covalent attachment of synthetic DNA to self-assembled monolayer films," *Nucleic Acids Research*, vol. 24, pp. 3031–9, Aug. 1996.

[70] R. Georgiadis, K. P. Peterlinz, and a. W. Peterson, "Quantitative measurements and modeling of kinetics in nucleic acid monolayer films using SPR spectroscopy," *Journal of the American Chemical Society*, vol. 122, pp. 3166–3173, Apr. 2000.

[71] J. S. Shumaker-Parry, R. Aebersold, and C. T. Campbell, "Parallel, quantitative measurement of protein binding to a 120-element double-stranded DNA array in real time using surface plasmon resonance microscopy," *Analytical Chemistry*, vol. 76, pp. 2071–82, Apr. 2004.

[72] L. K. Wolf, D. E. Fullenkamp, and R. M. Georgiadis, "Quantitative angle-resolved SPR imaging of DNA-DNA and DNA-drug kinetics," *Journal of the American Chemical Society*, vol. 127, pp. 17453–9, Dec. 2005.

[73] A. W. Wark, H. J. Lee, and R. M. Corn, "Long-range surface plasmon resonance imaging for bioaffinity sensors," *Analytical Chemistry*, vol. 77, pp. 3904–7, July 2005.

[74] S. M. Schreiner, D. F. Shudy, A. L. Hatch, A. Opdahl, L. J. Whitman, and D. Y. Petrovykh, "Controlled and efficient hybridization achieved with DNA probes immobilized solely through preferential DNA-substrate interactions.," *Analytical Chemistry*, vol. 82, pp. 2803–10, Apr. 2010.

[75] X. Su, Y.-J. Wu, R. Robelek, and W. Knoll, "Surface plasmon resonance spectroscopy and quartz crystal microbalance study of streptavidin film structure effects on biotinylated DNA assembly and target DNA hybridization," *Langmuir*, vol. 21, pp. 348–53, Jan. 2005.

[76] M. Lazerges, H. Perrot, E. Antoine, A. Defontaine, and C. Compere, "Oligonucleotide quartz crystal microbalance sensor for the microalgae Alexandrium minutum (Dinophyceae)," *Biosensors and Bioelectronics*, vol. 21, pp. 1355–1358, 2005.

[77] R. Lao, S. Song, H. Wu, L. Wang, Z. Zhang, L. He, and C. Fan, "Electrochemical interrogation of DNA monolayers on gold surfaces," *Analytical Chemistry*, vol. 77, pp. 6475–80, Oct. 2005.

[78] R. Levicky and A. Horgan, "Physicochemical perspectives on DNA microarray and biosensor technologies," *Trends in Biotechnology*, vol. 23, pp. 143–9, Mar. 2005.

[79] Z.-L. Zhang, D.-W. Pang, R.-Y. Zhang, J.-W. Yan, B.-W. Mao, and Y.-P. Qi, "Investigation of DNA orientation on gold by EC-STM," *Bioconjugate Chemistry*, vol. 13, no. 1, pp. 104–9, 2002.

[80] S. O. Kelley, J. K. Barton, N. M. Jackson, L. D. McPherson, A. B. Potter, E. M. Spain, M. J. Allen, and M. G. Hill, "Orienting DNA Helices on Gold Using Applied Electric Fields," *Langmuir*, vol. 14, pp. 6781–6784, Nov. 1998.

[81] A. V. Saprigin, C. W. Thomas, C. S. Dulcey, C. H. Patterson, and M. S. Spector, "Spectroscopic quantification of covalently immobilized oligonucleotides," *Surface and Interface Analysis*, vol. 37, pp. 24–32, Jan. 2004.

[82] M. R. Vilar, A. M. Botelho do Rego, A. M. Ferraria, Y. Jugnet, C. Noguès, D. Peled, and R. Naaman, "Interaction of self-assembled monolayers of DNA with electrons: HREELS and XPS studies," *The Journal of Physical Chemistry B*, vol. 112, pp. 6957–6964, June 2008.

[83] N. Ballav, P. Koelsch, and M. Zharnikov, "Orientation and ordering in monomolecular films of sulfur-modified homo-oligonucleotides on gold," *The Journal of Physical Chemistry C*, vol. 113, pp. 18312–18320, Oct. 2009.

[84] C. Howell, R. Schmidt, V. Kurz, and P. Koelsch, "Sum-frequency-generation spectroscopy of DNA films in air and aqueous environments," *Biointerphases*, vol. 3, pp. FC47–51, Sept. 2008.

[85] N. Samuel, C. Lee, L. Gamble, D. Fischer, and D. Castner, "NEXAFS characterization of DNA components and molecular-orientation of surface-bound DNA oligomers," *Journal of Electron Spectroscopy and Related Phenomena*, vol. 152, pp. 134–142, July 2006.

[86] C.-Y. Lee, H. E. Canavan, L. J. Gamble, and D. G. Castner, "Evidence of impurities in thiolated single-stranded DNA oligomers and their effect on DNA self-assembly on gold," *Langmuir*, vol. 21, pp. 5134–41, May 2005.

[87] C.-Y. Lee, P.-C. T. Nguyen, D. W. Grainger, L. J. Gamble, and D. G. Castner, "Structure and DNA hybridization properties of mixed nucleic acid/maleimide-ethylene glycol monolayers," *Analytical Chemistry*, vol. 79, pp. 4390–400, June 2007.

[88] H. F. Arlinghaus, M. Ostrop, O. Friedrichs, J. Feldner, U. Gunst, and D. Lipinsky, "DNA sequencing with ToF-SIMS," *Surface and Interface Analysis*, vol. 34, pp. 35–39, Aug. 2002.

[89] N. Winograd, "Prospects for imaging TOF-SIMS: from fundamentals to biotechnology," *Applied Surface Science*, vol. 203-204, pp. 13–19, 2003.

[90] J. D. Gelder, K. D. Gussem, P. Vandenabeele, and L. Moens, "Reference database of Raman spectra of biological molecules," *Journal of Raman Spectroscopy*, vol. 38, pp. 1133–1147, 2007.

[91] L. Q. Dong, J. Z. Zhou, L. L. Wu, P. Dong, and Z. H. Lin, "SERS studies of self-assembled DNA monolayer - characterization of adsorption orientation of oligonucleotide probes and their hybridized helices on gold substrate," *Chemical Physics Letters*, vol. 354, pp. 458–465, 2002.

[92] A. Barhoumi and N. J. Halas, "Label-Free Detection of DNA Hybridization Using Surface Enhanced Raman Spectroscopy.," *Journal of the American Chemical Society*, vol. 132, pp. 12792–12793, Aug. 2010.

[93] J. T. Woodward, M. L. Walker, C. W. Meuse, D. J. Vanderah, G. E. Poirier, and A. L. Plant, "Effect of an Oxidized Gold Substrate on Alkanethiol Self-Assembly," *Langmuir*, vol. 16, pp. 5347–5353, June 2000.

[94] K. F. Domke, D. Zhang, and B. Pettinger, "Tip-enhanced Raman spectra of picomole quantities of DNA nucleobases at Au(111)," *Journal of the American Chemical Society*, vol. 129, pp. 6708–9, May 2007.

[95] A. G. Lambert, P. B. Davies, and D. J. Neivandt, "Implementing the theory of sum frequency generation vibrational spectroscopy : a tutorial review," *Applied Spectroscopy Reviews*, vol. 40, pp. 103–145, 2005.

[96] Y. R. Shen and V. Ostroverkhov, "Sum-frequency vibrational spectroscopy on water interfaces: polar orientation of water molecules at interfaces," *Chemical Reviews*, vol. 106, pp. 1140–54, Apr. 2006.

[97] Z. Chen, Y. Shen, and G. A. Somorjai, "Studies of polymer surfaces by sum frequency generation spectroscopy," *Annual Review of Physical Chemistry*, vol. 53, pp. 437–465, 2002.

[98] S. Roke, "Nonlinear Optical Spectroscopy of Soft Matter Interfaces," *ChemPhysChem*, vol. 10, pp. 1380 – 1388, 2009.

[99] a. Hopkins, C. Mcfearin, and G. Richmond, "Investigations of the solid-aqueous interface with vibrational sum-frequency spectroscopy," *Current Opinion in Solid State and Materials Science*, vol. 9, pp. 19–27, Feb. 2005.

[100] O. Mermut, D. C. Phillips, R. L. York, K. R. McCrea, R. S. Ward, and G. a. Somorjai, "In situ adsorption studies of a 14-amino acid leucine-lysine peptide onto hydrophobic polystyrene and hydrophilic silica surfaces using quartz crystal microbalance, atomic force microscopy, and sum frequency generation vibrational spectroscopy," *Journal of the American Chemical Society*, vol. 128, pp. 3598–607, Mar. 2006.

[101] H. Asanuma, H. Noguchi, K. Uosaki, and H.-Z. Yu, "Metal cation-induced deformation of DNA self-assembled monolayers on silicon: vibrational sum frequency generation spectroscopy," *Journal of the American Chemical Society*, vol. 130, pp. 8016–22, June 2008.

[102] M. Ostblom, B. Liedberg, L. M. Demers, and C. a. Mirkin, "On the structure and desorption dynamics of DNA bases adsorbed on gold: a temperature-programmed study.," *The Journal of Physical Chemistry B*, vol. 109, pp. 15150–60, Aug. 2005.

[103] R. Hesse, P. Streubel, and R. Szargan, "Product or sum : comparative tests of Voigt, and product or sum of Gaussian and Lorentzian functions in the fitting of synthetic Voigt based X ray photoelectron spectra," *Surface and Interface Analysis*, vol. 39, pp. 381–391, 2007.

[104] K. Heister, M. Zharnikov, M. Grunze, and L. S. O. Johansson, "Adsorption of Alkanethiols and Biphenylthiols on Au and Ag Substrates : A High-Resolution X-ray Photoelectron Spectroscopy Study," *Journal of Physical Chemistry B*, vol. 105, pp. 4058–4061, May 2001.

[105] P. Batson, "Carbon 1s near-edge-absorption fine structure in graphite," *Physical Review B*, vol. 48, pp. 2608–2610, July 1993.

[106] R. Ahlrichts, M. Bär, M. Häser, H. Horn, and C. Kölmel, "Electronic structure calculations on worksatation computers: The program system turbomole," *Chemical Physics Letters*, vol. 162, pp. 165–169, 1989.

[107] J. P. Perdew, K. Burke, and M. Ernzerhof, "Generalized gradient approximation made simple," *Physical Review Letters*, vol. 77, pp. 3865–3868, 1996.

[108] S. Grimme, "Semiempirical GGA-type density functional constructed with a long-range dispersion correction," *Journal of Computational Chemistry*, vol. 27, pp. 1787–99, Nov. 2006.

[109] R. Maul, F. Ortmann, M. Preuss, K. Hannewald, and F. Bechstedt, "DFT studies using supercells and projector-augmented waves for structure, energetics, and dynamics of glycine, alanine, and cysteine," *Journal of Computational Chemistry*, vol. 28, pp. 1817–33, Aug. 2007.

[110] X. D. Zhu, H. Suhr, and Y. R. Shen, "Surface vibrational spectroscopy by infrared-visible sum frequency generation," *Physical Review B*, vol. 35, pp. 3047–3050, 1987.

[111] J. Hunt, P. Guyot-Sionnest, and Y. Shen, "Observation of C-H strech vibrations of monolayers of molecules optical sum-frequency generation," *Chemical Physics Letters*, vol. 133, pp. 189–192, 1987.

[112] A. Harris, E. Chidsey, N. Levinos, and D. Loiacono, "Monolayer vibrational spectroscopy by infrared-visible sum generation at metal and semiconductor surfaces," *Chemical Physics Letters*, vol. 141, no. 4, pp. 350–356, 1987.

[113] C. D. Bain, "Sum-frequency Vibrational Spectroscopy of the Solid/Liquid Interface," *Journal of the Chemical Society, Faraday Transactions*, vol. 91, pp. 1281–1296, 1995.

[114] L. Dreesen, C. Humbert, M. Celebi, J. Lemaire, A. Mani, P. Thiry, and A. Peremans, "Influence of the metal electronic properties on the sum-frequency generation spectra of dodecanethiol self-assembled monolayers on Pt (111), Ag (111) and Au (111) single crystals," *Applied Physics B: Lasers and Optics*, vol. 74, pp. 621–625, May 2002.

[115] D. Verreault, V. Kurz, C. Howell, and P. Koelsch, "Sample cells for probing solid/liquid interfaces with broadband sum-frequency-generation spectroscopy," *The Review of Scientific Instruments*, vol. 81, p. 063111, June 2010.

[116] M. Skoda, R. Jacobs, S. Zorn, and F. Schreiber, "Optimizing the PMIRRAS signal from a multilayer system and application to self-assembled monolayers in contact with liquids," *Journal of Electron Spectroscopy and Related Phenomena*, vol. 172, no. 1-3, pp. 21–26, 2009.

[117] A. Lagutchev, S. A. Hambir, and D. D. Dlott, "Nonresonant Background Suppression in Broadband Vibrational Sum-Frequency Generation Spectroscopy," *Journal of Physical Chemistry C Letters*, vol. 111, pp. 13645–13647, 2007.

[118] R. Maoz, J. Sagiv, D. Degenhardt, H. Moehwald, and P. Quint, "Hydrogen-bonded multilayers of self-assembling silanes: structure elucidation by combined Fourier transform infrared spectroscopy and X-ray scattering techniques," *Supramolecular Science*, vol. 2, pp. 9–24, 1995.

[119] I. V. Stiopkin, H. D. Jayathilake, A. N. Bordenyuk, and A. V. Benderskii, "Heterodyne-Detected Vibrational Sum Frequency Generation Spectroscopy," *Langmuir*, vol. 130, pp. 2271–2275, 2008.

[120] T. H. Ong, P. B. Davies, and C. D. Bain, "Sum-Frequency Spectroscopy of Monolayers of Alkoxy-Terminated Alkanethiols in Contact with Liquids," *Langmuir*, vol. 9, pp. 7155– 7164, 1993.

[121] T. H. Ong, R. N. Ward, P. B. Davies, and C. D. Bain, "Microscopic Basis of Wetting: An in Situ Study of the Interaction between Liquids and an Organic Monolayer," *Journal of the American Chemical Society*, vol. 114, pp. 6243–6245, 1992.

[122] N. Ward, B. Davies, and C. D. Bain, "Orientation of surfactants adsorbed on a hydrophobic surface," *Journal of Physical Chemistry*, vol. 97, pp. 7141–7143, 1993.

[123] M. Buck, "Ab initio calculations of vibrational spectra of 2-methoxy ethanol in the CH stretching range," *Physical Chemistry Chemical Physics*, vol. 5, pp. 18–25, 2003.

[124] A. J. Pertsin and M. Grunze, "Computer Simulation of Water near the Surface of Oligo(ethylene glycol)-Terminated Alkanethiol Self-Assembled Monolayers," *Langmuir*, vol. 16, pp. 8829–8841, Nov. 2000.

[125] M. Zolk, F. Eisert, J. Pipper, S. Herrwerth, W. Eck, M. Buck, and M. Grunze, "Solvation of Oligo (ethylene glycol) -Terminated Self-Assembled Monolayers Studied by Vibrational Sum Frequency Spectroscopy," *Langmuir*, vol. 16, pp. 5849–5852, 2000.

[126] C. Vericat, M. E. Vela, G. A. Benitez, J. A. M. Gago, and X. Torrelles, "Surface characterization of sulfur and alkanethiol self-assembled monolayers on Au (111)," *Journal of Physics: Condensed Matter*, vol. 18, pp. R867–R900, 2006.

[127] M. J. Stevens and G. S. Grest, "Simulations of water at the interface with hydrophilic self-assembled monolayers," *Biointerphases*, vol. 3, no. 3, pp. 13–22, 2008.

[128] A.-c. Yang and C.-i. Weng, "Influence of alkanethiol self-assembled monolayers with various tail," *The Journal of Chemical Physics*, vol. 129, p. 154710, 2008.

[129] M. Mezger, H. Reichert, S. Schöder, J. Okasinski, H. Schröder, H. Dosch, D. Palms, J. Ralston, and V. Honkimäki, "High-resolution in situ x-ray study of the hydrophobic gap at the water-octadecyl-trichlorosilane interface.," *Proceedings of the National Academy of Sciences of the United States of America*, vol. 103, pp. 18401–4, Dec. 2006.

[130] L. Dreesen, C. Humbert, P. Hollander, A. Mani, K. Ataka, P. Thiry, and A. Peremans, "Study of the water/poly(ethylene glycol) interface by IR-visible sum-frequency generation spectroscopy," *Chemical Physics Letters*, vol. 333, pp. 327–331, 2001.

[131] L. Baugh, T. Weidner, J. E. Baio, P.-C. T. Nguyen, L. J. Gamble, P. S. Stayton, and D. G. Castner, "Probing the orientation of surface-immobilized protein G B1 using ToF-SIMS, sum frequency generation, and NEXAFS spectroscopy," *Langmuir*, vol. 26, pp. 16434–41, Nov. 2010.

[132] C. D. Bain, E. B. Troughton, Y. T. Tao, J. Evall, G. M. Whitesides, and R. G. Nuzzo, "Formation of monolayer films by the spontaneous assembly of organic thiols from solution onto gold," *Journal of the American Chemical Society*, vol. 111, pp. 321–335, Jan. 1989.

[133] M. D. Porter, T. B. Bright, D. L. Allara, and C. E. D. Chidsey, "Spontaneously Organized Molecular Assemblies. 4. Structural Characterization of n-Alkyl Thiol Monolayers," *Journal of the American Chemical Society*, vol. 109, pp. 3559–3568, 1987.

[134] R. G. Nuzzo, L. H. Dubois, and D. L. Allara, "Fundamental Studies of Microscopic Wetting on Organic Surfaces . 1 . Formation and Structural Characterization of a Self-Consistent Series of Polyfunctional Organic Monolayers," *Journal of the American Chemical Society*, vol. 112, pp. 558–569, 1990.

[135] M. Himmelhaus, F. Eisert, M. Buck, and M. Grunze, "Self-Assembly of n-Alkanethiol Monolayers. A Study by IR-Visible Sum Frequency Spectroscopy (SFG)," *Journal of Physical Chemistry B*, vol. 104, pp. 576–584, 2000.

[136] M. Maccarini, R. Steitz, M. Himmelhaus, J. Fick, S. Tatur, M. Wolff, M. Grunze, J. Janec, R. R. Netz, G. Strasse, and D. Berlin, "Density Depletion at Solid-Liquid Interfaces : a Neutron Reflectivity Study," *Langmuir*, vol. 23, pp. 598–608, 2007.

[137] A. Vainrub and B. Pettitt, "Coulomb blockage of hybridization in two-dimensional DNA arrays," *Physical Review E*, vol. 66, pp. 23–26, Oct. 2002.

[138] N. Nishi, D. Hobara, M. Yamamoto, and T. Kakiuchi, "Chain-length-dependent change in the structure of self-assembled monolayers of n-alkanethiols on Au (111) probed by broad-bandwidth sum frequency generation spectroscopy," *Chemical Physics*, vol. 118, no. 4, pp. 17–19, 2003.

[139] G. R. Bell, C. D. Bain, and R. N. Ward, "Sum-frequency vibrational spectroscopy of soluble surfactants at the air/water interface," *Journal of the Chemical Society, Faraday Transactions*, vol. 92, no. 4, p. 515, 1996.

[140] W. Haiss, B. Roelfs, S. N. Port, E. Bunge, H. Baumga, and R. J. Nichols, "In-situ infrared spectroscopic studies of thymine adsorption on a Au (111) electrode," *Journal of Electroanalytical Chemistry*, vol. 454, pp. 107 – 113, 1998.

[141] E. L. Hommel and H. C. Allen, "The air/liquid interface of benzene, toluene, m-xylene, and mesitylene: a sum frequency, Raman, and infrared spectroscopic study," *The Analyst*, vol. 128, no. 6, p. 750, 2003.

[142] N. J. Tao, J. a. DeRose, and S. M. Lindsay, "Self-assembly of molecular superstructures studied by in situ scanning tunneling microscopy: DNA bases on gold (111)," *The Journal of Physical Chemistry*, vol. 97, pp. 910–919, Jan. 1993.

[143] T. Boland and B. D. Ratner, "Two-dimensional assembly of purines and pyrimidines on Au(111)," *Langmuir*, vol. 10, pp. 3845–3852, Oct. 1994.

[144] A. Bensimon, A. Simon, A. Chiffaudel, V. Croquette, F. Heslot, and D. Bensimon, "Alignment and sensitive detection of DNA by a moving interface," *Science*, vol. 265, pp. 7–9, 1994.

[145] J. Zheng, L. Li, S. Chen, and S. Jiang, "Molecular Simulation Study of Water Interactions with Oligo (Ethylene Glycol) - Terminated Alkanethiol Self-Assembled Monolayers," *Langmuir*, vol. 20, pp. 8931–8938, 2004.

[146] S. Peeters, T. Stakenborg, G. Reekmans, W. Laureyn, L. Lagae, A. Van Aerschot, and M. Van Ranst, "Impact of spacers on the hybridization efficiency of mixed self-assembled DNA/alkanethiol films," *Biosensors & Bioelectronics*, vol. 24, pp. 72–7, Sept. 2008.

[147] Y. Maeda, "IR spectroscopic study on the hydration and the phase transition of poly(vinyl methyl ether) in water," *Langmuir*, vol. 17, pp. 1737–1742, Mar. 2001.

[148] A. W. Peterson, R. J. Heaton, and R. Georgiadis, "Kinetic Control of Hybridization in Surface Immobilized DNA Monolayer Films," *Journal of the American Chemical Society*, vol. 122, pp. 7837–7838, 2000.

[149] M. Wirde, U. Gelius, T. Dunbar, and D. L. Allara, "Modification of self-assembled monolayers of alkanethiols on gold by ionizing radiation," *Nuclear Instruments and Methods in Physics Research Section B: Beam Interactions with Materials and Atoms*, vol. 131, pp. 245–251, 1997.

[150] R. K. Campen, T. T. M. Ngo, M. Sovago, J.-M. Ruysschaert, and M. Bonn, "Molecular restructuring of water and lipids upon the interaction of DNA with lipid monolayers," *Journal of the American Chemical Society*, vol. 132, pp. 8037–47, June 2010.

[151] M. Zharnikov and M. Grunze, "Modification of thiol-derived self-assembling monolayers by electron and x-ray irradiation: Scientific and lithographic aspects," *Journal of Vacuum Science & Technology B: Microelectronics and Nanometer Structures*, vol. 20, p. 1793, Oct. 2002.

[152] C. Howell, R. Maul, W. Wenzel, and P. Koelsch, "Interactions of hydrophobic and hydrophilic self-assembled monolayers with water as probed by sum-frequency-generation spectroscopy," *Chemical Physics Letters*, vol. 494, pp. 193–197, July 2010.

[153] J. Stoehr, *NEXAFS Spectroscopy, Springer Series in Surface Science 25*. Berlin: SPringer-Verlag, 1992.

[154] Y. Zubavichus, A. Shaporenko, M. Grunze, M. Zharnikov, and V. Korolkov, "Is X-ray absorption spectroscopy sensitive to the amino acid composition of functional proteins?," *The journal of physical chemistry. B*, vol. 112, pp. 4478–80, Apr. 2008.

[155] A. Jain, Y. Gupta, R. Agrawal, S. K. Jain, and P. Khare, "Biofilms - a microbial life perspective: a critical review," *Critical Reviews in Theraputic Drug Carrier Systems*, vol. 24, pp. 393–443, 2007.

[156] R. Patel, "Biofilms and antimicrobial resistance," *Clinical Orthopaedics and Related Research*, vol. 437, pp. 41–47, 2005.

[157] E. D. Hay, *Cell biology of the extracellular matrix*. Springer, 2nd ed., 2007.

[158] I. Vlodavsky, Z. Fuks, R. Ishai-Michaeli, P. Bashkin, E. Levi, G. Korner, R. Bar-Shavit, and M. Klagsbrun, "Extracellular matrix-resident basic fibroblast growth factor: implication for the control of angiogenesis," *Journal of Cellular Biochemistry*, vol. 45, pp. 167–76, Feb. 1991.

[159] A. Cretu and P. C. Brooks, "Impact of the non-cellular tumor microenvironment on metastasis: potential therapeutic and imaging opportunities," *Journal of Cellular Physiology*, vol. 213, pp. 391–402, Nov. 2007.

[160] S. M. Pupa, S. Ménard, S. Forti, and E. Tagliabue, "New insights into the role of extracellular matrix during tumor onset and progression.," *Journal of Cellular Physiology*, vol. 192, pp. 259–67, Sept. 2002.

[161] P.-J. Wipff, D. B. Rifkin, J.-J. Meister, and B. Hinz, "Myofibroblast contraction activates latent TGF-beta1 from the extracellular matrix.," *The Journal of cell biology*, vol. 179, pp. 1311–23, Dec. 2007.

[162] L. J. Kaufman, C. P. Brangwynne, K. E. Kasza, E. Filippidi, V. D. Gordon, T. S. Deisboeck, and D. a. Weitz, "Glioma expansion in collagen I matrices: analyzing collagen concentration-dependent growth and motility patterns.," *Biophysical journal*, vol. 89, pp. 635–50, July 2005.

[163] G. Bernard, M. Auger, J. Soucy, and R. Pouliot, "Physical characterization of the stratum corneum of an in vitro psoriatic skin model by ATR-FTIR and Raman spectroscopies," *Biochimica et Biophysica Acta*, vol. 1770, pp. 1317–1323, 2007.

[164] D. F. Coutinho, I. H. Pashkuleva, C. M. Alves, A. P. Marques, N. M. Neves, and R. L. Reis, "The effect of chitosan on the in vitro biological performance of chitosan-poly(butylene succinate) blends.," *Biomacromolecules*, vol. 9, pp. 1139–45, Apr. 2008.

[165] W. He, X. Guo, and M. Zhang, "Transdermal permeation enhancement of N-trimethyl chitosan for testosterone," *International Journal of Pharmaceutics*, vol. 356, pp. 82–87, 2008.

[166] A. Heredia, H. J. van der Strate, I. Delgadillo, V. A. Basiuk, and E. G. Vrieling, "Analysis of organo-silica interactions during valve formation in synchronously growing cells of the diatom Navicula pelliculosa.," *Chembiochem*, vol. 9, pp. 573–84, Mar. 2008.

[167] J. Wang, S.-H. Lee, and Z. Chen, "Quantifying the ordering of adsorbed proteins in situ," *The Journal of Physical Chemistry B*, vol. 112, pp. 2281–90, Feb. 2008.

[168] J. Wang, Z. Paszti, M. L. Clarke, X. Chen, and Z. Chen, "Deduction of structural information of interfacial proteins by combined vibrational spectroscopic methods," *The Journal of Physical Chemistry B*, vol. 111, pp. 6088–95, May 2007.

[169] X. Chen, J. Wang, J. J. Sniadecki, M. A. Even, and Z. Chen, "Probing r-Helical and -Sheet Structures of Peptides at Solid/Liquid Interfaces with SFG," *Langmuir*, vol. 21, pp. 2662–2664, 2005.

[170] R. L. York, O. Mermut, D. C. Phillips, K. R. Mccrea, R. S. Ward, and G. A. Somorjai, "Influence of Ionic Strength oh the Adsorption of a Model Peptide on Hydrophobic polystyrene surfaces : insight from SFG vibrational spectroscopy," *Journal of Physical Chemistry C*, vol. 111, pp. 8866–8871, 2007.

[171] D. Phillips, R. York, O. Mermut, K. McCrea, R. Ward, and G. Somorjai, "Side Chain, Chain Length, and Sequence Effects on Amphiphilic Peptide Adsorption at Hydrophobic and Hydrophilic Surfaces Studied by Sum-Frequency Generation Vibrational Spectroscopy and Quartz Crystal Microbalance," *Journal of Physical Chemistry C*, vol. 111, pp. 255–261, Jan. 2007.

[172] J. Wang, M. a. Even, X. Chen, A. H. Schmaier, J. H. Waite, and Z. Chen, "Detection of amide I signals of interfacial proteins in situ using SFG," *Journal of the American Chemical Society*, vol. 125, pp. 9914–5, Aug. 2003.

[173] I. Rocha-Mendoza, D. R. Yankelevich, M. Wang, K. M. Reiser, C. W. Frank, and A. Knoesen, "Sum frequency vibrational spectroscopy: the molecular origins of the optical second-order nonlinearity of collagen," *Biophysical Journal*, vol. 93, pp. 4433–44, Dec. 2007.

[174] S.-Y. Jung, S.-M. Lim, F. Albertorio, G. Kim, M. C. Gurau, R. D. Yang, M. a. Holden, and P. S. Cremer, "The Vroman effect: a molecular level description of fibrinogen displacement," *Journal of the American Chemical Society*, vol. 125, pp. 12782–6, Oct. 2003.

[175] X. Chen, L. B. Sagle, and P. S. Cremer, "Urea orientation at protein surfaces," *Journal of the American Chemical Society*, vol. 129, pp. 15104–5, Dec. 2007.

[176] Y. R. Shen, "Surface probed by second-harmonic and sum-frequency generation," *Nature*, vol. 337, pp. 519–525, 1989.

[177] S. Ye, K. T. Nguyen, S. V. Le Clair, and Z. Chen, "In situ molecular level studies on membrane related peptides and proteins in real time using sum frequency generation vibrational spectroscopy.," *Journal of structural biology*, vol. 168, pp. 61–77, Oct. 2009.

[178] T. Weidner, N. F. Breen, G. P. Drobny, and D. G. Castner, "Amide or amine: determining the origin of the 3300 cm(-1) NH mode in protein SFG spectra using 15N isotope labels.," *The Journal of Physical Chemistry B*, vol. 113, pp. 15423–6, Nov. 2009.

[179] S. Le Clair, K. Nguyen, and Z. Chen, "Sum Frequency Generation Studies on Bioadhesion: Elucidating the Molecular Structure of Proteins at Interfaces.," *The Journal of Adhesion*, vol. 85, pp. 484–511, Aug. 2009.

[180] M. M. Wintrobe and J. W. Landsberg, "A standardized technique for the blood sedimentation test," *The American Journal of Medical Sciences*, vol. 189, pp. 102–114, 1935.

[181] C. Godin and A. Caprani, "Effect of blood storage on erythrocyte/wall interactions: implications for surface charge and rigidity," *European Biophysics Journal*, vol. 26, pp. 175–182, June 1997.

[182] P. E. Laibinis, R. G. Nuzzo, and G. M. Whitesides, "Structure of monolayers formed by coadsorption of two n-alkanethiols of different chain lengths on gold and its relation to wetting," *The Journal of Physical Chemistry*, vol. 96, pp. 5097–5105, June 1992.

Eidesstattliche Erklärung

Ich erkläre hiermit, dass ich die vorgelegte Dissertation selbst verfasst und mich keiner anderen als der von mir ausdrücklich bezeichneten Quellen und Hilfen bedient habe. Ausserdem, habe ich an keiner anderen Stelle ein Prüfungsverfahren beantragt bzw. die Dissertation in dieser oder anderer Form bereits anderweitig als Prüfungsarbeit verwendet oder einer anderen Fakultät als Dissertation vorgelegt.

Caitlin Howell

Heidelberg, den 27 Juli 2011